Fall 12-18-2014

A Computational Study of Procyanidin Binding to Histatin 5 and Thermodynamic Properties of Hofmeister-Anion Binding to a Hydrophobic Cavitand

Joshua Shraberg
University of New Orleans, jshraber@my.uno.edu

A Computational Study of Procyanidin Binding to Histatin 5
and
Thermodynamic Properties of Hofmeister-Anion Binding to a Hydrophobic Cavitand

A Dissertation

Submitted to the Graduate Faculty of the
University of New Orleans
in partial fulfillment of the
requirements for the degree of

Doctor of Philosophy
in
Chemistry

by

Joshua Shraberg

B.S. Tulane University, 2001
M.S. Tulane University, 2002

December, 2014

Dedication

For Claire

Acknowledgement

I would like to thank my advisor Dr. Steven Rick for his teaching and assistance throughout my Ph.D. studies. I would also like to thank my committee members Dr. Richard Cole, Dr. Mark Trudell and Dr. David Mobley for their valuable discussion and comments and to acknowledge Dr. Richard Cole for his collaboration and Dr. Bruce Gibb for his support and collaboration. I would also like to thank Dr. Michel Laguerre, Dr. Michael P. Williamson, Dr. James Gumbart, Dr. Anders Bennick, and Dr. Christopher M. Summa for their valuable discussion and assistance.

Table of Contents

List of Figures

List of Tables

Abstract

This dissertation will present the following two studies: A Computational Study of Procyanidin Binding to Histatin 5 and Thermodynamic Properties of Hofmeister-Anion Binding to a Hydrophobic Cavitand.

A Computational Study of Procyanidin Binding to Histatin 5

Abstract

Various studies suggest tannins act as antioxidants, anticarcinogens, cardio-protectants, anti-inflammatory agents, and antimicrobials. However, more investigation is needed to examine the bioavailability of tannins. Tannins bind to salivary peptides by hydrophilic and hydrophobic mechanisms. Electrospray Ionization Mass Spectrometry (ESI-MS) has been used to assess both hydrophilic and hydrophobic components of protein complexes. ESI-MS could potentially be an effective tool for screening the bioavailability of tannins. Weaker binding tannins are predicted to be more highly absorbed by the body, and should therefore exhibit greater bioavailability. Rannulu and Cole have used ESI-MS to measure binding affinities of procyanidin tannin stereoisomers for salivary peptides in aqueous solution. The condensed tannins procyanidin B1, B2, B3, and B4 demonstrated significantly different binding affinities (binding strengths) for the Histatin 5 salivary peptide. The procyanidin-Histatin 5 binding mechanisms in the ESI-MS experiments by Rannulu and Cole were investigated using the FRED docking program combined with molecular dynamics optimization in the AMBER software suite. The simulations suggest residual liquid-phase binding interactions in procyanidin-Histatin 5 complexes are maintained in the gas phase under conditions resembling those in ESI-MS experiments, though the gas-phase interaction energies were enhanced. Increased hydrogen bonding and decreased π-π stacking interactions were also detected in gas versus liquid-phase procyanidin-Histatin 5 complexes. In addition, simulation results suggest multiple conformations of procyanidins bind Histatin 5 at several sites and procyanidin binding does not fix the Histatin 5 peptide backbone. The simulations agree with previous studies which indicate aromatic Histatin 5 residues are responsible for procyanidin-Histatin 5 binding and tannins can bind salivary peptides in multiple conformations.

Introduction and Background

Plant tannins are water-soluble polyphenolic secondary metabolites having molecular weights between 500 and 3000 Da, and possessing unique properties such as the ability to precipitate alkaloids, gelatin, and other flexible proteins in addition to participating in typical phenolic reactions.[1] Tannins have generally been classified as either hydrolyzable (gallotannins and ellagitannins) or condensed based on their ability to readily undergo or resist hydrolysis.[2] A more rigorous classification system based on structural characteristics and chemical properties distributes the tannins into four major groups: gallotannins, ellagitannins, complex tannins, and condensed tannins (Figure 1.1).[3] Gallotannins consist of polyol, catechin, or triterpenoid cores esterified to gallic acid (Figure 1.2(d)) or meta-depsidically linked gallic acid derivatives (Figure 1.1(a)). Ellagitannins are similar to gallotannins and also possess at least two galloyl units oxidatively coupled through a C-C bond, but lack glycosidically linked catechin units (Figure 1.1(b)). Complex tannins contain catechin units glycosidically linked to a gallotannin or ellagitannin (Figure 1.1(c)) and condensed tannins are oligomers or polymers of flavan-3-ol derivatives with the C4 of one flavan-3-ol unit linked to C6 or C8 of another flavan-3-ol unit (Figure 1.1(d)).

Tannins are present in a variety of plant foods in quantities up to several grams *per* kilogram (Table 1.1).[4,5] The intake of flavonoids (the class of polyphenols that includes condensed tannins) in the U.S. is estimated to be approximately 20 milligrams *per* day, though other estimates range up to 1 gram *per* day.[4,6] Tannins have been found to produce hepatotoxicity, carcinogenesis, and anti-nutritional effects in animal studies.[7] However, other studies indicate tannins act as antioxidants, anticarcinogens, cardio-protectants, anti-inflammatory agents, and antimicrobials. More investigation to determine the potential health benefits and adverse effects of tannins as well as their mechanism(s) of action and bioavailability is therefore warranted.[7,8]

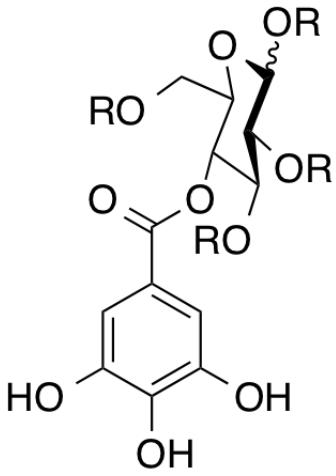

1.1(a) gallotannins (R = gallic acid)

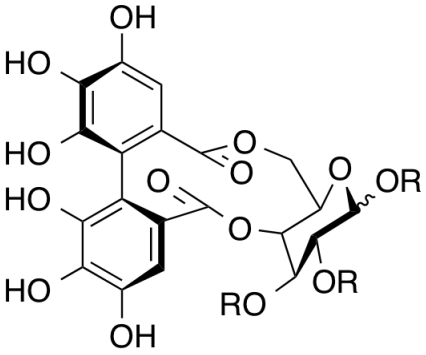

1.1(b) ellagitannins (R = gallic acid)

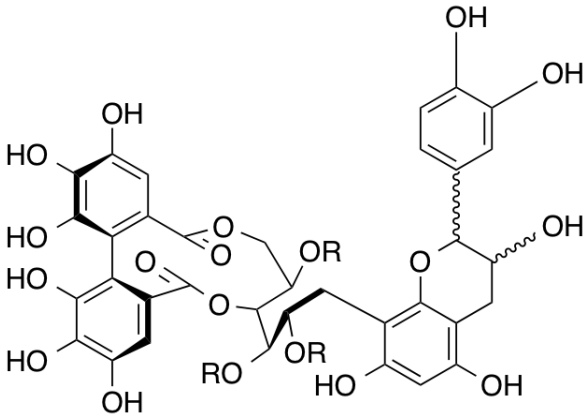

1.1(c) complex tannins (R = gallic acid)

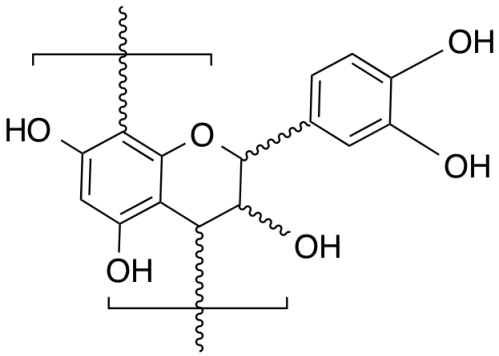

1.1(d) condensed tannins

Figure 1.1. Tannin classification

Table 1.1. Typical tannin-containing foods

Beverages	Berries
Tea	Strawberries
Coffee	Blueberries
Cocoa	Raspberries
Cider	Red currants
Red wine	
Beer	Legumes
	Common beans
Fruits	Pinto beans
Apple	Fava beans
Banana	Cowpeas
Persimmon	
	Other
Cereals	Condiments
Barley	
Sorghum	

Tannins bind and precipitate peptides with extended flexible conformations such as gelatin, though binding affinities of tannins for a particular peptide can vary considerably.[9] Tannins bind salivary peptides even more strongly than gelatin and are believed to be responsible for the sensation of astringency associated with consumption of foods with high tannin content (Table 1.1).[4,10] In addition, condensed tannin-salivary peptide complexes remain relatively insoluble under conditions typically found in the digestive tract.[11,12]

A significant portion of the salivary peptidome is generated through proteolysis of six classes of protein species secreted by the major salivary glands: acidic Proline Rich Proteins (aPRPs), basic Proline Rich Proteins (bPRPs), glycosylated Proline Rich Proteins (gPRPs), Histatins, Statherin, and Cystatins.[13–15] Salivary peptides are involved in maintaining oral health, lubrication, and digestion.[13,16,17] Proline Rich Proteins (PRPs), including aPRPs, bPRPs, and gPRPs, constitute up to 70% of secreted salivary proteins and tannin binding is proposed to be the main function of bPRPs.[14,18–23] The Histatins are a family of cationic histidine-rich peptides secreted by the parotid and submandibular/sublingual glands.[24–26] Of the twelve known Histatins, Histatins 4 through 12 are proteolytically cleaved from Histatin 3, while Histatin 2 is a proteolytic fragment of Histatin 1

(Table 1.2).[25,27] Histatins are believed to contribute to innate immunity, and Histatin 5 demonstrates potent antifungal activity against *Candida albicans* in particular.[28] 2D NMR studies indicate that Histatin 5 assumes a random coil in aqueous solution.[29,30] Histatin 5 has a propensity to adopt transient helical conformations in DMSO, but a definitive global minimum energy conformation is lacking.[29] Also, tertiary structural changes in Histatin 5 were not observed upon binding EGCG.[31]

Table 1.2. Amino acid sequences of Histatins 1 through 12

Histatin 1: DSHEKRHHGYRRKFHEKHHSHREFPFYGDYGSNYLYDN
Histatin 2: RKFHEKHHSHREFPFYGDYGSNYLYDN
Histatin 3: DSHAKRHHGYKRKFHEKHHSHRGYRSNYLDYN
Histatin 4: RKFHEKHHSHRGYRSNYLYDN
Histatin 5: DSHAKRHHGYKRKFHEKHHSHRGY
Histatin 6: DSHAKRHHGYKRKFHEKHHSHRGYR
Histatin 7: RKFHEKHHSHRGY
Histatin 8: KFHEKHHSHRGY
Histatin 9: RKFHEKHHSHRGYR
Histatin 10: KRHEKHHSHRGYR
Histatin 11: KRHHGYKR
Histatin 12: KRHHGYK

Various analytical techniques have been used to study tannin-protein binding, including: precipitation/centrifugation analysis,[32] competitive binding assays,[9] enzyme-linked immunosorbent assay (ELISA) style assays,[33] nephelometry,[34] isothermal titration calorimetry (ITC),[35–40] nuclear magnetic resonance (NMR) spectroscopy,[41–43] and mass spectrometry (MS).[44–47] Histatins bind

more strongly to tannins than most other salivary peptides.[48,49] One precipitation/centrifugation study concluded Histatins 3 and 5 bind condensed tannins more strongly than Histatin 1.[12] Another study using combined chromatographic and proteomics based approaches concluded Histatin 1 has the highest affinity for condensed tannins among the Histatins.[49] The authors of the latter study noted, however, that their experimental methods and conditions were significantly different from the former.[49] The effects of several structural features of condensed tannins on tannin-peptide binding have been assessed, including: type of interflavanoid bond linkage (C4-C8 or C4-C6), monomer stereochemistry (catechin versus epicatechin), esterification of galloyl groups to the C3 hydroxyl group, the hydroxylation pattern of the B ring, and the degree of polymerization (Figure 1.2).[34,36] In addition, the degree of polymerization and the presence and arrangement of specific functional groups have been found to influence the antioxidant properties of tannins.[50,51]

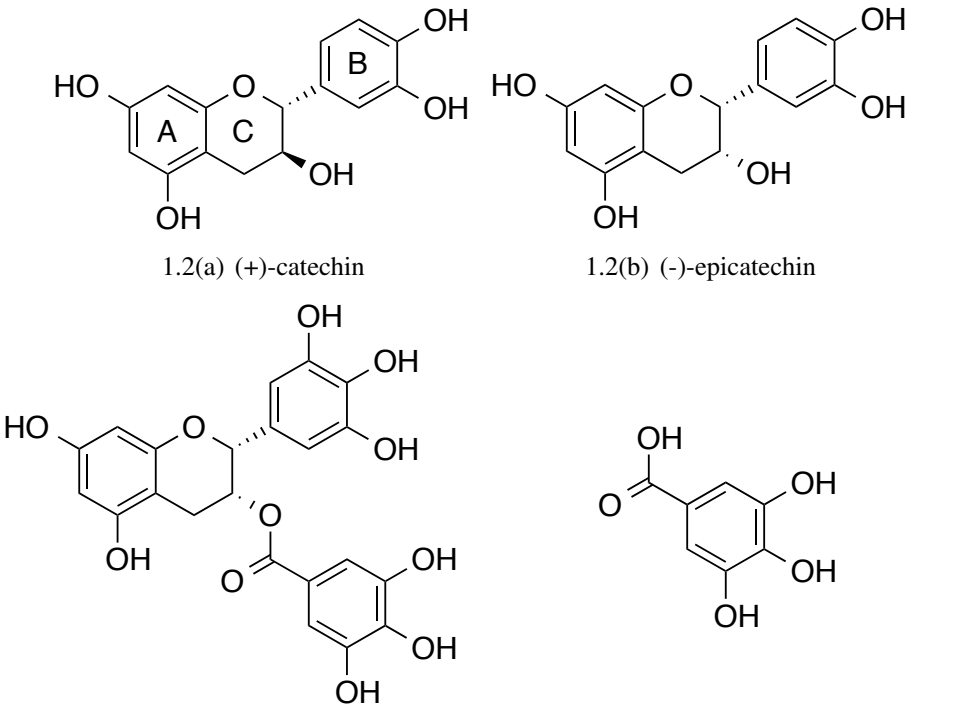

1.2(a) (+)-catechin

1.2(b) (-)-epicatechin

1.2(c) epigallocatechin gallate (EGCG)

1.2(d) gallic acid

Figure 1.2. Procyanidin monomers

ESI-MS has been successfully applied to the study of tannin-PRP interactions to determine

the relative binding affinities and stoichiometries of tannin-peptide complexes, and to investigate the overall architecture of the tannin-peptide complex.[44,45] The tannin-peptide complexes possessed a similar charge state distribution to the unbound peptide and collision-induced dissociation (CID) was used as a means to determine the relative binding affinities of several condensed tannin monomers for procyanidin B2.[44,45] Some studies indicate salivary peptides bind tannins most efficiently at or near their isoelectric point.[32] However, Histatin 5, whose isoelectric point is estimated to be around 10.3 (Table 1.3), was observed to bind and precipitate more epigallocatechin gallate (EGCG) (Figure 1.2(c)) at pH 3.0 than pH 7.4.[12,52] Thus, peptide neutrality is not a necessary condition for effective binding of some tannins to Histatin 5.[12]

Table 1.3. Amino acid sequence and physical properties of Histatin 5 (pI: Isoelectric Point)

Histatin 5 amino acid sequence	charge at neutral pH	pI
DSHAKRHHGYKRKFHEKHHSHRGY	+5	10.5

ESI-MS has been used to study numerous types of noncovalent protein complexes, including: protein-protein, protein-peptide, protein-nucleic acid, protein-small molecule, and polypeptide-metal ion complexes, and to assess both hydrophilic and hydrophobic components of protein complexes.[53–55] Stoichiometry data is readily obtained from ESI-MS studies and ESI-MS can complement other bioanalytical techniques such as analytical ultracentrifugation and X-ray crystallography as well as UV, IR, fluorescence, and NMR spectroscopy.[53] In addition, ESI-MS has notable advantages with respect to other biophysical methods, including high sensitivity, specificity, and speed.[53] The power of ESI-MS to measure relative binding affinities of tannin stereoisomers for salivary peptides could enable it as an effective tool for screening the bioavailability of tannins. Weaker binding tannins are predicted to be more susceptible to absorption from the gut and thus have higher bioavailability, though other factors including complexation with bile salts can influence the bioavailability of tannins as well.[12,31,78]

The condensed tannins procyanidin B1, B2, B3, and B4 are dimeric diastereomers of (+)-catechin and (-)-epicatechin units (Figures 1.2(a) and 1.2(b)) with the structures: epicatechin-(4$\beta\rightarrow$8)-catechin, epicatechin-(4$\beta\rightarrow$8)-epicatechin, catechin-(4$\alpha\rightarrow$8)-catechin, and catechin-(4$\alpha\rightarrow$8)-epicatechin, respectively (Figure 1.3).[7] Procyanidin B1, B2, B3, and B4 adopt two distinct minimum energy conformations (rotamers) in aqueous solution corresponding to a 'compact' rotamer with π-π stacked monomers forming a dihedral angle at the interflavanoid bond of +95° or an 'extended' unstacked rotamer with a dihedral angle of -81° (Figure 1.4).[56]

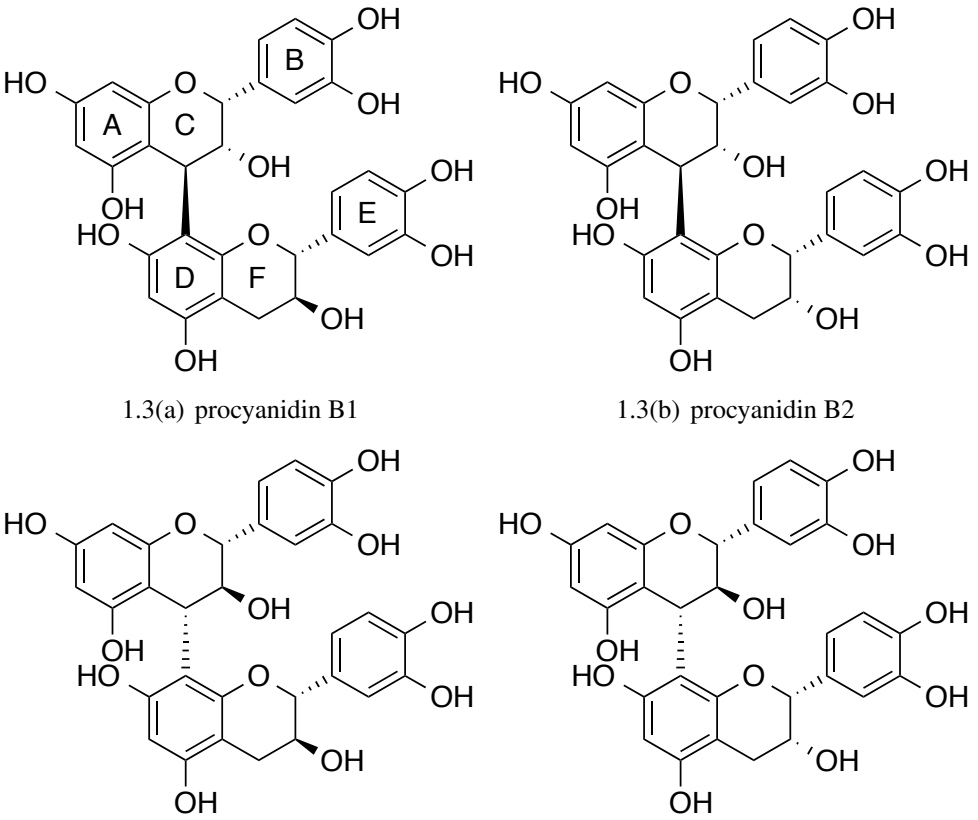

1.3(a) procyanidin B1

1.3(b) procyanidin B2

1.3(c) procyanidin B3

1.3(d) procyanidin B4

Figure 1.3. Procyanidin B1, B2, B3, and B4

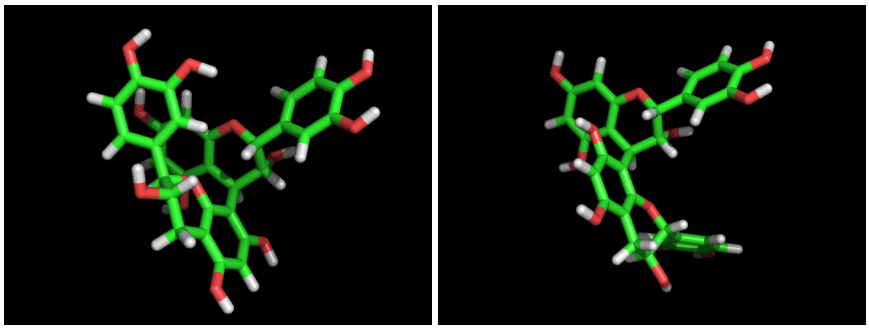

1.4(a) procyanidin B1 compact rotamer 1.4(b) procyanidin B1 extended rotamer

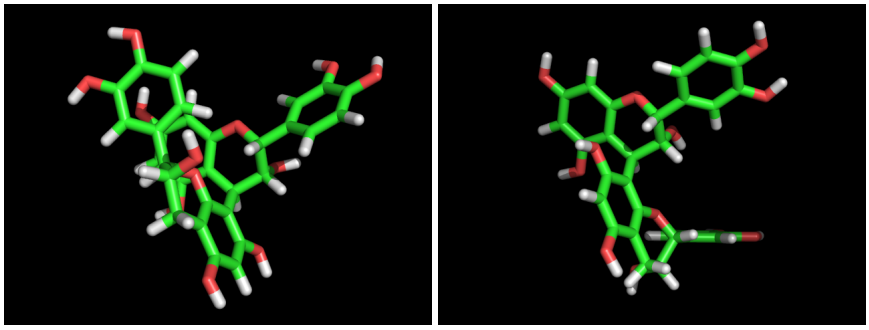

1.4(c) procyanidin B2 compact rotamer 1.4(d) procyanidin B2 extended rotamer

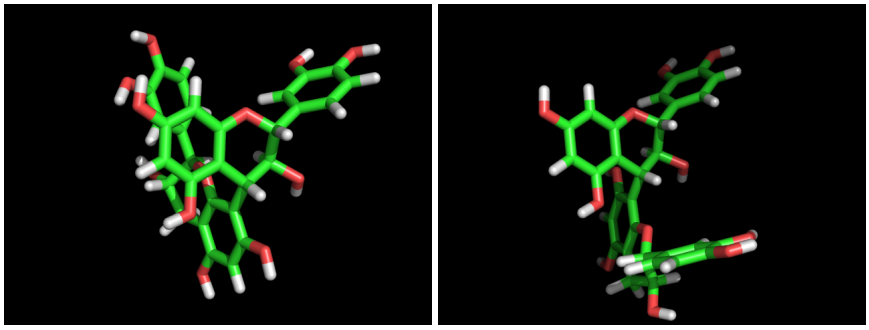

1.4(e) procyanidin B3 compact rotamer 1.4(f) procyanidin B3 extended rotamer

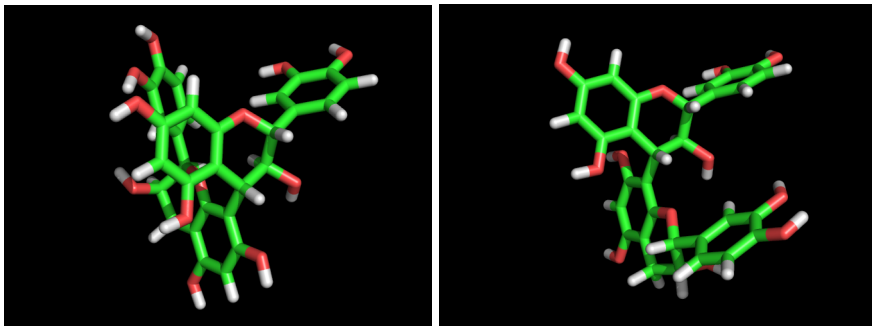

1.4(g) procyanidin B4 compact rotamer 1.4(h) procyanidin B4 extended rotamer

Figure 1.4. Compact and extended rotamers of procyanidin B1, B2, B3, and B4*

*atomic coordinates of compact and extended rotamers of procyanidin B1, B2, B4, and the compact rotamer of procyanidin B3 provided by Dr. Michel Laguerre, Institut Européen de Chimie et de Biologie, 33607 Pessac, France.

Rannulu and Cole used ESI-MS to probe the relative binding affinities (relative binding strengths) of procyanidin B1, B2, B3, and B4 for the Histatin 5 salivary peptide in aqueous solution. The ESI-MS studies used 10 μM Histatin 5 and 40 μM of procyanidin B1, B2, B3, and B4 at acidic pH. Binding strength quotients were calculated for each procyanidin diastereomer using equation (1).[57]

binding strength quotient =

$$\frac{\text{sum of peak intensities for all charge states and stoichiometries of the tannin-peptide complex}}{\text{sum of peak intensities for all charge states of the unbound peptide}} \quad (1)$$

The relative binding affinities of procyanidin diastereomers in solution were ranked according to their corresponding binding strength quotients: B1 > B4 > B2 > B3 (Table 1.4). Rannulu and Cole also determined gas-phase dissociation quotients (the resistance of procyanidin-Histatin 5 complexes to collision-induced dissociation (CID)) for each procyanidin diastereomer.

Table 1.4. ESI-MS binding strength quotients and gas-phase dissociation quotients (averaged over several trials) +/- 1 standard deviation of procyanidin B1, B2, B3 and B4 with Histatin 5 (PCB: Procyanidin B)

PCB	Binding strength quotient	Rank
PCB1	0.36 +/- 0.01	1
PCB4	0.32 +/- 0.02	2
PCB2	0.27 +/- 0.03	3
PCB3	0.210 +/- 0.004	4
PCB	**Gas-phase dissociation quotient**	**Rank**
PCB4	1.4 +/- 0.2	1
PCB2	4.1 +/- 0.5	2
PCB1	8 +/- 3	3
PCB3	14 +/- 3	4

The gas-phase dissociation quotients were calculated using equation (2). The relative binding

gas-phase dissociation quotient =

$$\frac{\text{sum of peak intensities for the dissociated product ions}}{\text{peak intensity for the precursor ion}} \tag{2}$$

affinities of procyanidin diastereomers in the gas phase were ranked according to their corresponding gas phase dissociation quotients: B4 $>$ B2 $>$ B1 $>$ B3 (Table 1.4). The binding strength quotients and gas-phase dissociation quotients of procyanidins somewhat differed, suggesting that the relative binding affinities of procyanidins in solution and in the gas phase might also differ.

The Fast Rigid Exhaustive Docking (FRED) program performs rigid-body docking of a set of ligand conformers to a fixed protein receptor in implicit aqueous solvent.[58,59] FRED calculates a score for each pose using an empirical scoring function and ranks the ligands according to their scores. A lower score corresponds to a stronger binding pose, and the rank of each ligand corresponds ideally to its relative binding affinity. FRED also outputs atomic coordinates for the highest ranked poses of docked ligands, which can be subjected to further optimization. The compact and extended rotamers of procyanidin B1, B2, B3, and B4 were docked to Histatin 5 with FRED, and subsequently optimized in molecular dynamics (MD) simulations using the Assisted Model Building with Energy Refinement (AMBER) software suite[42] to further investigate procyanidin-Histatin 5 binding mechanisms in the ESI-MS experiments by Rannulu and Cole.

Methods

In-house scripts for processing MD trajectory data were written using Python 2.5.6 or Fortran 90 unless otherwise indicated. Two-dimensional chemical structures were drawn with ChemDraw version 13.0.[61] Three-dimensional structures were rendered in PyMOL version 1.3[62] or VMD version 1.9.1[46] and data were plotted with gnuplot version 4.4.

Atomic coordinates for the compact and extended rotamers of procyanidin B1, B2, and B4, and the compact rotamer of procyanidin B3 were provided by Dr. Michel Laguerre of the Institut Européen de Chimie et de Biologie, Pessac, France. The extended rotamer of procyanidin B3 was obtained by manual rotation of the interflavanoid bond of the compact procyanidin B3 rotamer in PyMOL.

Structural data for the Histatin 5 peptide was not available from a protein structure database. A Histatin 5 structure was therefore generated with CS23D2.0,[64] a web server for protein structure prediction from sequence data and NMR chemical shifts. Proton chemical shifts for Histatin 5 in 10 mM phosphate/H_2O buffer from a conformational study of Histatin 5 by Lajoie et al. were used as input for CS23D2.0 (Table 1.5).[29] CS23D2.0 was executed with the "number of GAFolder iterations" set to 100. The final structure reliability for Histatin 5 generated by CS23D2.0 was output as poor. Secondary structure analysis with PyMOL indicated a helical conformation for most of the length of the Histatin 5 structure. Further optimization of side chain rotamers of the Histatin 5 structure was performed manually using the PyMOL Mutagenesis Wizard to reduce steric clashes of side chain heavy atoms. Simulations of the resulting structure were implemented with the *sander* module of AMBER 9[42] using the ff03 force field[65] with periodic boundary conditions. All bond lengths were constrained with the SHAKE algorithm and long-range electrostatics were treated with the particle-mesh Ewald (PME) method. The Histatin 5 structure was neutralized by addition of 5 chloride ions and solvated in a box of 986 TIP3P[66] explicit waters. Fifty cycles of the steepest descent method followed by 50 cycles of conjugate gradient minimization were used with

Table 1.5. ^{1}H NMR chemical shifts for Histatin 5 in 10 mM phosphate/H_2O buffer at pH 7.5 (Data are from "D. Brewer, H. Hunter, and G. Lajoie. NMR Studies of the Antimicrobial Salivary Peptides Histatin 3 and Histatin 5 in Aqueous and Nonaqueous Solution. *Biochem. Cell Biol.*, *76*: 247–256, **1998**, Table 1")

Residue	NH	CαH	CβH	Others
Asp1	4.25	2.72		
Ser2	8.73	4.39	3.76, 3.82	
His3	8.54	4.61	3.15, 3.25	4H 7.26, 2H 8.23
Ala4	8.15	4.22	1.32	
Lys5	8.36	4.20	1.61	CγH 1.35, CδH 1.72, CεH 2.91, NH 7.49
Arg6	8.24	4.19	1.61	CγH 1.52, CδH 3.10, NH 7.11
His7	8.50	4.61	3.09, 3.15	4H 7.21, 2H 8.23
His8	8.58	4.62	3.10, 3.16	4H 7.22, 2H 8.20
Gly9	8.47	3.87		
Tyr10	8.08	4.50	2.92	3,5H 7.11, 2,6H 6.73
Lys11	8.21	4.21	1.62	CγH 1.29, CδH 1.72, CεH 2.91, NH 7.49
Arg12	8.25	4.20	1.64	CγH 1.57, CδH 3.10 NH 7.09
Lys13	8.26	4.22	1.51	CγH 1.23, 1.30, CδH 1.62, CεH 2.75, NH 7.69
Phe14	8.19	4.51	2.79, 2.94	2,6H 7.13, 3,5H 7.24, 4H 7.31
His15	8.67	4.67	3.12, 3.23	4H 7.20, 2H 8.34
Glu16	8.29	4.21	1.88, 1.94	CγH 2.23
Lys17	8.28	4.20	1.62	CγH 1.35, CδH 1.69, CεH 2.91, NH 7.49
His18	8.53	4.60	3.14, 3.19	4H 7.21, 2H 8.23
His19	8.37	4.58	3.07, 3.16	4H 7.15, 2H 8.20
Ser20	8.44	4.37	3.77, 3.87	
His21	8.62	4.67	3.11, 3.20	4H 7.22, 2H 8.23
Arg22	8.42	4.26	1.69, 1.73	CγH 1.53, CδH 2.85, NH 7.11
Gly23	8.42	3.86		
Tyr24	8.05	4.53	2.89, 2.94	3,5H 6.73, 2,6H 7.19

an 8 Å nonbonded cutoff to minimize the system. The system was equilibrated for 10 ps in MD simulations with a 9 Å nonbonded cutoff and a 1 fs time step under constant volume and temperature (NVT) conditions at 298 K using the weak coupling algorithm with a 0.5 ps time constant, followed by 140 ps of equilibration under constant temperature and pressure (NTP) conditions at 298 K and 1 bar. MD simulations were subsequently run under constant NTP conditions at 600 K for up to 0.5 ns, then cooled to 298 K at random time steps in order to obtain conformers potentially sampled by a Histatin 5 random coil. Six Histatin 5 conformers were selected for further analysis.

All atom and backbone atom root-mean-square deviations (RMSDs) of the six conformers were measured using the RMSD trajectory tool plugin in VMD. All atom RMSDs between pairs of the six conformers ranged from 3.4 to 9.1 Å, while backbone RMSDs ranged from 2.0 to 8.3 Å.

Receptor files were prepared in OEB format from the six Histatin 5 conformers with the FRED receptor GUI.[58,59] Receptor files were created by extending a box around the volume of each conformer and the inner and outer contours were disabled. FRED was used with the default scoring function, Chemgauss3, to dock the compact and extended rotamers of procyanidin B1, B2, B3, and B4 to each Histatin 5 conformer. The Chemgauss3 score for each ligand is a sum of the following components: steric, desolvation, acceptor, donor, and metal. The steric component accounts for increased van der Waals interactions between the docked ligand and the receptor, and desolvation of hydrogen bond acceptors and donors on the receptor by lipophilic ligand atoms. The desolvation component assesses an energy penalty for interactions between hydrogen bond donors/acceptors on the ligand with solvent waters that are blocked by the receptor. The acceptor component accounts for interactions between hydrogen bond acceptors on the ligand and hydrogen bond donors on the receptor, whereas the donor component accounts for interactions of hydrogen bond donors on the ligand with hydrogen bond acceptors on the receptor. The metal component accounts for interactions between ligand metal coordinating atoms and metals on the receptor, but was not applicable in this instance. The clash scale was set to 0.25, 0.5, or 0.75. A higher clash scale invokes a stricter energy penalty for steric clashes between atoms. A clash scale of 0.75 did not yield docking solutions for every procyanidin rotamer docked with FRED. However, every procyanidin diastereomer bound Histatin 5 in the ESI-MS experiments by Rannulu and Cole. In order to avoid omission of relevant docking solutions due to an overly conservative clash scale, only docking simulations with the clash scale set to 0.25 were subjected to further analysis.

The highest ranked poses of the compact and extended rotamers of procyanidin B1, B2, B3, and B4 docked to the six Histatin 5 conformers with FRED were optimized in liquid-phase and

gas-phase MD simulations with the *sander* module of AMBER 11 using the ff03 force field. The SHAKE algorithm was used to constrain bond lengths involving hydrogens. Partial charges for procyanidin atoms were fit to electrostatic potentials derived from closed-shell restricted Hartree-Fock calculations with the augmented cc-pVTZ basis set using the NWChem software package version 6.1.[67] Additional parameters for the procyanidins were obtained from the gaff[68] parameter set in the antechamber[69] module of AMBER.

Liquid-phase MD optimization of procyanidins docked to Histatin 5 conformers was performed under periodic boundary conditions. Long-range electrostatics were handled with the PME method. Docked structures were neutralized by addition of 5 chloride ions and solvated in boxes of approximately 800 to 1100 TIP3P explicit waters. Each system was minimized with 50 cycles of the steepest descent method followed by 50 cycles of conjugate gradient minimization using a 12 Å nonbonded cutoff. Equilibration was performed for 10 ps with a 12 Å nonbonded cutoff and a 1 fs time step under NVT conditions at 298 K using Langevin dynamics temperature regulation with a collision frequency of 1 ps^{-1}, followed by 160 ps of equilibration under constant NTP conditions at 298K and 1 bar. MD simulations were subsequently run under constant NTP conditions at 298 K for 1 ns. The total energy of a liquid-phase optimized Histatin 5 conformer bound to the compact and extended rotamers of procyanidin B1 remained roughly constant throughout the 1 ns trajectories, indicating simulations of liquid-phase optimized procyanidin-Histatin 5 complexes were stable (Figure 1.5). All-atom and backbone-atom RMSDs of the Histatin 5 conformer bound to the compact and extended rotamers of procyanidin B1 during the last 100 ps of equilibration followed by 1 ns of MD optimization in the liquid phase were assessed with respect to the initial configuration using the AMBER ptraj program. Following equilibration, backbone-atom RMSDs of the Histatin 5 conformer bound to the compact and extended rotamers of procyanidin B1 gradually increased throughout the 1 ns trajectories, while all-atom RMSDs appeared to remain stable (Figure 1.6). Liquid-phase simulations of unbound compact and extended rotamers of procyanidin B1, B2, B3, and B4 were run for 1 ns at 298 K using a similar method. No conformational changes

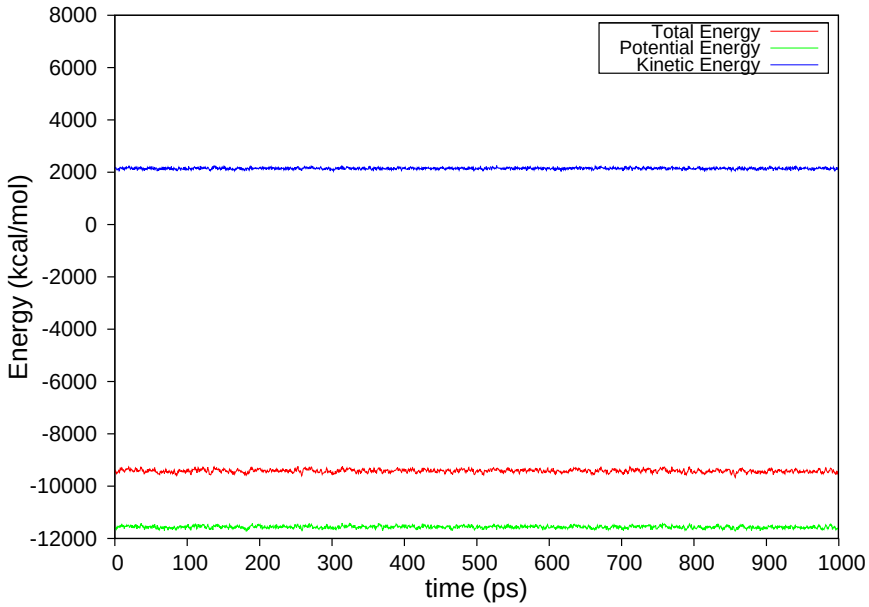

1.5(a) compact rotamer of procyanidin B1 bound to Histatin 5

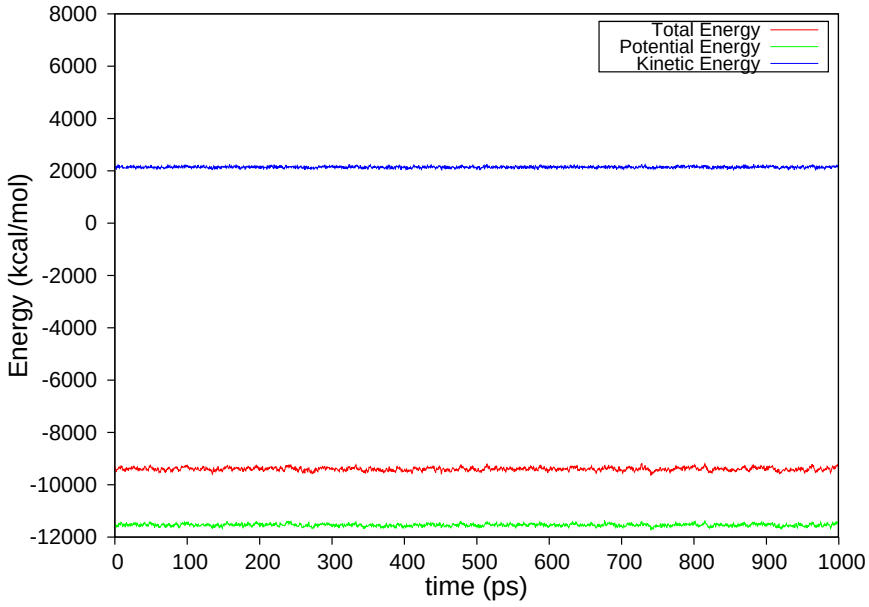

1.5(b) extended rotamer of procyanidin B1 bound to Histatin 5

Figure 1.5. Total, potential, and kinetic energy of the compact and extended rotamers of procyanidin B1 bound to a Histatin 5 conformer during 1 ns of MD simulation in the liquid phase (kcal/mol)

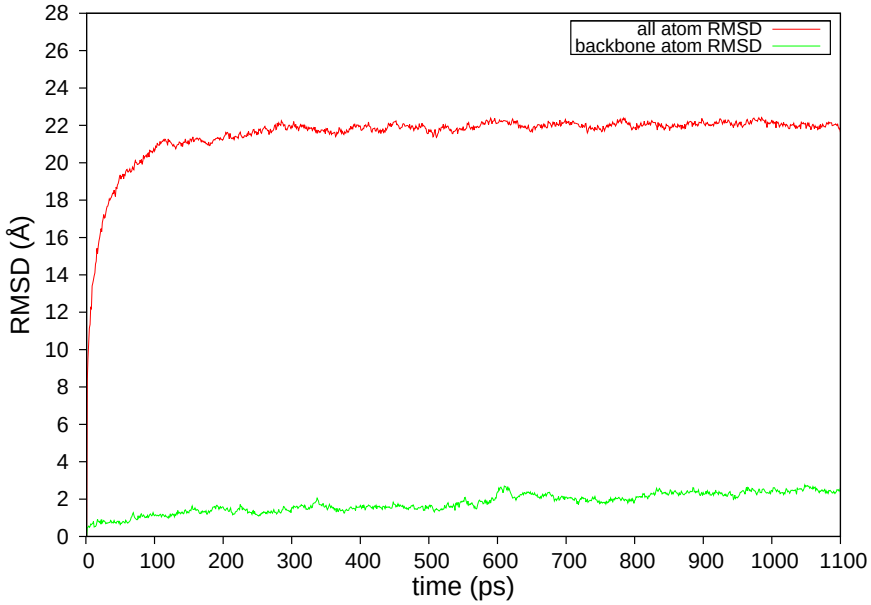

1.6(a) compact rotamer of procyanidin B1 bound to Histatin 5

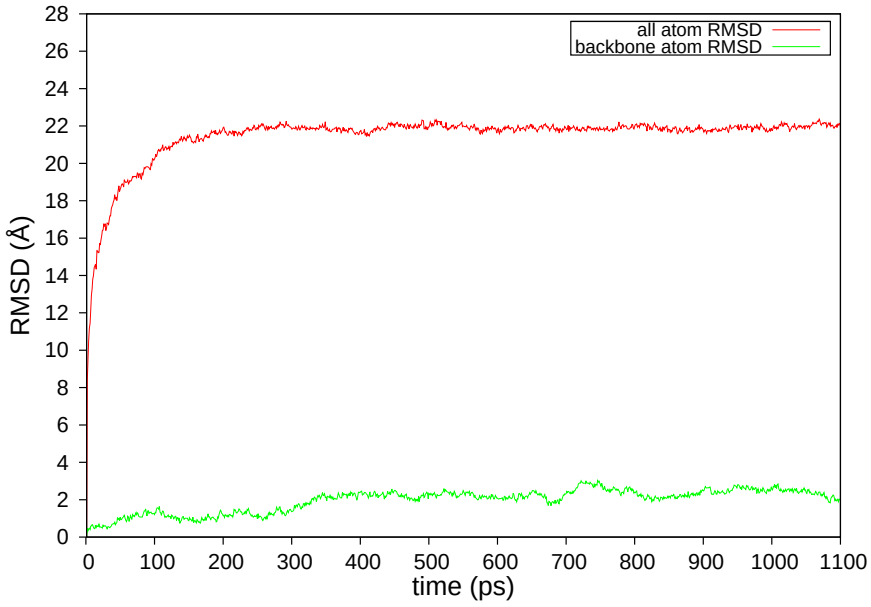

1.6(b) extended rotamer of procyanidin B1 bound to Histatin 5

Figure 1.6. RMSDs of compact and extended rotamers of procyanidin B1 bound to a Histatin 5 conformer during the last 100 ps of equilibration and 1 ns of MD simulation in the liquid phase (Å)

were observed between compact and extended forms in liquid-phase simulations of bound and unbound procyanidins.

The strongest peaks observed for procyanidin-Histatin 5 complexes in the ESI-MS studies by Rannulu and Cole had a 1:1 binding stoichiometry and a net charge of +5. In addition, the charge state distribution of procyanidin-Histatin 5 complexes was the same as for the unbound peptide. Thus, it was assumed Histatin 5 possessed all the charge contained in the complexes, while procyanidins bound as neutral species. Gas-phase MD optimization of procyanidins docked to Histatin 5 conformers was performed *in vacuo* with periodic boundary conditions disabled and the electrostatic interactions calculated directly. Docked structures were not neutralized by addition of ions in order to simulate the +5 net charge of procyanidin-Histatin 5 complexes in the ESI-MS experiments by Rannulu and Cole. Each system was minimized with 50 cycles of the steepest descent method followed by 50 cycles of conjugate gradient minimization using a nonbonded cutoff of 999 Å. The systems were equilibrated for 170 ps with a 999 Å nonbonded cutoff at a constant temperature of 298 K using Langevin dynamics temperature regulation with a collision frequency of 1 ps^{-1}. The temperature was increased from 298 K to 448 K during an additional 100 ps of equilibration as done in previous studies to simulate typical conditions in ESI-MS experiments.[70–74] MD simulations were subsequently run under constant temperature conditions at 448 K for 1 ns. The total energy of a gas-phase optimized Histatin 5 conformer bound to the compact and extended rotamers of procyanidin B1 remained roughly constant, indicating simulations of gas-phase optimized procyanidin-Histatin 5 complexes were stable (Figure 1.7). Following equilibration, significant fluctuations in all-atom and backbone-atom RMSDs of the gas-phase optimized Histatin 5 conformer bound to the compact and extended rotamers of procyanidin B1 were observed most likely due to the high temperature conditions used in the simulations (Figure 1.8). Gas-phase simulations of unbound compact and extended rotamers of procyanidin B1, B2, B3, and B4 were run for 1 ns at 448 K using a similar method. No conformational changes were observed between compact and extended forms in the gas-phase simulations of bound and unbound procyanidins.

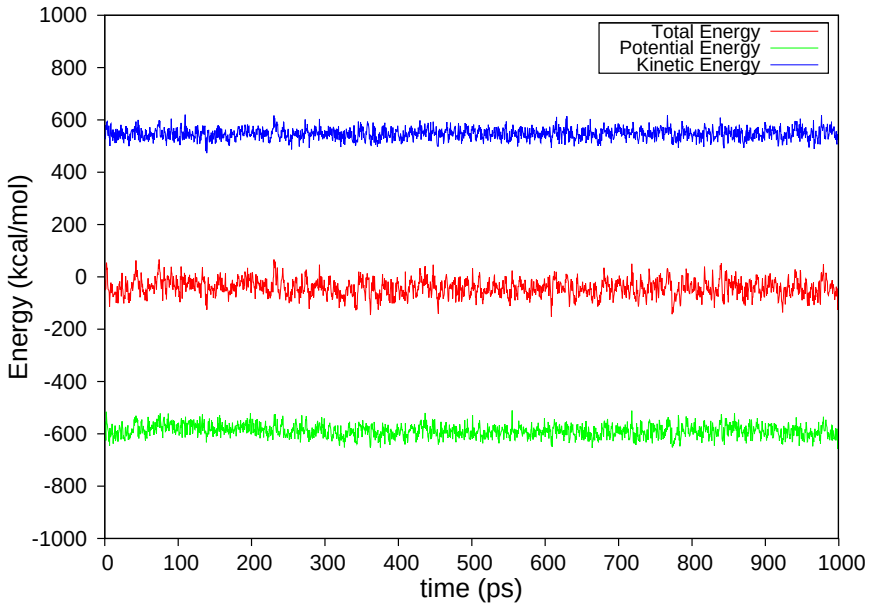

1.7(a) compact rotamer of procyanidin B1 bound to Histatin 5

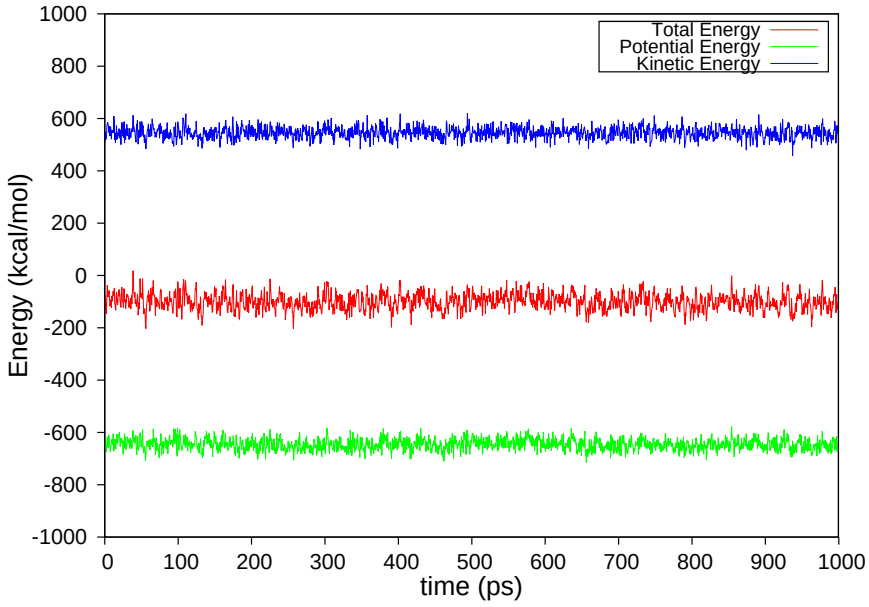

1.7(b) extended rotamer of procyanidin B1 bound to Histatin 5

Figure 1.7. Total, potential, and kinetic energy of the compact and extended rotamers of procyanidin B1 bound to a Histatin 5 conformer during 1 ns of MD simulation in the gas phase (kcal/mol)

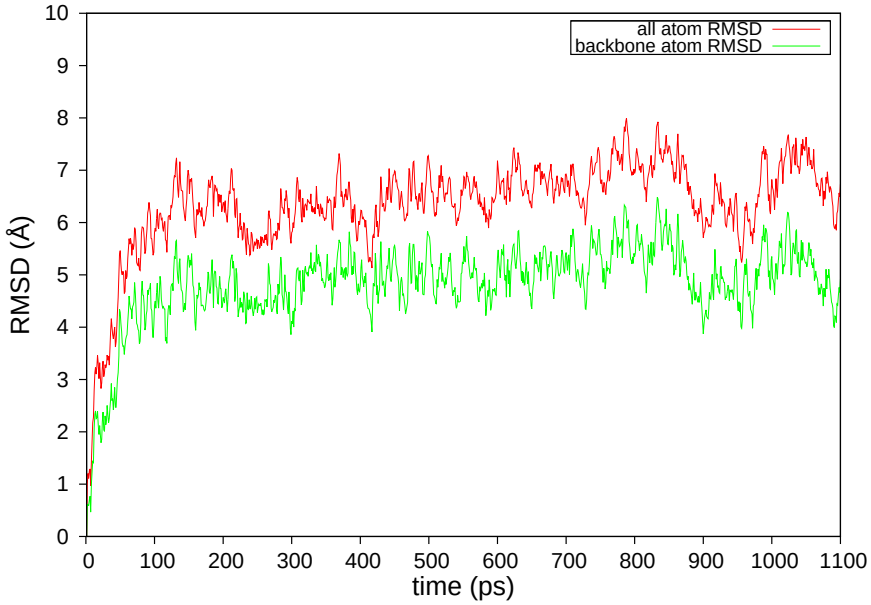

1.8(a) compact rotamer of procyanidin B1 bound to Histatin 5

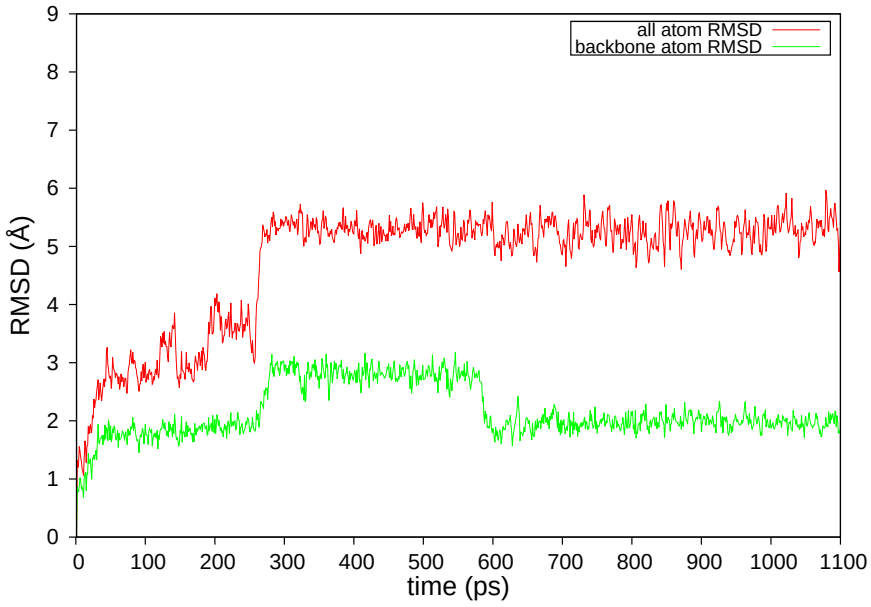

1.8(b) extended rotamer of procyanidin B1 bound to Histatin 5

Figure 1.8. RMSDs of compact and extended rotamers of procyanidin B1 bound to a Histatin 5 conformer during the last 100 ps of equilibration and 1 ns of MD simulation in the gas phase (Å)

Results and Data Analysis

Docked Procyanidin-Histatin 5 Complexes

To compare the docking scores of procyanidin diastereomers with their relative binding affinities derived from ESI-MS, relative binding affinities (relative binding strengths) of the compact and extended rotamers of procyanidin B1, B2, B3, and B4 were calculated by averaging their docking scores for the six Histatin 5 conformers using equation (3), and relative binding affinities of the procyanidin diastereomers were calculated with equation (4). However, the docking score

procyanidin rotamer relative binding affinity =

$$\frac{\text{sum of rotamer docking scores for each Histatin 5 conformer}}{\text{number of Histatin 5 conformers}} \tag{3}$$

procyanidin diastereomer relative binding affinity =

$$\frac{\text{compact + extended rotamer relative binding affinity}}{\text{2 rotamers } \textit{per} \text{ diastereomer}} \tag{4}$$

distributions of each procyanidin diastereomer were too similar to provide sufficient data to rank the calculated relative binding affinities of the procyanidin diastereomers (Figure 1.9 and Table S1).

Interatomic distances of nearest-neighbor atoms of procyanidin rotamers docked to the six Histatin 5 conformers were assessed manually with the PyMOL Measurement Wizard. Various hydrogen bond forming atoms of the procyanidin polyphenol rings exhibited interatomic distances of approximately 3 Å with side chain and backbone hydrogen bonding atoms of Histatin 5 (Figure 1.10). In addition, π-π stacking orientations and interatomic distances approximating the sum

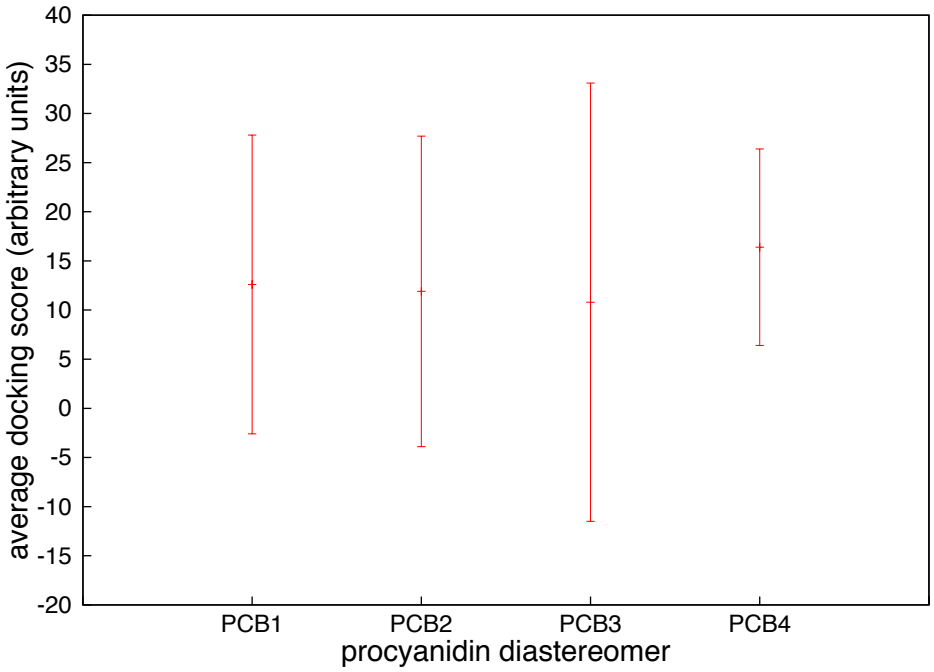

Figure 1.9. Average docking scores of procyanidin B1, B2, B3, and B4 (PCB1, PCB2, PCB3, and PCB4) for six conformers of Histatin 5 +/- 2 standard deviations

of van der Waals radii were observed between procyanidin polyphenol rings and phenylalanine, tyrosine, and histidine rings of Histatin 5 (Figure 1.10(a)).

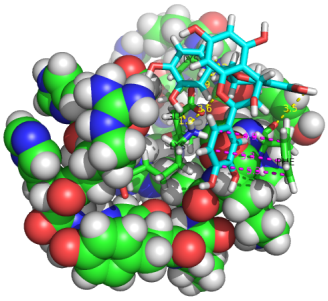

1.10(a) procyanidin B1 compact rotamer docked to Histatin 5

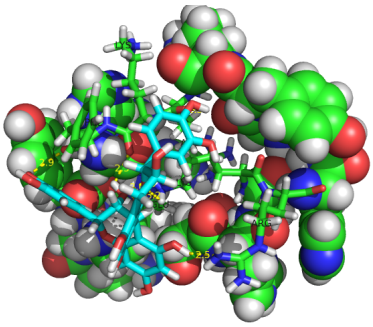

1.10(b) procyanidin B1 extended rotamer docked to Histatin 5

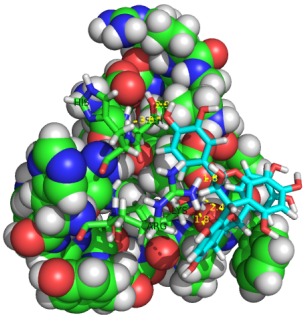

1.10(c) procyanidin B2 compact rotamer docked to Histatin 5

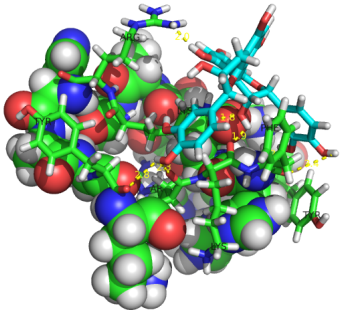

1.10(d) procyanidin B2 extended rotamer docked to Histatin 5

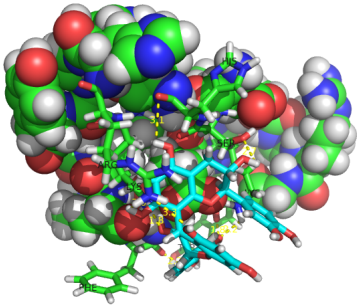

1.10(e) procyanidin B3 compact rotamer docked to Histatin 5

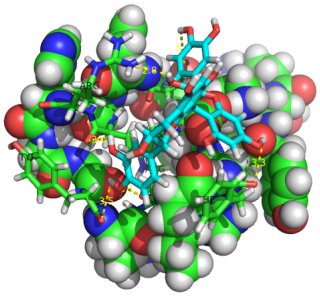

1.10(f) procyanidin B3 extended rotamer docked to Histatin 5

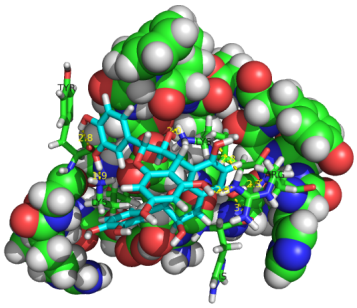

1.10(g) procyanidin B4 compact rotamer docked to Histatin 5

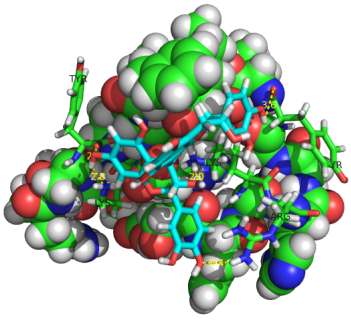

1.10(h) procyanidin B4 extended rotamer docked to Histatin 5

Figure 1.10. Interatomic distances of hydrogen bond forming atoms (dashed yellow lines) and π-π stacking atoms (dashed magenta lines) of compact and extended rotamers of procyanidin B1, B2, B3, and B4 and a Histatin 5 conformer

Optimized Procyanidin-Histatin 5 Complexes

Procyanidin-Histatin 5 Binding Energies

Following liquid and gas-phase optimization of procyanidin diastereomers docked to the six Histatin 5 conformers, procyanidin-Histatin 5 binding energies were calculated using their direct interaction energies (without solvent-mediated interactions such as bridging water molecules) according to equation (5), and averaged over the 1 ns trajectories using an in-house perl script.

procyanidin-Histatin 5 binding energy =

energy of procyanidin-Histatin 5 complex - Histatin 5 self energy - procyanidin self energy (5)

The direct interaction energy of each procyanidin-Histatin 5 complex was used as an approximation to its potential energy of binding (binding energy) and, by extension, binding affinity. To compare the procyanidin-Histatin 5 binding energies of optimized procyanidin diastereomers with the relative binding affinities derived from ESI-MS, relative binding affinities of the compact and extended rotamers of procyanidin B1, B2, B3, and B4 were calculated by averaging their procyanidin-Histatin 5 binding energies for the six Histatin 5 conformers using equation (6), and relative binding affinities of the procyanidin diastereomers were calculated with equation (4).

procyanidin rotamer relative binding affinity =

$$\frac{\text{sum of procyanidin rotamer-Histatin 5 binding energies for each Histatin 5 conformer}}{\text{number of Histatin 5 conformers}} \quad (6)$$

The calculated relative binding affinities of liquid and gas-phase optimized procyanidin B1, B2, B3, and B4 were ranked according to their average procyanidin-Histatin 5 binding

energies: B1 > B4 > B2 > B3 and B2 > B4 > B3 > B1, respectively (Figure 1.11 and Table S3). The calculated relative binding affinities of liquid-phase optimized procyanidin diastereomers were consistent with the relative binding relative binding affinities derived from ESI-MS binding strength quotients, though their average procyanidin-Histatin 5 binding energies were similar to each other (Figure 1.11(a) and Table 1.4). The calculated relative binding affinities of gas-phase optimized procyanidin diastereomers were inconsistent with the relative binding affinities derived from ESI-MS gas-phase dissociation quotients, though again their average procyanidin-Histatin 5 binding energies were similar to one another (Figure 1.11(b) and Table 1.4). In addition, the distributions of procyanidin-Histatin 5 binding energies for the six Histatin 5 conformers were small in both the liquid and gas phase (Figure 1.11).

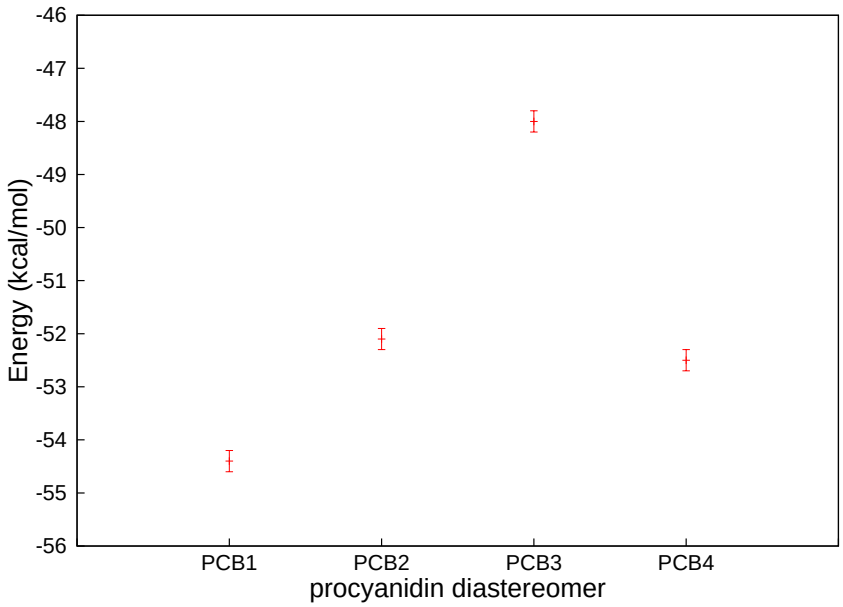

1.11(a) liquid-phase procyanidin-Histatin 5 binding energies

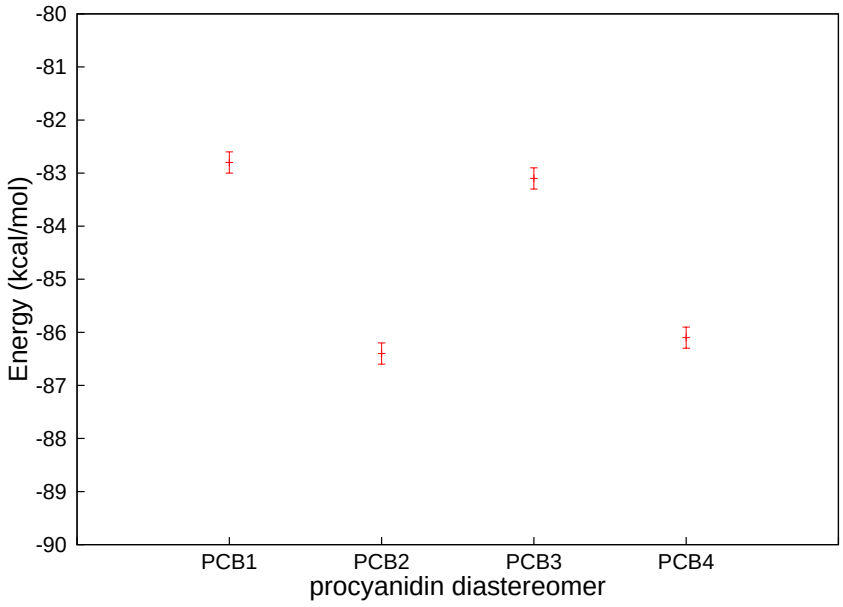

1.11(b) gas-phase procyanidin-Histatin 5 binding energies

Figure 1.11. Average procyanidin-Histatin 5 binding energies of procyanidin B1, B2, B3, and B4 (PCB1, PCB2, PCB3, and PCB4) for six conformers of Histatin 5 during liquid and gas-phase simulations +/- about 2 standard errors (kcal/mol)

Procyanidin Ligand Strain

The self energies of procyanidin ligands bound to Histatin 5 and self energies of unbound procyanidins were averaged over their 1 ns trajectories using an in-house perl script. The self energy can be defined as the sum of intramolecular Lennard-Jones and Coulombic interaction energies as well as bond stretching, bond angle bending, and torsional energy terms. However, only Lennard-Jones and Coulombic interaction energies were used to calculate the self energies of the procyanidin ligands. The self energies of bound compact and extended rotamers of procyanidin B1, B2, B3, and B4 were calculated by averaging their self energies in complex with the six Histatin 5 conformers using equation (7). Strain induced by binding of procyanidin rotamers to Histatin 5 was measured as the difference between the self energies of bound and unbound rotamers using equation (8) and strain energies for the procyanidin diastereomers were calculated with equation (9).

bound procyanidin rotamer self energy =

$$\frac{\text{sum of bound rotamer self energies for each Histatin 5 conformer}}{\text{number of Histatin 5 conformers}} \tag{7}$$

procyanidin rotamer strain energy =

$$\text{bound - unbound rotamer self energy} \tag{8}$$

procyanidin diastereomer strain energy =

$$\frac{\text{compact + extended rotamer strain energy}}{\text{2 rotamers } \textit{per} \text{ diastereomer}} \tag{9}$$

The strain energy would include the loss of hydrogen bonds and other favorable non-bonding intramolecular interactions as well as increases in bond stretching, bond angle bending, and torsional energies, though only Lennard-Jones and Coulombic interactions were included in this instance. The strain energies of liquid-phase optimized procyanidin diastereomers resembled each other (Figure 1.12(a)). Strain energies of gas-phase optimized procyanidin diastereomers were also similar to each other (Figure 1.12(b)). In addition, strain energies of the liquid-phase optimized procyanidin diastereomers were similar to the gas phase (Figure 1.12 and Table S5).

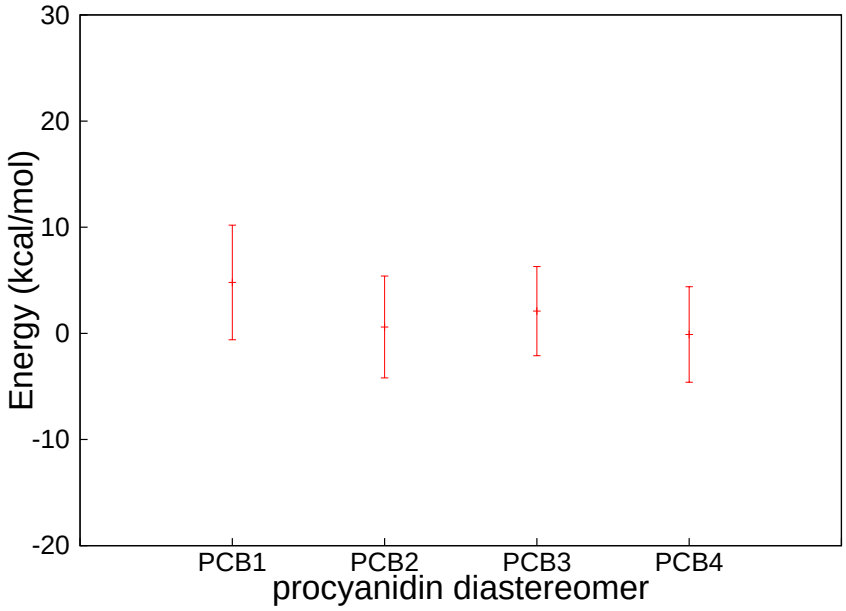

1.12(a) strain energies of liquid-phase procyanidins

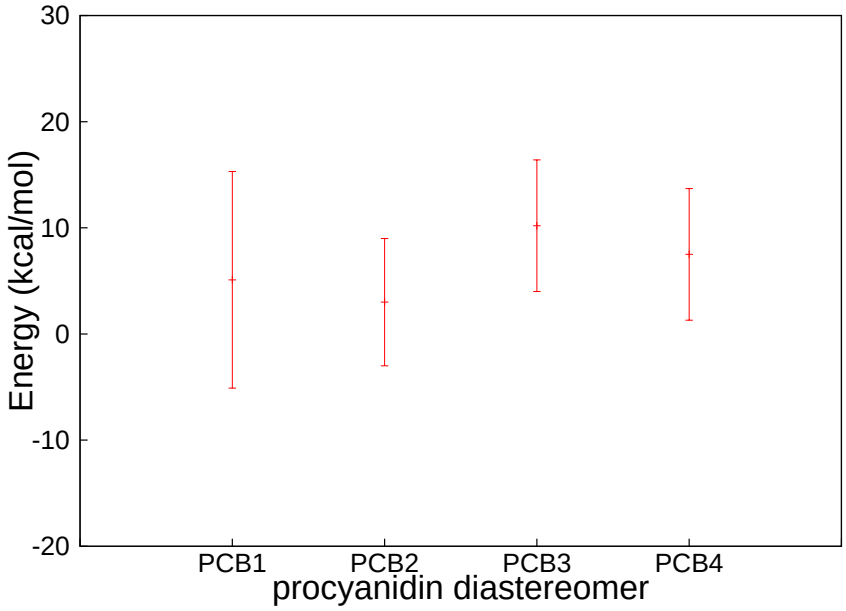

1.12(b) strain energies of gas-phase procyanidins

Figure 1.12. Strain energies of procyanidin B1, B2, B3, and B4 (PCB1, PCB2, PCB3, and PCB4) during liquid and gas-phase simulations +/- about 2 standard errors (kcal/mol)

Compact and Extended Procyanidin Rotamer Energies

The difference between the self energy of the compact and extended rotamer of bound procyanidins was calculated with equation (10), and the difference in the self energy of the compact and extended rotamer of unbound procyanidins was calculated with equation (11). The compact

bound procyanidin rotamer self energy difference =

$$\text{compact - extended bound rotamer self energy} \tag{10}$$

unbound procyanidin rotamer self energy difference =

$$\text{compact - extended unbound rotamer self energy} \tag{11}$$

rotamers of bound and unbound procyanidin B1, B2, and B4 exhibited lower energies than the extended rotamers in both the liquid and gas phase, while the extended rotamer of procyanidin B3 had a somewhat lower energy than the compact rotamer (Figure 1.13 and Table S7). The differences in the self energies of compact and extended rotamers of unbound procyanidins in the liquid phase resembled those in the gas phase (Figure 1.13). Differences in the self energies of bound compact and extended procyanidin rotamers in the liquid phase also resembled those in the gas phase (Figure 1.13). In addition, differences in the self energies of compact and extended rotamers of unbound procyanidins resembled bound procyanidins in both the liquid (Figure 1.13(a)) and gas phase (Figure 1.13(b)).

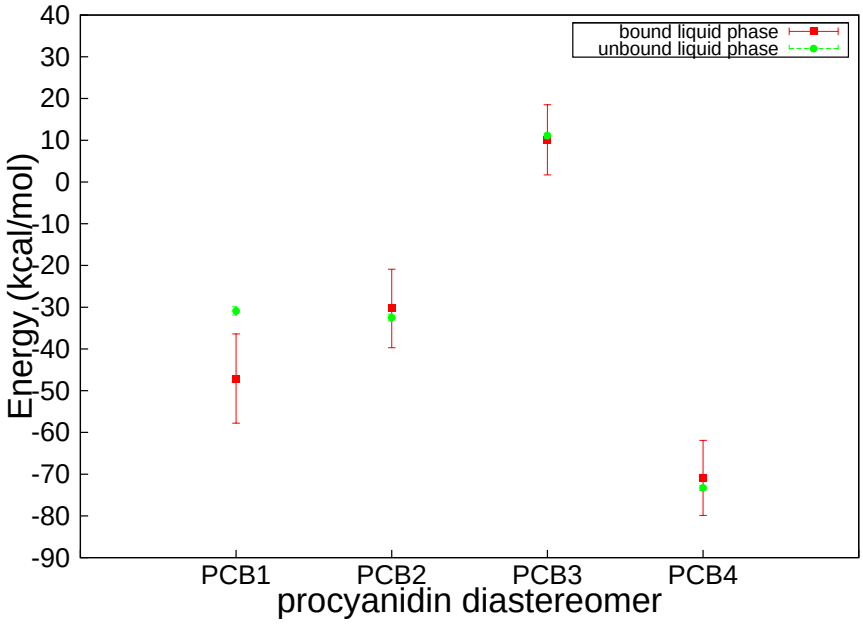

1.13(a) compact - extended rotamer self energies of liquid-phase procyanidins

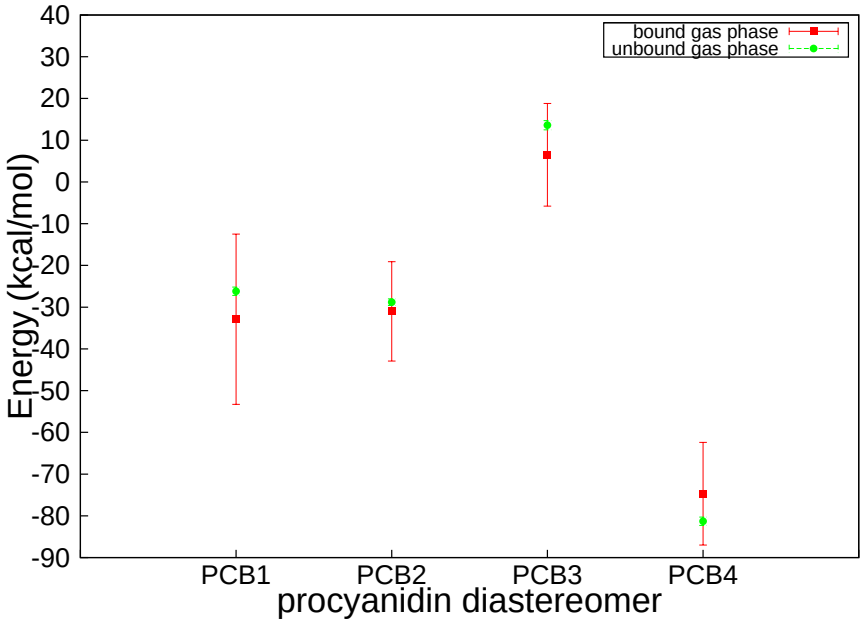

1.13(b) compact - extended rotamer self energies of gas-phase procyanidins

Figure 1.13. Average compact - extended rotamer self energies of procyanidin B1, B2, B3, and B4 (PCB1, PCB2, PCB3, and PCB4) bound to six Histatin 5 conformers and unbound procyanidins during liquid and gas-phase simulations +/- about 2 standard errors (kcal/mol)

Procyanidin-Histatin 5 Binding Modes

To investigate potential binding modes of optimized procyanidin-Histatin 5 complexes, binding energy distributions of the compact and extended rotamers of procyanidin B1, B2, B3 and B4 were calculated for the six Histatin 5 conformers using energies output every 1000 time steps during the one nanosecond trajectories. Probabilities of procyanidin-Histatin 5 binding energies in each trajectory were plotted in histograms containing twenty bins ranging from the minimum to maximum binding energy of the trajectory. The binding energy distributions of almost all gas-phase procyanidin rotamers exhibited a single maxima for each of the six Histatin 5 conformers (Figure 1.14). The binding energy distributions of most liquid-phase rotamers also exhibited a single maxima for each Histatin 5 conformer, though several liquid-phase rotamers displayed two maxima for some conformers (Figure 1.15). Structures of the procyanidin-Histatin 5 complexes corresponding to the energy distribution maxima were inspected visually to determine the binding characteristics of potential procyanidin-Histatin 5 binding modes. Procyanidin B1, B2, B3, and B4 bound multiple sites on the six Histatin 5 conformers in multiple ligand conformations in both the gas and liquid phase (Figures 1.16 and 1.17, respectively). Gas-phase binding modes mostly exhibited structural characteristics representative of hydrogen bonding interactions, i.e. interatomic distances of around 3 Å between hydrogen bond forming atoms of procyanidins and side chain and backbone hydrogen bonding atoms of Histatin 5 (Figure 1.16). However, gas-phase binding modes also exhibited π-π stacking orientations and interatomic distances approximating the sum of van der Waals radii between procyanidin polyphenol rings and phenylalanine, tyrosine, and histidine rings of Histatin 5 (Figure 1.16). The majority of liquid-phase binding modes exhibited hydrogen bonding and π-π stacking characteristics (Figure 1.17).

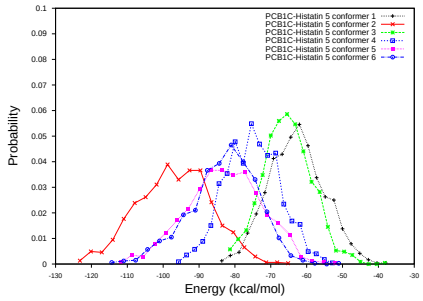

1.14(a) procyanidin B1 compact rotamer

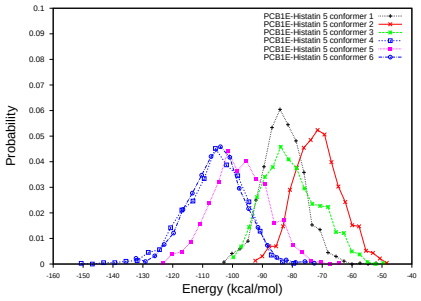

1.14(b) procyanidin B1 extended rotamer

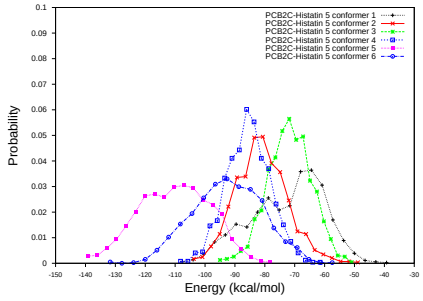

1.14(c) procyanidin B2 compact rotamer

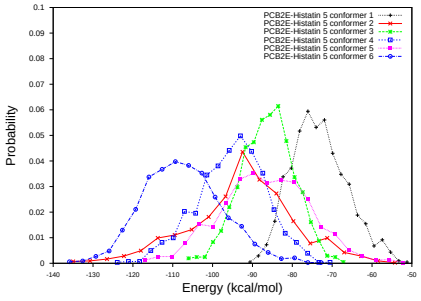

1.14(d) procyanidin B2 extended rotamer

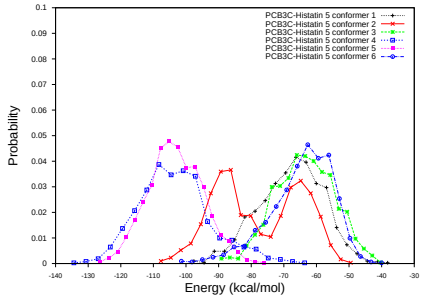

1.14(e) procyanidin B3 compact rotamer

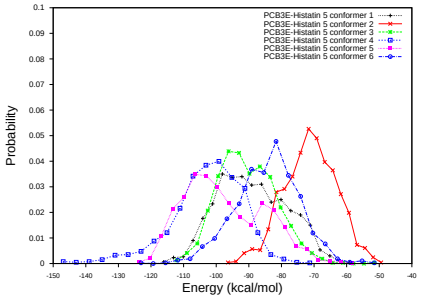

1.14(f) procyanidin B3 extended rotamer

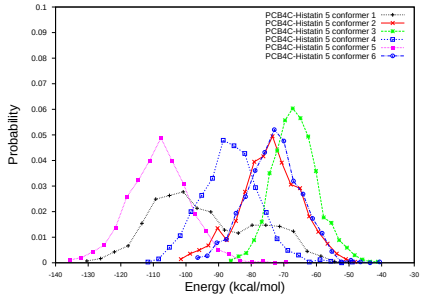

1.14(g) procyanidin B4 compact rotamer

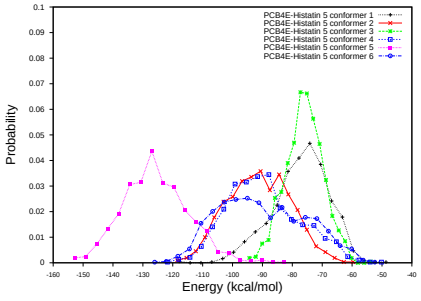

1.14(h) procyanidin B4 extended rotamer

Figure 1.14. Binding energy distributions of gas-phase procyanidins and Histatin 5 (kcal/mol)

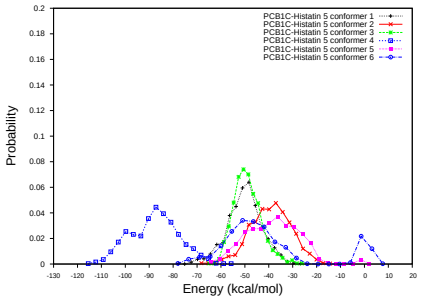

1.15(a) procyanidin B1 compact rotamer

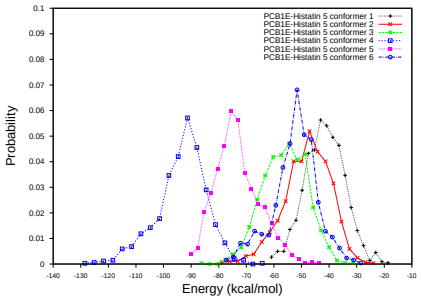

1.15(b) procyanidin B1 extended rotamer

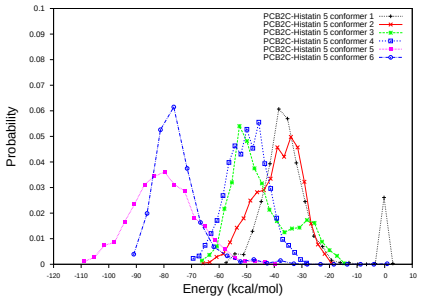

1.15(c) procyanidin B2 compact rotamer

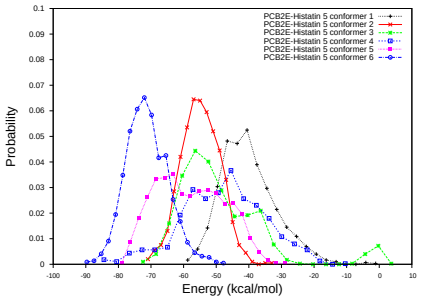

1.15(d) procyanidin B2 extended rotamer

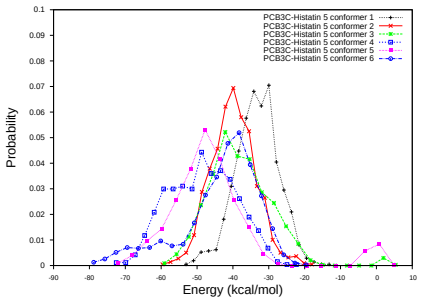

1.15(e) procyanidin B3 compact rotamer

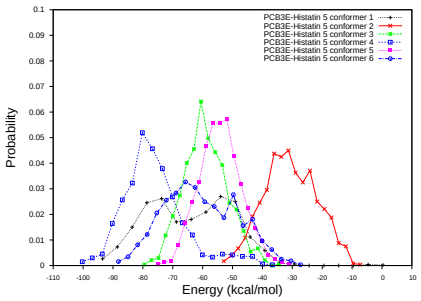

1.15(f) procyanidin B3 extended rotamer

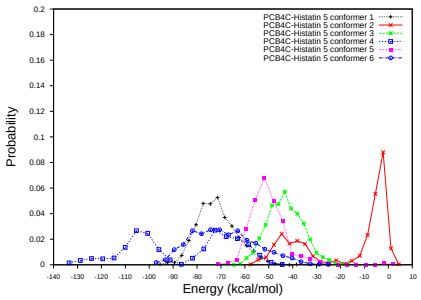

1.15(g) procyanidin B4 compact rotamer

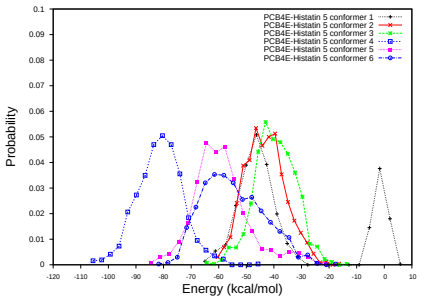

1.15(h) procyanidin B4 extended rotamer

Figure 1.15. Binding energy distributions of liquid-phase procyanidins and Histatin 5 (kcal/mol)

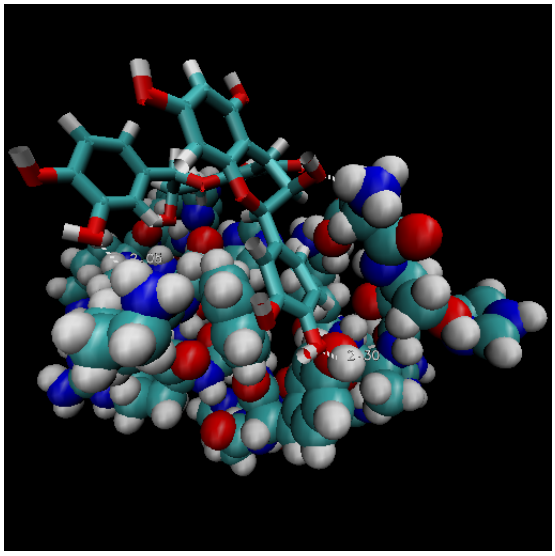

1.16(a) a potential binding mode of the procyanidin B2 compact rotamer and Histatin 5

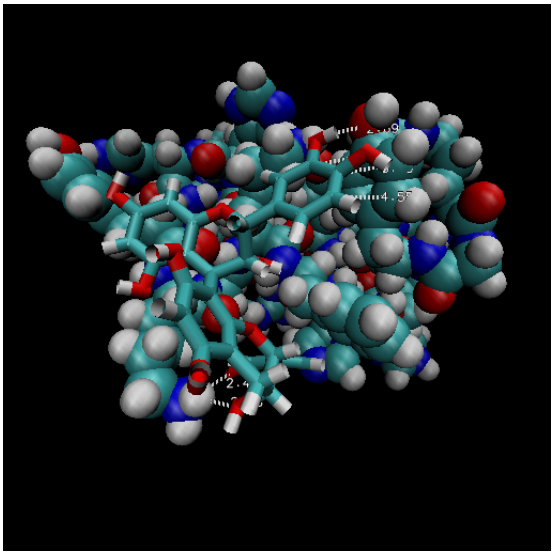

1.16(b) a potential binding mode of the procyanidin B2 extended rotamer and Histatin 5

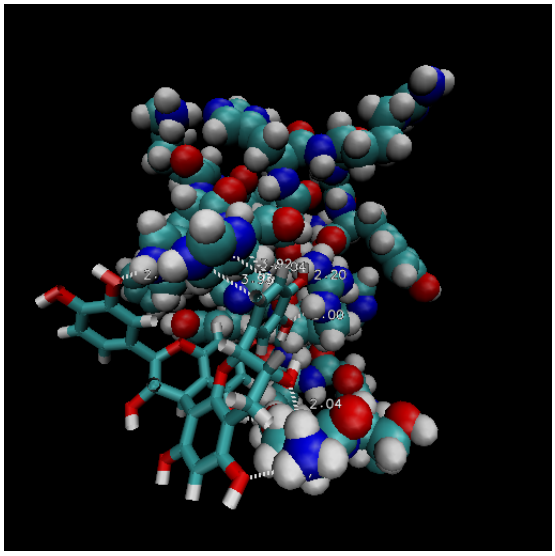

1.16(c) a potential binding mode of the procyanidin B4 compact rotamer and Histatin 5

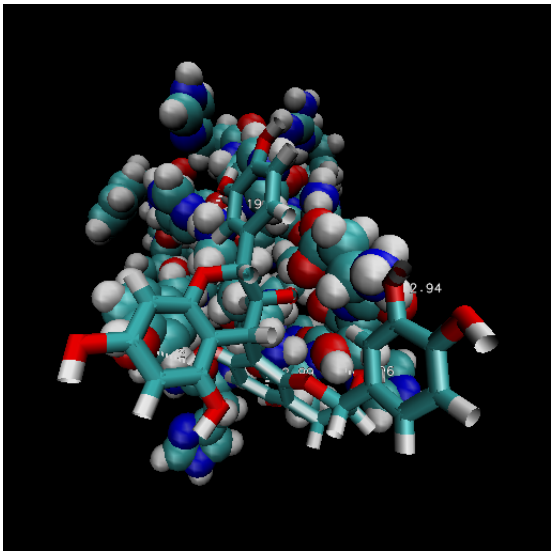

1.16(d) a potential binding mode of the procyanidin B4 extended rotamer and Histatin 5

Figure 1.16. Potential binding modes of gas-phase optimized procyanidin rotamers and a conformer of Histatin 5

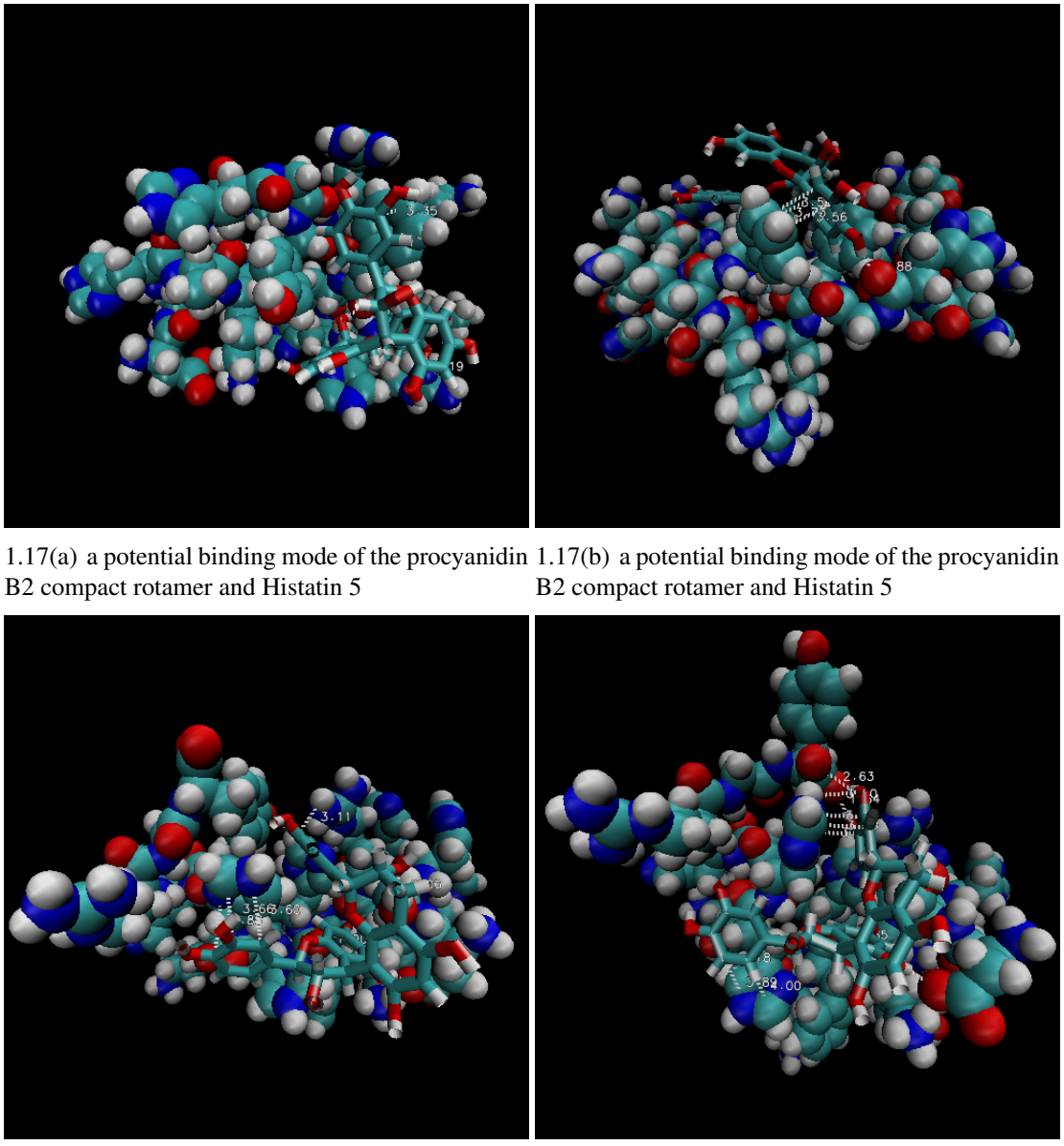

1.17(a) a potential binding mode of the procyanidin B2 compact rotamer and Histatin 5

1.17(b) a potential binding mode of the procyanidin B2 compact rotamer and Histatin 5

1.17(c) a potential binding mode of the procyanidin B4 compact rotamer and Histatin 5

1.17(d) a potential binding mode of the procyanidin B4 compact rotamer and Histatin 5

Figure 1.17. Potential binding modes of liquid-phase optimized procyanidin rotamers and a conformer of Histatin 5

Procyanidin-Histatin 5 Intermolecular Interactions

The percentage of nearest-neighbor atom contacts within a distance of 4 Å between procyanidin diastereomers and each residue of Histatin 5 was calculated by averaging the number of contacts over the 1 ns trajectories using an in-house tcl script in VMD. To compare the percentage of nearest-neighbor contacts in liquid versus gas-phase optimized procyanidin-Histatin 5 complexes, the average percentage of contacts of each rotamer of procyanidin B1, B2, B3, and B4 for the six Histatin 5 conformers was calculated with equation (12), and the average percentage of contacts of each procyanidin diastereomer was calculated with equation (13). More nearest-neighbor contacts were observed in gas

average percentage of procyanidin rotamer contacts =

$$\frac{\text{sum of percentage of rotamer contacts for each Histatin 5 conformer}}{\text{number of Histatin 5 conformers}} \tag{12}$$

average percentage of procyanidin diastereomer contacts =

$$\frac{\text{compact + extended average percentage of rotamer contacts}}{\text{2 rotamers } \textit{per} \text{ diastereomer}} \tag{13}$$

versus liquid-phase optimized procyanidin-Histatin 5 complexes, though the relative number of contacts in the gas phase was similar to that in the liquid phase (Figures 1.18-1.21).

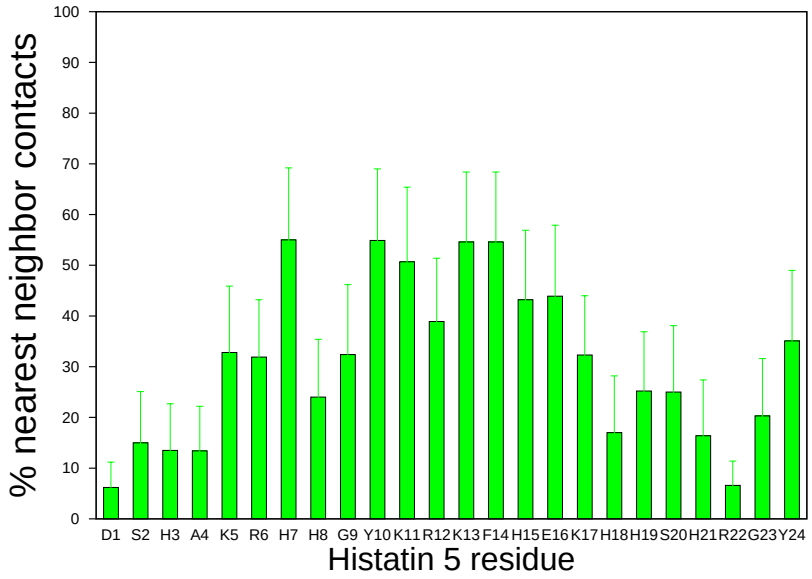

1.18(a) percentage of contacts between liquid-phase optimized procyanidin B1 and Histatin 5

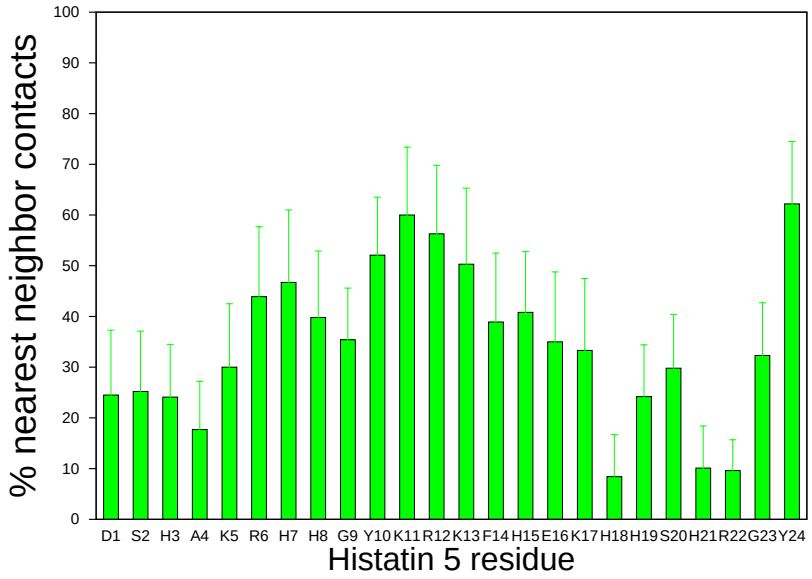

1.18(b) percentage of contacts between gas-phase optimized procyanidin B1 and Histatin 5

Figure 1.18. Average percentage of nearest-neighbor atom contacts less than 4 Å between procyanidin B1 and six conformers of Histatin 5 during liquid and gas-phase simulations with standard errors

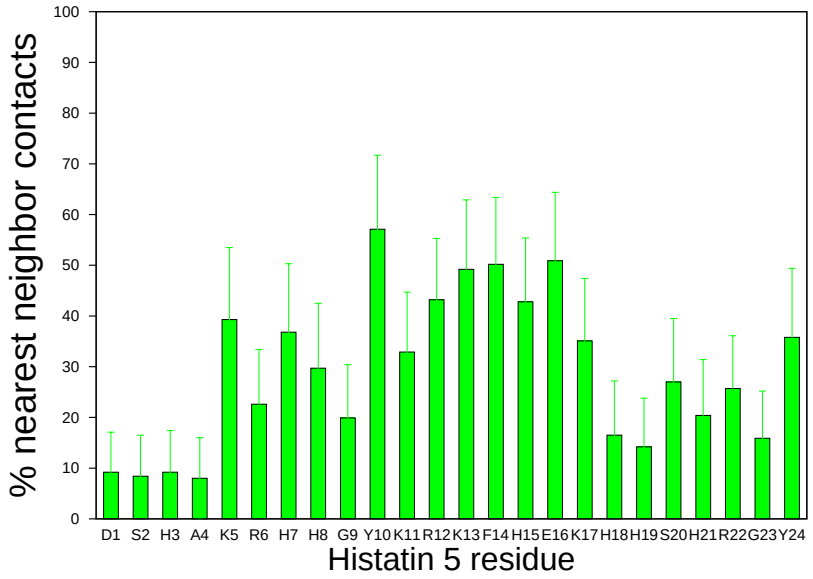

1.19(a) percentage of contacts between liquid-phase optimized procyanidin B2 and Histatin 5

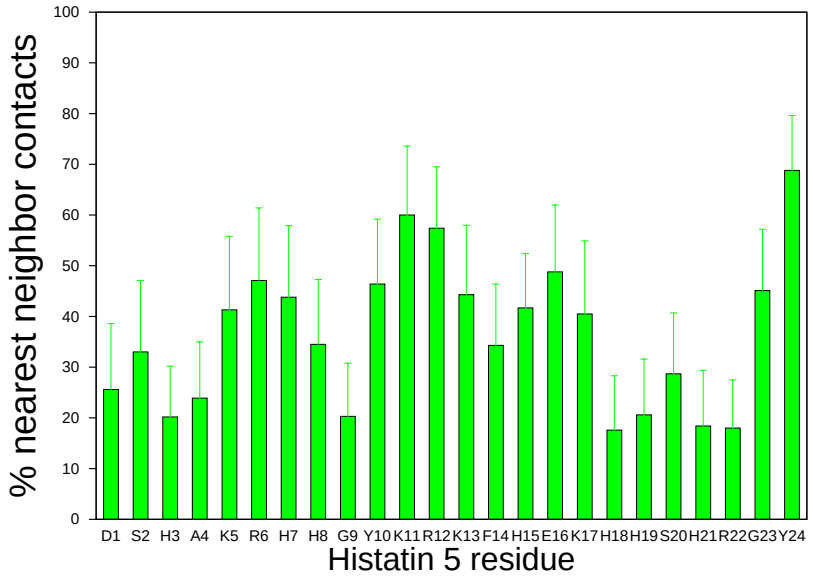

1.19(b) percentage of contacts between gas-phase optimized procyanidin B2 and Histatin 5

Figure 1.19. Average percentage of nearest-neighbor atom contacts less than 4 Å between procyanidin B2 and six conformers of Histatin 5 during liquid and gas-phase simulations with standard errors

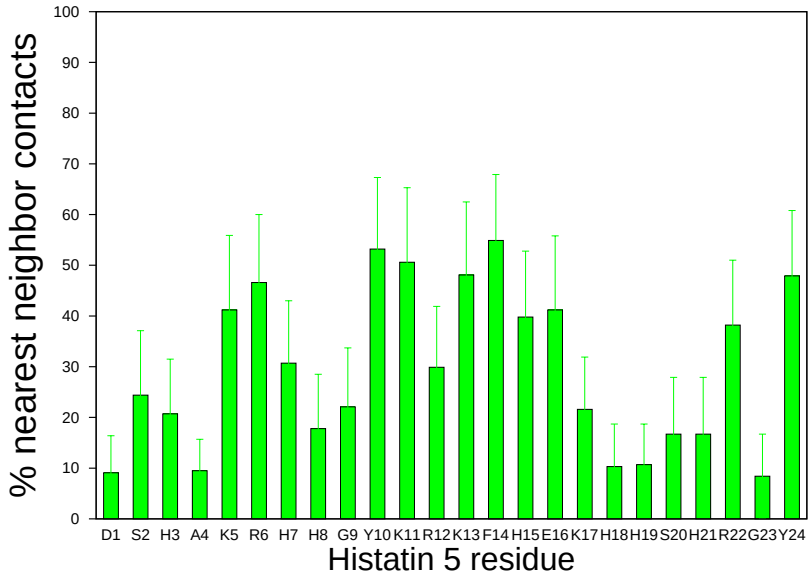

1.20(a) percentage of contacts between liquid-phase optimized procyanidin B3 and Histatin 5

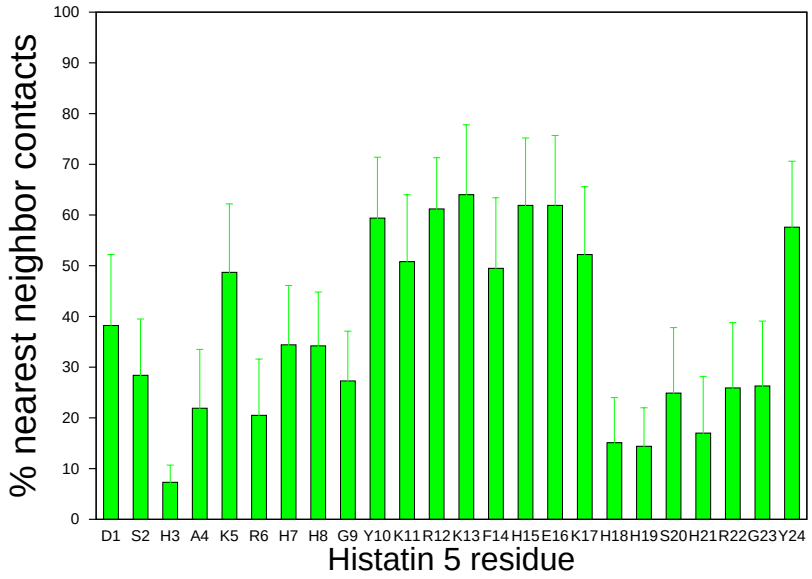

1.20(b) percentage of contacts between gas-phase optimized procyanidin B3 and Histatin 5

Figure 1.20. Average percentage of nearest-neighbor atom contacts less than 4 Å between procyanidin B3 and six conformers of Histatin 5 during liquid and gas-phase simulations with standard errors

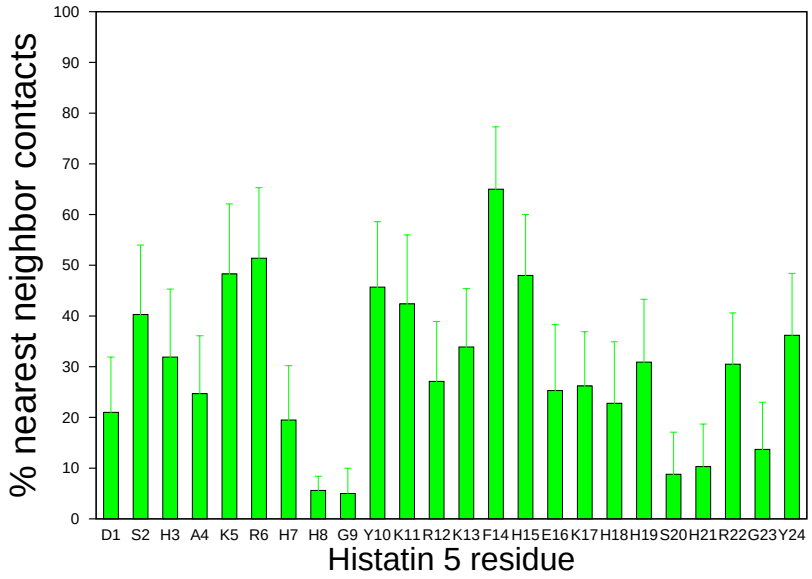

1.21(a) percentage of contacts between liquid-phase optimized procyanidin B4 and Histatin 5

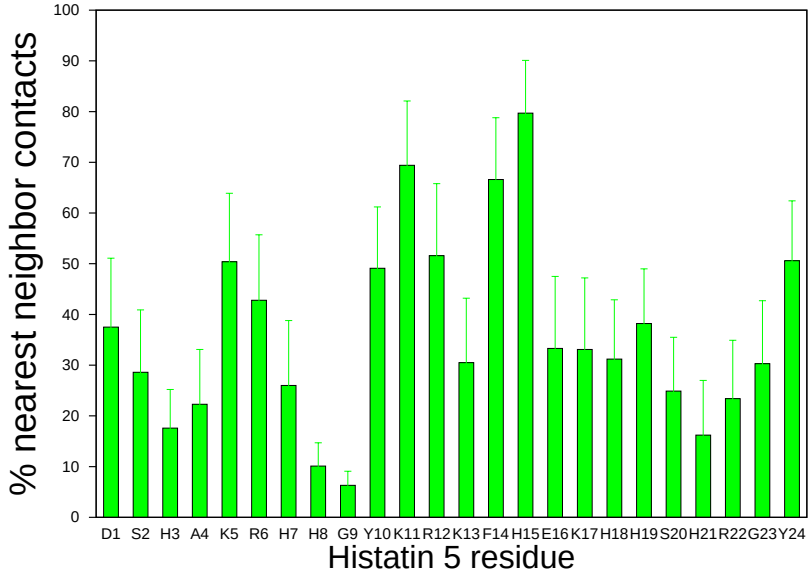

1.21(b) percentage of contacts between gas-phase optimized procyanidin B4 and Histatin 5

Figure 1.21. Average percentage of nearest-neighbor atom contacts less than 4 Å between procyanidin B4 and six conformers of Histatin 5 during liquid and gas-phase simulations with standard errors

The average percentage of nearest-neighbor contacts for all four procyanidin diastereomers (procyanidin B1, B2, B3, and B4) was calculated as well using equation (14). More contacts

average percentage of contacts for the four procyanidin diastereomers =

$$\frac{\text{sum of average percentage of contacts for each diastereomer}}{\text{number of Histatin 5 diastereomers}} \tag{14}$$

were observed in the gas versus liquid-phase optimized procyanidin-Histatin 5 complexes, though the relative number of contacts in the gas phase was similar to that in the liquid phase (Figure 1.22). In addition, the relative number of contacts of the procyanidin-Histatin 5 complexes resembled average changes in the proton chemical shifts of Histatin 5 residues upon titration with EGCG as determined in 2D NMR studies by Bennick et al (Figures 1.18-1.23).[31]

The percentage of intermolecular π-π stacking interactions in procyanidin-Histatin 5 complexes was assessed by averaging the number of intermolecular carbon-carbon or carbon-nitrogen contacts less than 4.0 Å between procyanidin polyphenol rings and aromatic side chain atoms of Histatin 5 over the 1 ns trajectories using an in-house tcl script in VMD, and by visual inspection for π-π stacking orientations between the procyanidin polyphenol rings and aromatic side chains of Histatin 5. The criteria for π-π stacking between procyanidins and Histatin 5 were: intermolecular carbon-carbon or carbon-nitrogen contacts less than 4.0 Å and parallel stacked orientations between procyanidin polyphenol rings and the aromatic side chains of phenylalanine, tyrosine, or histidine. In addition, carbon-carbon and carbon-nitrogen bond distances between procyanidin polyphenol rings and aromatic side chains of Histatin 5 were measured with VMD. To compare

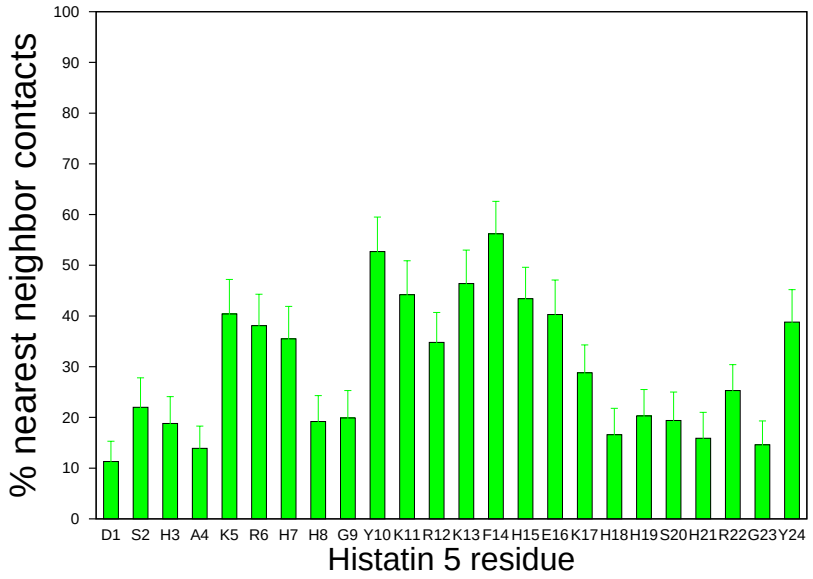

1.22(a) percentage of contacts between four procyanidin diastereomers and Histatin 5 during liquid-phase optimization

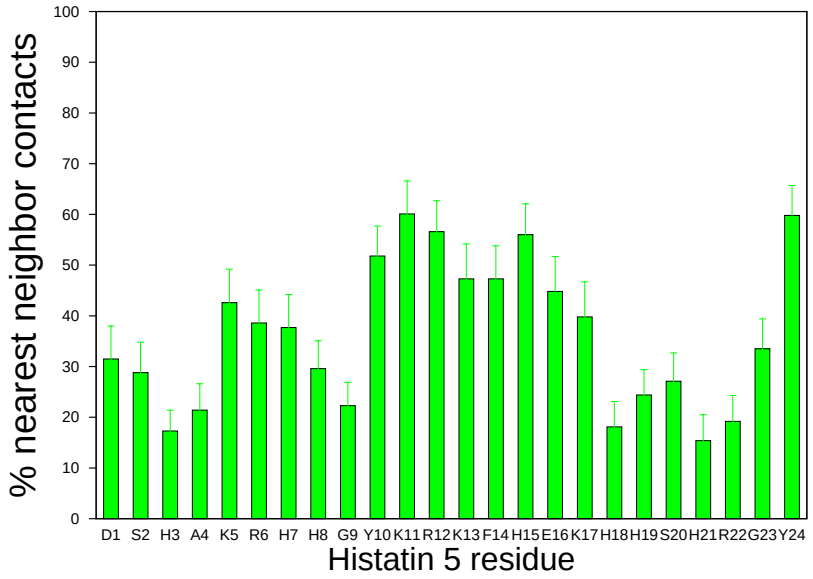

1.22(b) percentage of contacts between four procyanidin diastereomers and Histatin 5 during gas-phase optimization

Figure 1.22. Average percentage of nearest-neighbor atom contacts less than 4 Å between four procyanidin diastereomers (procyanidin B1, B2, B3, and B4) and six conformers of Histatin 5 during liquid and gas-phase simulations with standard errors

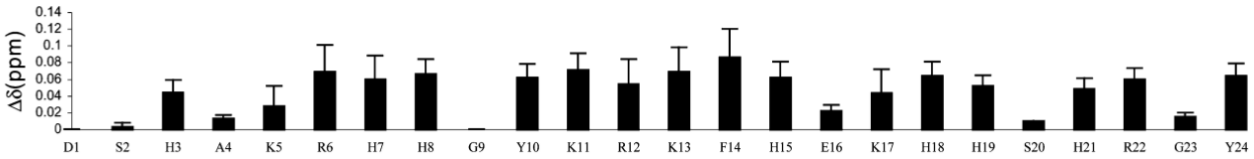

Figure 1.23. Average changes in ^{1}H NMR chemical shifts of Histatin 5 residues upon titration with EGCG with standard deviations (Data are from "K. Wroblewski and R. Muhandiram and A. Chakrabartty and A. Bennick. The Molecular Interaction of Human Salivary Histatins with Polyphenolic Compounds. *Eur. J. Biochem.*, *268*: 4384–4397, **2001**, Table 4")

π-π stacking in liquid versus gas-phase optimized procyanidin-Histatin 5 complexes, the average percentage of π-π stacking of each rotamer of procyanidin B1, B2, B3, and B4 for the six Histatin 5 conformers was calculated using equation (15), and the average percentage of π-π stacking of each procyanidin diastereomer was calculated with equation (16).

average percentage of procyanidin rotamer π-π stacking =

$$\frac{\text{sum of the percentage of rotamer } \pi\text{-}\pi \text{ stacking for each Histatin 5 conformer}}{\text{number of Histatin 5 conformers}} \qquad (15)$$

average percentage of procyanidin diastereomer π-π stacking =

$$\frac{\text{compact + extended average percentage of rotamer } \pi\text{-}\pi \text{ stacking}}{\text{2 rotamers } \textit{per} \text{ diastereomer}} \qquad (16)$$

The average percentage of carbon-carbon and carbon-nitrogen contacts was greater in liquid versus gas-phase optimized procyanidin-Histatin 5 complexes, though the relative number of carbon-carbon and carbon-nitrogen contacts in the gas phase was similar to that in the liquid phase (Figures 1.24-1.27). In addition, both liquid and gas-phase optimized procyanidin-Histatin 5 complexes exhibited parallel stacked orientations between procyanidin polyphenol rings and

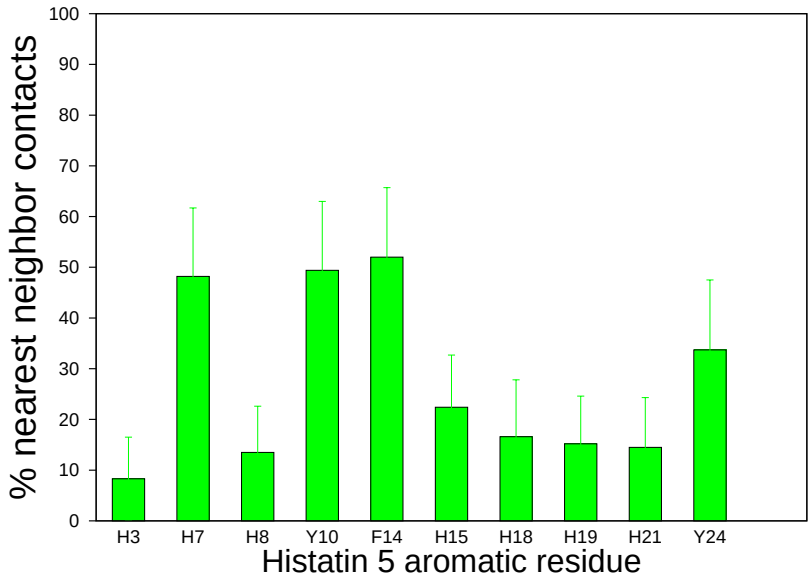

1.24(a) percentage of contacts between liquid-phase optimized procyanidin B1 and Histatin 5

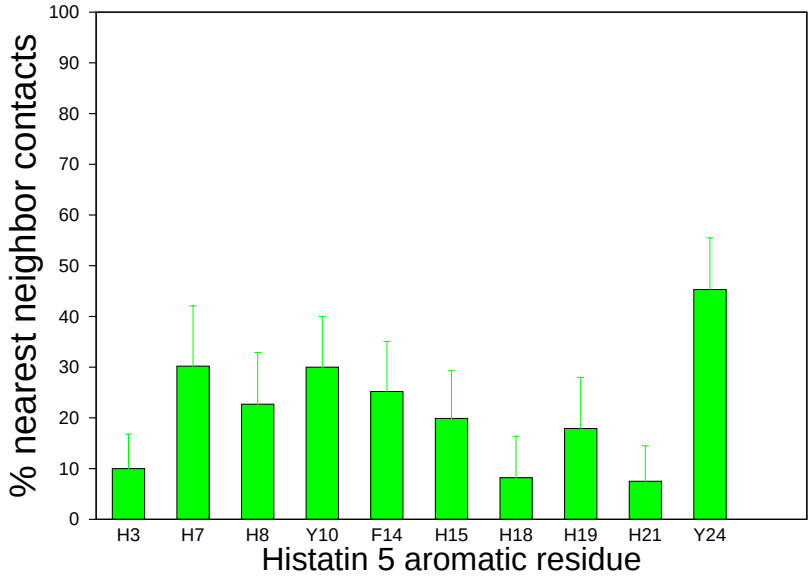

1.24(b) percentage of contacts between gas-phase optimized procyanidin B1 and Histatin 5

Figure 1.24. Average percentage of carbon-carbon and carbon-nitrogen contacts less than 4 Å between procyanidin B1 and six conformers of Histatin 5 during liquid and gas-phase simulations with standard errors

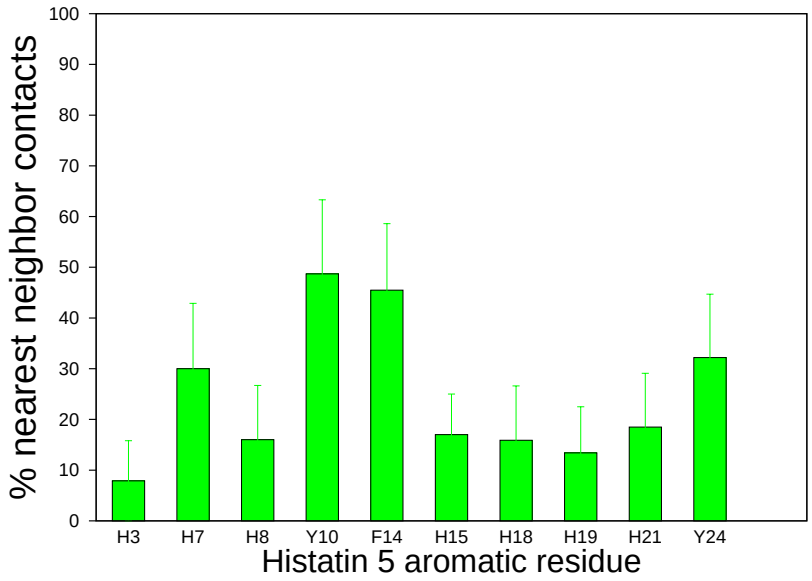

1.25(a) percentage of contacts between liquid-phase optimized procyanidin B2 and Histatin 5

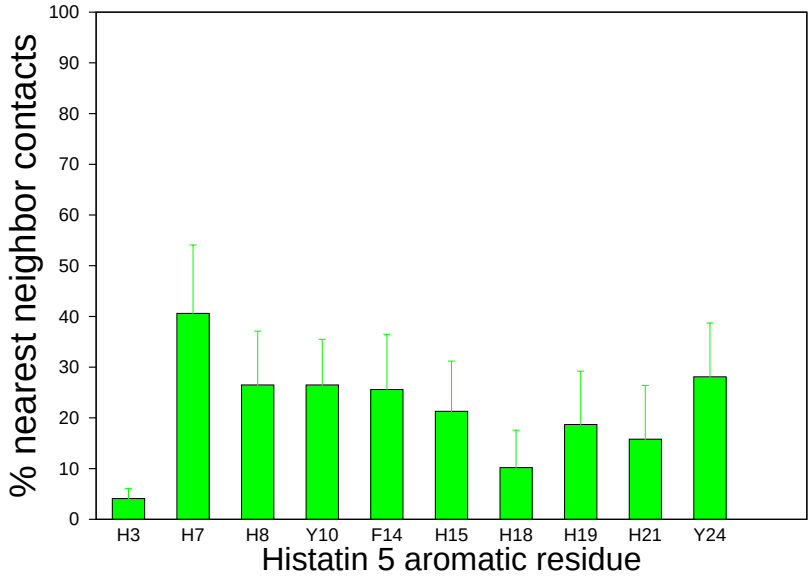

1.25(b) percentage of contacts between gas-phase optimized procyanidin B2 and Histatin 5

Figure 1.25. Average percentage of carbon-carbon and carbon-nitrogen contacts less than 4 Å between procyanidin B2 and six conformers of Histatin 5 during liquid and gas-phase simulations with standard errors

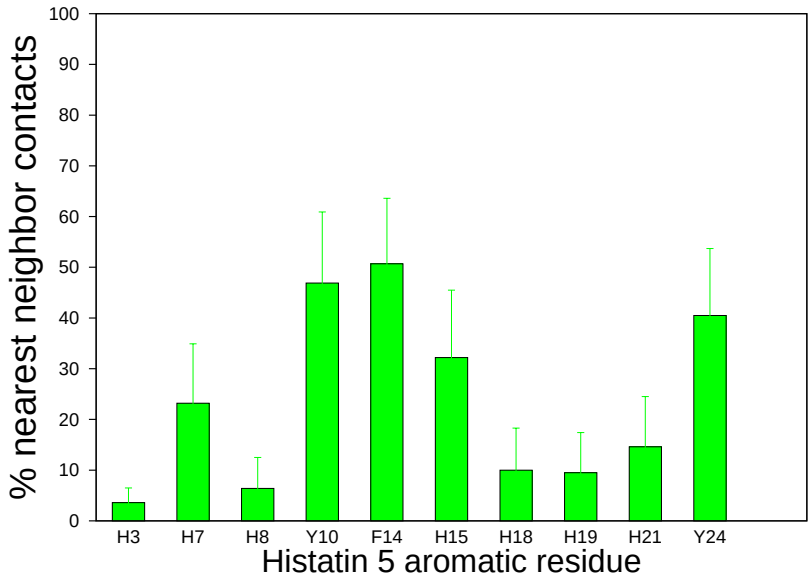

1.26(a) percentage of contacts between liquid-phase optimized procyanidin B3 and Histatin 5

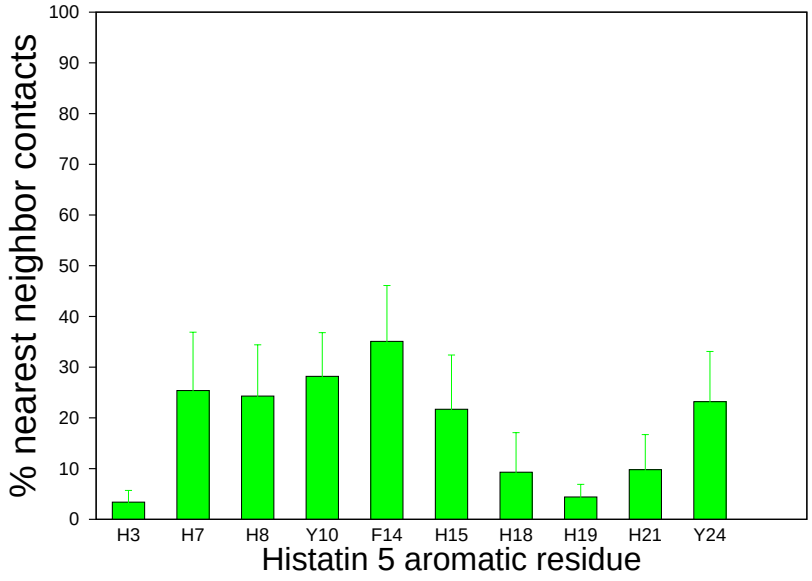

1.26(b) percentage of contacts between gas-phase optimized procyanidin B3 and Histatin 5

Figure 1.26. Average percentage of carbon-carbon and carbon-nitrogen contacts less than 4 Å between procyanidin B3 and six conformers of Histatin 5 during liquid and gas-phase simulations with standard errors

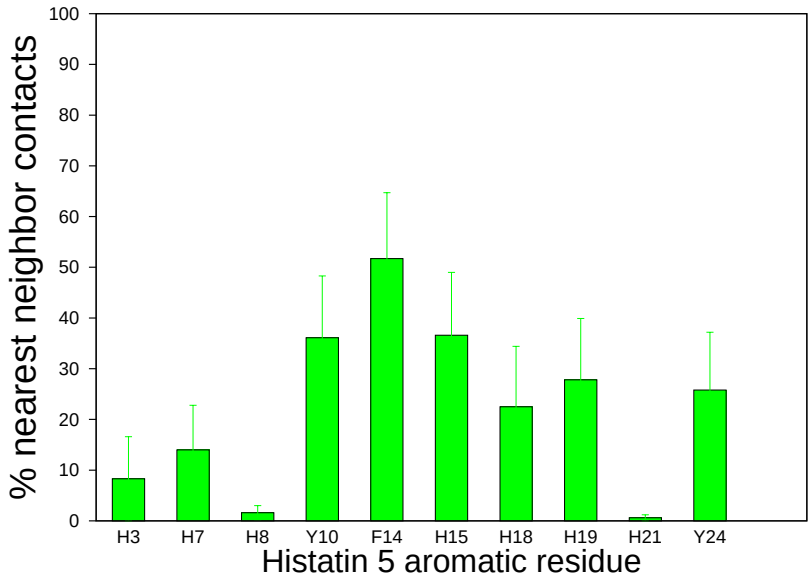

1.27(a) percentage of contacts between liquid-phase optimized procyanidin B4 and Histatin 5

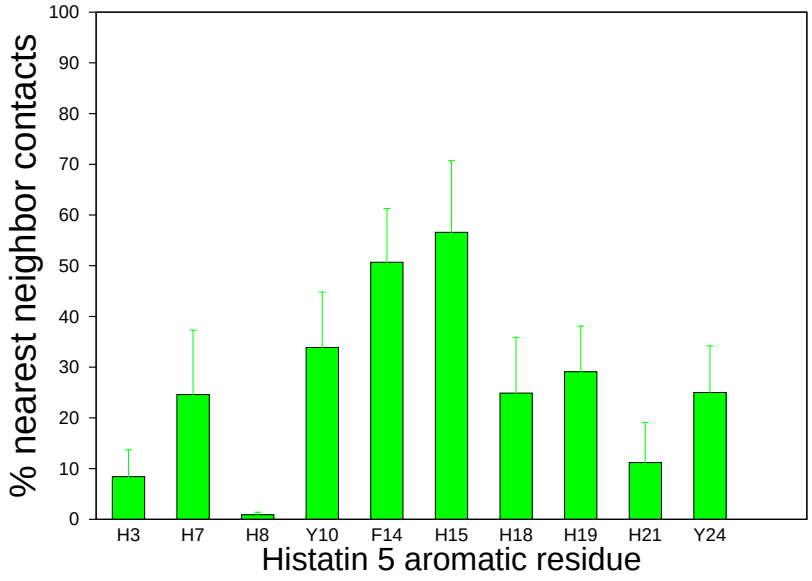

1.27(b) percentage of contacts between gas-phase optimized procyanidin B4 and Histatin 5

Figure 1.27. Average percentage of carbon-carbon and carbon-nitrogen contacts less than 4 Å between procyanidin B4 and six conformers of Histatin 5 during liquid and gas-phase simulations with standard errors

aromatic side chains of phenylalanine, tyrosine, and histidine (Figure 1.28). The average percentage of carbon-carbon and carbon-nitrogen contacts for all four procyanidin diastereomers (procyanidin B1, B2, B3, and B4) was calculated as well using equation (17). More carbon-carbon

average percentage of π-π stacking for the four procyanidin diastereomers =

$$\frac{\text{sum of average percentage of } \pi\text{-}\pi \text{ stacking for each diastereomer}}{\text{number of Histatin 5 diastereomers}} \tag{17}$$

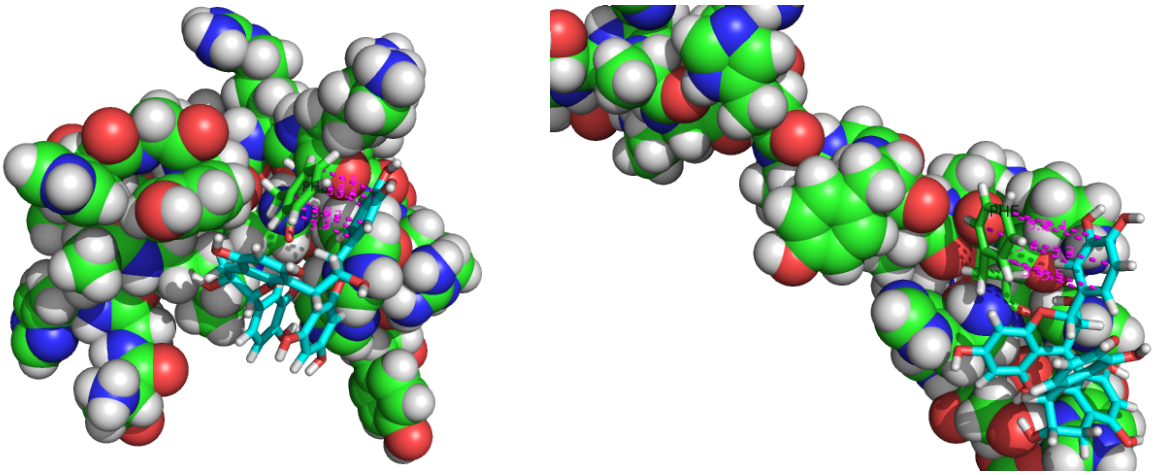

1.28(a) π-π stacking between the compact rotamer of procyanidin B1 and phenylalanine 14 of Histatin 5 during liquid-phase optimization

1.28(b) π-π stacking between the compact rotamer of procyanidin B1 and phenylalanine 14 of Histatin 5 during gas-phase optimization

Figure 1.28. Intermolecular π-π stacking (dashed magenta lines) between a polyphenol ring of the compact rotamer of procyanidin B1 and phenylalanine 14 of a Histatin 5 conformer during liquid and gas-phase simulations

and carbon-nitrogen contacts were observed in the liquid versus gas-phase optimized procyanidin-Histatin 5 complexes, though the relative number of carbon-carbon and carbon-nitrogen contacts in the gas phase was similar to that in the liquid phase (Figure 1.29). Additionally, carbon-carbon and carbon-nitrogen bond distances between procyanidin polyphenol rings and aromatic side chains of Histatin 5 were similar in the gas and liquid phase (Figures 1.30 and 1.31).

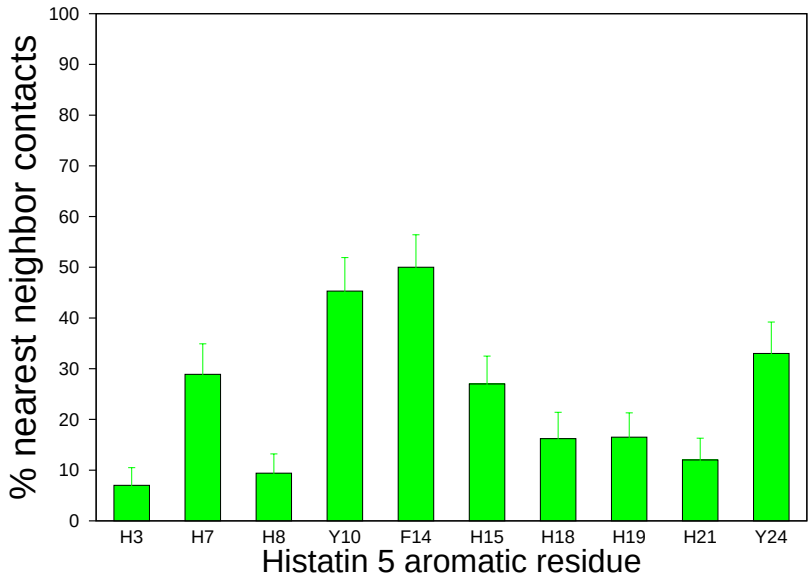

1.29(a) percentage of contacts between four procyanidin diastereomers and Histatin 5 during liquid-phase optimization

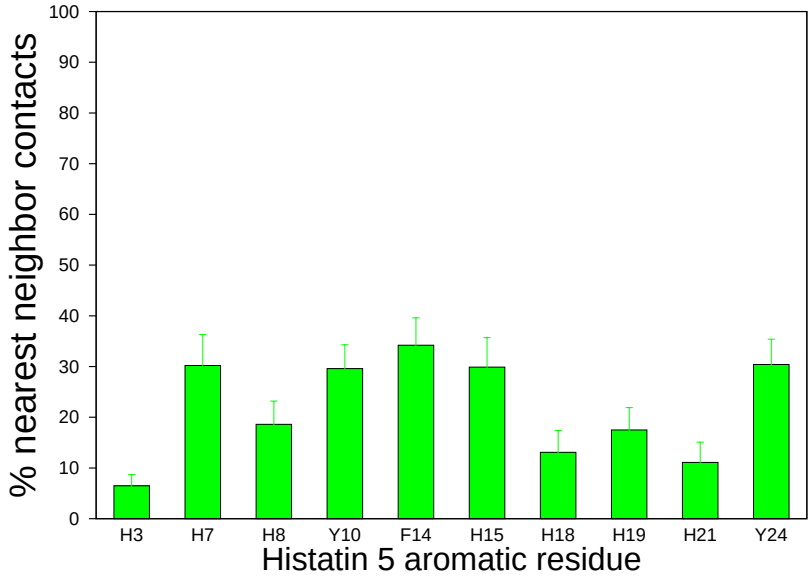

1.29(b) percentage of contacts between four procyanidin diastereomers and Histatin 5 during gas-phase optimization

Figure 1.29. Average percentage of carbon-carbon and carbon-nitrogen contacts less than 4 Å between four procyanidin diastereomers (procyanidin B1, B2, B3, and B4) and six conformers of Histatin 5 during liquid and gas-phase simulations with standard errors

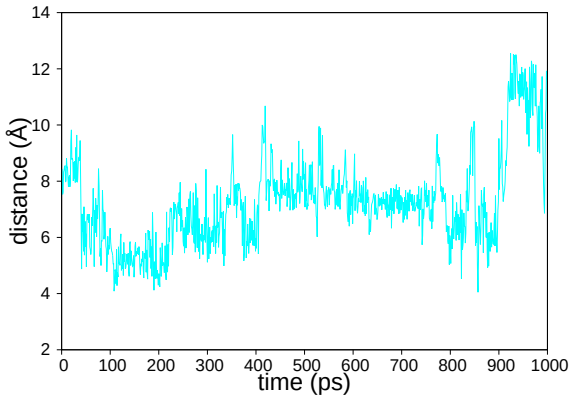

1.30(a) distance between procyanidin B1 and γC of phenylalanine 14

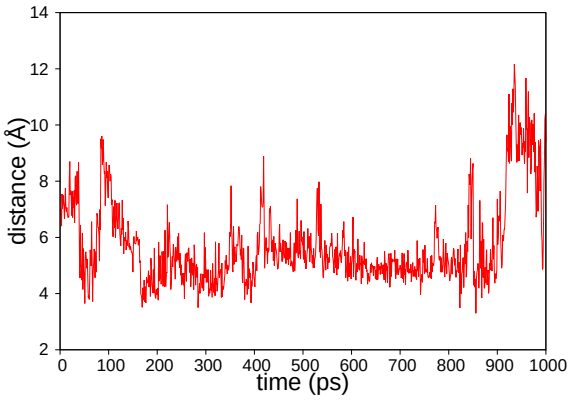

1.30(b) distance between procyanidin B1 and δ^1C of phenylalanine 14

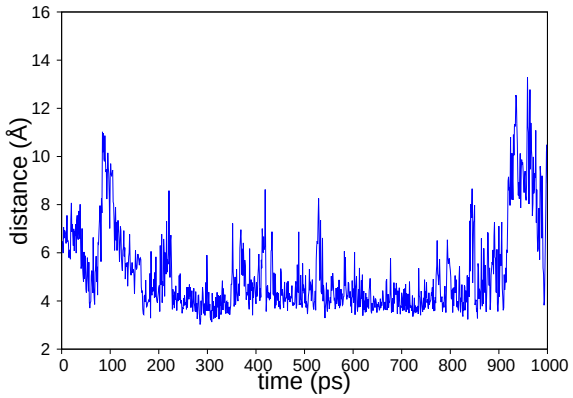

1.30(c) distance between procyanidin B1 and ε^1C of phenylalanine 14

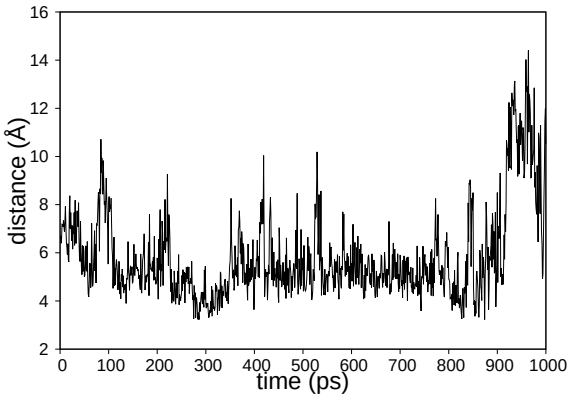

1.30(d) distance between procyanidin B1 and ζC of phenylalanine 14

Figure 1.30. Carbon-carbon bond distances between a polyphenol ring of the compact rotamer of procyanidin B1 and phenylalanine 14 of a Histatin 5 conformer in the gas phase

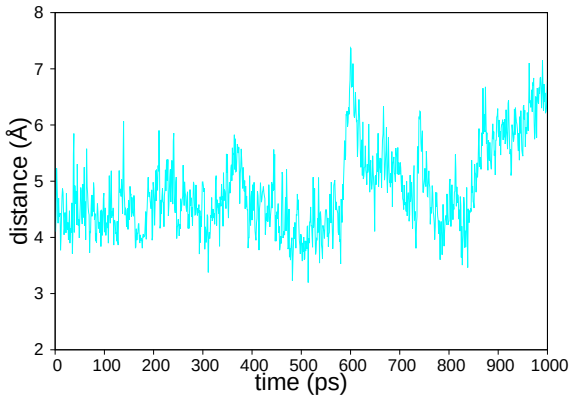

1.31(a) distance between procyanidin B1 and γC of phenylalanine 14

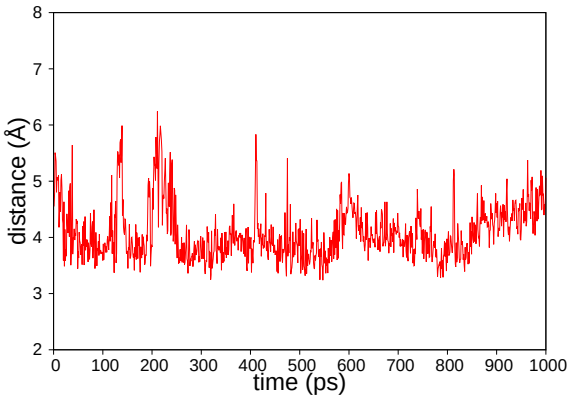

1.31(b) distance between procyanidin B1 and δ^1C of phenylalanine 14

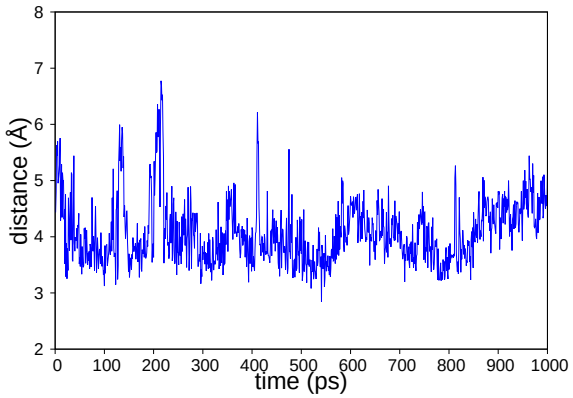

1.31(c) distance between procyanidin B1 and ε^1C of phenylalanine 14

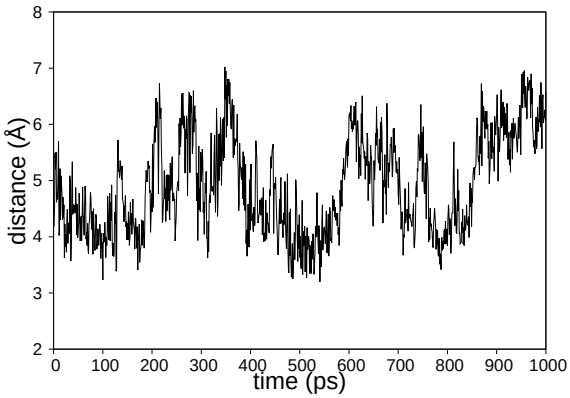

1.31(d) distance between procyanidin B1 and ζC of phenylalanine 14

Figure 1.31. Carbon-carbon bond distances between a polyphenol ring of the compact rotamer of procyanidin B1 and phenylalanine 14 of a Histatin 5 conformer in the liquid phase

Intermolecular hydrogen bonding between procyanidin rotamers and a Histatin 5 conformer was assessed with the HBonds Plugin in VMD using a donor-acceptor cutoff distance of 3.2 Å and a 20° cutoff angle. A greater number of Histatin 5 residues participated in hydrogen bonding in gas-phase versus liquid-phase procyanidin-Histatin 5 complexes (Table 1.6). In addition, the percentage of hydrogen bonding during the 1 ns trajectories was greater for gas versus liquid-phase procyanidin rotamers (Table 1.6).

Table 1.6. Percentage of intermolecular hydrogen bonding during gas and liquid-phase simulations of procyanidin B1-Histatin 5 complexes (PCB1: procyanidin B1, Side: Side Chain Atom, Main: Main Chain Atom, Standard three letter abbreviations are used for amino acid residues of Histatin 5 followed by the residue number)

1.6(a) gas-phase optimized compact rotamer of procyanidin B1 and a Histatin 5 conformer

donor	acceptor	hydrogen bonds
TYR10-Side	PCB1	2.5%
LYS13-Side	PCB1	19.6%
PCB1	HIS15-Side	15.3%
HIS15-Side	PCB1	2.1%
HIS19-Side	PCB1	3.1%
PCB1	TYR24-Side	0.1%
PCB1	PHE14-Main	7.3%
HIS18-Side	PCB1	5.7%
PCB1	HIS19-Side	3.8%
PCB1	TYR10-Side	1.0%
PCB1	LYS13-Main	6.4%
TYR24-Side	PCB1	0.4%
PCB1	SER20-Side	0.1%
ARG22-Side	PCB1	0.9%
PCB1	HIS18-Main	0.5%

1.6(b) liquid-phase optimized compact rotamer of procyanidin B1 and a Histatin 5 conformer

donor	acceptor	hydrogen bonds
PCB1	PHE14-Main	42.5%
LYS5-Side	PCB1	1.8%
PCB1	ALA4-Main	0.4%
LYS17-Side	PCB1	0.1%
HIS15-Side	PCB1	1.3%
PCB1	HIS18-Side	0.2%

1.6(c) gas-phase optimized extended rotamer of procyanidin B1 and a Histatin 5 conformer

donor	acceptor	hydrogen bonds
PCB1	HIS15-Side	1.3%
ARG6-Side	PCB1	4.9%
ASP1-Main	PCB1	21.3%
LYS5-Side	PCB1	14.5%
PCB1	TYR10-Side	0.1%
PCB1	ASP1-Side	56.7%
TYR10-Side	PCB1	0.6%
PCB1	PHE14-Main	1.1%
SER2-Side	PCB1	29.6%
SER2-Main	PCB1	13.5%
PCB1	SER2-Side	2.1%

1.6(d) liquid-phase optimized extended rotamer of procyanidin B1 and a Histatin 5 conformer

donor	acceptor	hydrogen bonds
PCB1	PHE14-Main	6.9%
LYS13-Side	PCB1	1.7%
LYS5-Side	PCB1	3.6%
ARG22-Side	PCB1	1.2%
TYR10-Side	PCB1	0.9%

Discussion

Tannin binding to salivary peptides is attributed to both hydrophilic and hydrophobic mechanisms.[75,76] Predominantly hydrophilic binding interactions have been proposed for condensed tannins through hydrogen bonding of their phenolic hydroxyl groups, whereas hydrolyzable tannins have been suggested to bind via mostly hydrophobic interactions through π-π stacking of their phenolic rings.[51] However, condensed tannins were found to bind proline rings of PRPs via π-π stacking of their polyphenol rings, and the relative binding affinities of a selection of tannins, including both hydrolyzable tannins and condensed tannin monomers, corresponded to the number of aromatic rings available for π-π stacking.[31,77,78] In addition, the binding mechanism for the condensed tannin diastereomers procyanidin B1, B2, B3, and B4 to the 14 residue PRP IB7$_{14}$ was found to depend on the concentration of procyanidins, with hydrophilic interactions occurring at concentrations below the critical micelle concentration (CMC), while above the CMC, both hydrophilic and hydrophobic interactions were observed.[42,43]

Association constants for self aggregation of procyanidin diastereomers were measured to be around 6 M^{-1}.[79] 2D NMR studies of procyanidin binding to IB7$_{14}$ were performed below their self association constants, though self aggregation was taken into account when calculating procyanidin-IB7$_{14}$ dissociation constants.[42,43] The procyanidin-IB7$_{14}$ binding studies used 1 mM peptide and 1 to 7 mM of procyanidins in 12% ethanol and 5 mM acetic acid at pH 3.5.[43] CMCs for procyanidin B1, B2, B3, and B4 range from 19 to 28 mM.[79] The procyanidin-IB7$_{14}$ binding studies demonstrated that the tendency for procyanidin diastereomers to adopt the extended versus compact rotamer determined their relative binding affinities for IB7$_{14}$ in aqueous solution.[42,43] Below the CMC and at a tannin:peptide molar ratio > 2, the tendency for procyanidin diastereomers to adopt the extended rotamer correlated with the amount of IB7$_{14}$ peptide precipitated. Above the CMC, the conformational preference of procyanidins did not influence their binding to IB7$_{14}$ due to the effects of tannin aggregation. Procyanidin B2 had the highest percentage of extended rotamer (45%), followed by B4(17%), B1(8%), and B3(5%).[56] Below the CMC, the dissociation

constants of procyanidin B1, B2, B3, and B4 for $IB7_{14}$ were calculated to be 2.9 mM, 1.1 mM, 8.0 mM, and 2.5 mM, respectively, and the number of $IB7_{14}$ binding sites for procyanidin B1, B2, B3, and B4 were found to be 3.0, 3.2, 3.0, and 3.5, respectively. Thus, the relative binding affinities of the procyanidin diastereomers for $IB7_{14}$ were ranked: $B2 > B4 > B1 > B3$. Since the ESI-MS studies by Rannulu and Cole used procyanidins at concentrations below their CMCs, both compact and extended rotamers of procyanidin B1, B2, B3, and B4 were docked to the six Histatin 5 conformers with FRED to adequately sample the most significant conformations contributing to procyanidin binding to Histatin 5.

PRPs possess a large number of tandem repeated proline-rich binding sites, which contributes to their high tannin binding affinities.[80,81] In addition, PRPs have a tendency to adopt a left handed polyproline-II (PPII) helix in which the protein backbone is extended and flexible.[41,82,83] The extended conformation of PRPs increases the availability of tannin binding sites when compared with more globular proteins such as BSA.[34,80] Changes in the tertiary structure of 19mer and 22mer PRPs upon tannin binding were not observed with 2D NMR.[84,85] However, tertiary structural changes have been observed upon binding of tannins to longer peptides such as a 209 residue proline-rich dephosphorylated β-casein protein and the 70 residue PRP IB-5.[19,86,87] Dissociation constants for flavan-3-ol binding to IB-5 could not be measured with ITC most likely due to conformational changes in the peptide upon tannin binding.[86] 2D NMR studies indicate EGCG binds residual PPII helical structures on IB-5, resulting in increased structural content of the peptide.[88] Furthermore, below the CMC, procyanidin B3 was observed to bind $IB7_{14}$ via anchorage to specific sites on the protein backbone, resulting in reduced conformational disorder of the peptide.[41]

2D NMR studies have shown that Histatin 5 adopts a random coil in aqueous solution.[29,30] Intrinsically unstructured proteins (IUPs) like Histatin 5 have been found to possess a high net charge and/or a large number of polar amino acids.[89,90] Histatin 5 possesses a net charge of +5 in aqueous solution at neutral pH as well as a large number of polar and aromatic residues, including histi-

dine, tyrosine, phenylalanine, lysine, and arginine (Table 1.3).[52] 2D NMR studies of Histatin 5 binding to EGCG used 3 mM peptide and 12.6 mM EGCG in 100 mM oxalate buffer.[31] In the EGCG-Histatin 5 binding studies, the EGCG-Histatin 5 dissociation constant was determined to be about 1 mM with 6.6 EGCG binding sites *per* peptide, though another study detected little or no binding and precipitation of Histatin 5 by EGCG.[31,78] In addition, no changes in the tertiary structure of Histatin 5 were detected upon binding EGCG.[31] Significant changes in the average chemical shifts of aromatic residues of Histatin 5, including histidine, tyrosine, and phenylalanine, and also the basic residues arginine and lysine were detected upon binding EGCG (Figure 1.23).[31] Moreover, site directed mutagenesis of histidine, tyrosine/phenylalanine, lysine, or arginine residues of Histatin 7, a C-terminal fragment of Histatin 5, resulted in loss of EGCG binding to the altered sites. Despite minor decreases in average chemical shifts of unaltered residues of Histatin 7, the pattern of binding for the remaining amino acids did not change. The average chemical shift changes of Histatin 5 and Histatin 7 upon binding EGCG were concluded to be due to hydrophobic interactions between aromatic rings of EGCG and histidine imidazole rings, the aromatic side chains of phenylalanine and tyrosine, and hydrophobic sections of the side chains of lysine and arginine.[31] Thus, it was hypothesized that histidine, tyrosine, phenylalanine, lysine, and arginine residues of Histatin 5 could bind procyanidin B1, B2, B3, and B4 in multiple peptide backbone conformations in aqueous solution. The protein structure prediction web server CS23D2.0 was used to obtain atomic coordinates for Histatin 5, followed by random selection of six potential Histatin 5 conformers from long MD simulations of the CS23D2.0 generated Histatin 5 structure with the *sander* module of AMBER. Histatin 5 receptors were prepared from the six Histatin 5 conformers using the FRED receptor GUI with the inner and outer contours disabled to allow for docking of procyanidins to multiple tannin binding sites on Histatin 5.

Refinement of docked ligands using a molecular mechanics force field improves identification of hits in virtual drug screening.[91,92] Structures of procyanidins docked to six Histatin 5 conformers were optimized in MD simulations with the *sander* module of AMBER. As in aqueous

solution, Histatin 5 had a +5 net charge during liquid-phase optimization of procyanidins docked to the Histatin 5 conformers, which was neutralized by the addition of 5 chloride ions.[52] Unbound Histatin 5 and procyanidin-Histatin 5 complexes had a +5 net charge in the EMS-MS experiments by Rannulu and Cole, though unbound procyanidins were neutral. Therefore, during gas-phase optimization, structures of procyanidins docked to the six Histatin 5 conformers were not neutralized by addition of chloride ions in order to simulate the +5 net charge of procyanidin-Histatin 5 complexes in the ESI-MS experiments by Rannulu and Cole.

In order to compare the docking scores of procyanidin B1, B2, B3, and B4 with their relative binding affinities derived from ESI-MS, relative binding affinities of the procyanidin diastereomers were calculated by averaging their docking scores for the six potential Histatin 5 conformers. However, the similarity of docking score distributions of the procyanidin diastereomers precluded ranking their calculated relative binding affinities (Figure 1.9). In addition, the interatomic distances of docked procyanidins and six Histatin 5 conformers were assessed with the PyMOL Measurement Wizard. Potential hydrogen bonding interactions were observed between hydrogen bond forming atoms of the procyanidin polyphenol rings and side chain and backbone hydrogen bonding atoms of Histatin 5 (Figure 1.10). In addition, potential π-π stacking interactions were observed between procyanidin polyphenol rings and phenylalanine, tyrosine, and histidine rings of Histatin 5 (Figure 1.10(a)).

The procyanidin-Histatin 5 binding energies of optimized procyanidin B1, B2, B3, and B4 were compared to their relative binding affinities derived from ESI-MS by averaging their procyanidin-Histatin 5 binding energies for the six Histatin 5 conformers. The average procyanidin-Histatin 5 binding energies of gas-phase procyanidin-Histatin 5 complexes were around 30 kcal/mol lower than the liquid phase, most likely due to enhanced electrostatic interactions in the gas phase and/or loss of solvent mediated interactions in the liquid phase since only direct interaction energies (without solvent-mediated interactions) were used to calculate the

procyanidin-Histatin 5 binding energies (Figure 1.11).[44,45] The calculated relative binding affinities of liquid-phase procyanidin diastereomers were consistent with the relative binding affinities derived from ESI-MS, though their average procyanidin-Histatin 5 binding energies were similar to each other (Figure 1.11(a) and Table 1.4). However, the calculated relative binding affinities of gas-phase procyanidin diastereomers were not consistent with the relative binding affinities derived from ESI-MS, though again their average procyanidin-Histatin 5 binding energies were comparable to each other, suggesting the general relationship among the relative binding affinities of liquid-phase procyanidin diastereomers does not change appreciably in the gas phase (Figure 1.11(b) and Table 1.4). In addition, the binding energies of each procyanidin diastereomer for the six Histatin 5 conformers were similar as evidenced by the narrowness of their distributions (Figure 1.11).

Strain energies of procyanidin B1, B2, B3, and B4 induced by binding Histatin 5 were calculated as the difference between the self energies of bound and unbound procyanidins. The strain energies were small enough to be neglected in calculations of the relative binding affinities of the procyanidin diastereomers for Histatin 5 (Figure 1.12). The strain energies of liquid-phase procyanidins were similar to each other, indicating little or no difference in the strain induced in each procyanidin ligand upon binding Histatin 5 (Figure 1.12(a)). The strain energies of gas-phase procyanidin diastereomers were also similar to each other, again indicating that differences in the strain induced in each procyanidin ligand upon binding Histatin 5 were small (Figure 1.12(b)). Additionally, the strain energies of liquid and gas-phase procyanidin diastereomers were similar (Figure 1.12).

Differences in the self energies of compact and extended rotamers of procyanidin B1, B2, B3, and B4 in complex with Histatin 5 were calculated by subtracting the average self energy of the extended rotamer for the six Histatin 5 conformers from the average self energy of the compact rotamer for the six Histatin 5 conformers. Differences in the self energies of compact

and extended rotamers of unbound procyanidin diastereomers were calculated by subtracting the self energy of the extended rotamer from the self energy of the compact rotamer. The compact π-π stacked rotamers of procyanidin B1, B2, and B4 exhibited lower energies than the extended unstacked rotamers in agreement with previous studies (Figure 1.13).[56] However, the extended rotamer of procyanidin B3 had a somewhat lower energy than the compact rotamer possibly due to the method used for calculation of the procyanidin self energies which included only the Lennard-Jones and Coulombic energy terms or perhaps insufficient sampling during the 1 ns MD trajectories (Figure 1.13). Differences in the self energies of compact and extended rotamers of procyanidins complexed with Histatin 5 in liquid-phase simulations resembled those in the gas phase, indicating the self energies of compact and extended rotamers of liquid-phase bound procyanidins did not change relative to one another in the gas phase (Figure 1.13). Differences in the self energies of compact and extended rotamers of unbound procyanidins in liquid-phase simulations also resembled the gas phase, again indicating the self energies of compact and extended rotamers of liquid-phase unbound procyanidins did not change relative to one another in the gas phase (Figure 1.13). In addition, differences in the self energies of compact and extended rotamers of unbound procyanidins resembled those of bound procyanidins in the liquid (Figure 1.13(a)) and gas phase (Figure 1.13(b)).

NMR studies employing time-averaged Nuclear Overhauser Effects (NOEs) demonstrated that multiple conformations of EGCG bound several sites of a PRP heptapeptide.[93] Visual inspection of structures corresponding to maxima in the energy distributions of optimized procyanidin-Histatin 5 complexes suggests that the compact and extended conformations of procyanidin B1, B2, B3, and B4 bind multiple sites on Histatin 5 as well (Figures 1.16 and 1.17). In addition, both gas and liquid-phase binding modes of procyanidin-Histatin 5 complexes exhibited hydrogen bonding and π-π stacking characteristics, though gas-phase binding modes appeared to exhibit more hydrogen bonding and less π-π stacking than liquid-phase binding modes as expected (Figures 1.16 and 1.17).

The percentage of nearest-neighbor contacts in liquid-phase procyanidin-Histatin 5 complexes was compared with the percentage of nearest-neighbor contacts in the gas phase by averaging the percentage of contacts of each procyanidin diastereomer for the six Histatin 5 conformers. The number of nearest-neighbor contacts in gas-phase procyanidin-Histatin 5 complexes was greater than the liquid phase, though the relative number of contacts in the gas phase resembled that in the liquid phase, suggesting some residual liquid-phase contacts may be retained in gas-phase procyanidin-Histatin 5 complexes (Figures 1.18-1.21). The average percentage of nearest-neighbor contacts for the four procyanidin diastereomers was also greater in the gas versus liquid phase, though the relative number of contacts in the gas phase resembled that in the liquid phase, again suggesting some residual liquid-phase contacts were retained in the gas phase (Figure 1.22).

The percentage of intermolecular π-π stacking in liquid-phase procyanidin-Histatin 5 complexes was compared with the percentage of π-π stacking in the gas phase by averaging the percentage of aromatic carbon-carbon or carbon-nitrogen contacts between procyanidin diastereomers and Histatin 5 for the six Histatin 5 conformers, and by visual inspection for intermolecular π-π stacking characteristics. The average percentage of carbon-carbon and carbon-nitrogen contacts was greater in liquid versus gas-phase procyanidin-Histatin 5 complexes, though the relative number of carbon-carbon and carbon-nitrogen contacts in the gas phase resembled that in the liquid phase, suggesting some residual π-π stacking was retained in the gas-phase procyanidin-Histatin 5 complexes (Figures 1.24-1.27). Additionally, π-π stacking characteristics were visually detected in both liquid and gas-phase procyanidin-Histatin 5 complexes (Figure 1.28). The average percentage of carbon-carbon and carbon-nitrogen contacts for all four procyanidin diastereomers was also greater in the liquid versus gas phase, though the relative number of carbon-carbon and carbon-nitrogen contacts in the gas phase resembled that in the liquid phase (Figure 1.29). In addition, carbon-carbon and carbon-nitrogen bond distances between the procyanidin diastereomers and Histatin 5 were similar in the gas and liquid phase, suggesting some

residual π-π stacking was retained in the gas-phase complexes (Figures 1.30 and 1.31).

Intermolecular hydrogen bonding in liquid-phase procyanidin-Histatin 5 complexes was compared with hydrogen bonding in the gas phase using the HBonds Plugin in VMD. The number of Histatin 5 residues involved in hydrogen bonding was greater for gas versus liquid-phase procyanidin-Histatin 5 complexes (Table 1.6). Also, the percentage of hydrogen bonding during the MD simulations was greater for gas versus liquid-phase complexes (Table 1.6). Thus, a greater number and percentage of hydrogen bonding interactions were observed in gas versus liquid-phase procyanidin-Histatin 5 complexes, though fewer π-π stacking interactions, most likely due to the reduced permittivity of the gas phase.[44,45]

Calculations of the procyanidin-Histatin 5 binding energies of procyanidin B1, B2, B3, and B4 using liquid-phase optimization of procyanidin-Histatin 5 complexes were unable to definitively reproduce the relative binding affinities of procyanidin diastereomers derived from ESI-MS binding strength quotients. Also, calculations of the procyanidin-Histatin 5 binding energies of procyanidin B1, B2, B3, and B4 using gas-phase optimization of procyanidin-Histatin 5 complexes did not coincide with the relative binding affinities of procyanidin diastereomers derived from ESI-MS gas-phase dissociation quotients. Again, it should be noted that only direct interaction energies between the procyanidin ligands and Histatin 5 were included in these calculations without the effects of solvent and other components of the system. Free energy calculations, which include entropic and desolvation effects not taken into account in docking and MD simulations, could be used to more accurately estimate the relative binding affinities derived from ESI-MS.[55,57,59,60,97,98,100–104] Also, molecular mechanics force fields have been reported to be too rigid to accurately model tannin conformations in solution.[105] Interestingly, no interconversions between compact and extended rotamers of the procyanidin diastereomers were observed during one nanosecond MD simulations of the unbound or bound procyanidins in the liquid or gas phase. In addition, the binding strength quotients of procyanidin B1, B2, B3, and B4 for Histatin 5 were of the same order of magnitude

and the gas-phase dissociation quotients of procyanidin B1, B2, B3, and B4 for Histatin 5 were of the same order of magnitude. Dissociation constants of the procyanidin diastereomers for $IB7_{14}$ from previous studies (vide supra) were also of the same order of magnitude.[43] Thus, the algorithms and force fields used in this study were unable to effectively reproduce the relative binding affinities of procyanidin diastereomers for Histatin 5 as determined in the ESI-MS experiments by Rannulu and Cole. However, analogous to previous studies, the correspondence between binding mode characteristics, including procyanidin-Histatin 5 binding energies, ligand self energies, nearest-neighbor contacts, hydrophobic contacts, and carbon-carbon/carbon-nitrogen bond distances in liquid and gas-phase MD simulations suggests that residual structural features of liquid-phase procyanidin-Histatin 5 complexes may be retained under gas-phase ESI-MS conditions, though simulations were run for only one nanosecond.[70–74] It should be noted that the procyanidin-Histatin 5 binding energies and the self energies of bound procyanidins were weighted equally when averaged over the six Histatin 5 conformers, though Boltzmann weighted averages would seem more appropriate. However, assuming the conformations sampled by a Histatin 5 random coil should be relatively close in energy and the energy differences between the compact and extended rotamers of each procyanidin are small enough to be neglected, averages of the procyanidin-Histatin 5 binding energies and procyanidin self energies using equal weights could be applicable in this instance.

The relative number of nearest-neighbor contacts between Histatin 5 residues and procyanidin diastereomers resembled average changes in proton chemical shifts of Histatin 5 residues upon titration with EGCG as determined by Bennick et al.[31] such that a greater number of contacts corresponded to a larger average chemical shift change (Figures 1.18-1.23). The average chemical shift changes are suggested to be due to hydrophobic interactions between aromatic rings of EGCG and aromatic side chains of histidine, phenylalanine, and tyrosine, and also hydrophobic sections of the side chains of lysine and arginine. A significant number of contacts were observed for histidine, tyrosine, and phenylalanine, and also arginine and lysine during optimization

of procyanidin-Histatin 5 complexes. Despite sampling only six potential Histatin 5 conformers as well as current limitations in modeling tannins with molecular mechanics force fields, these data suggest procyanidins bind a diverse array of peptide backbone conformations sampled by a Histatin 5 random coil in aqueous solution via mostly hydrophobic and π-π stacking interactions between procyanidin polyphenol rings and histidine, phenylalanine, tyrosine, lysine, and arginine residues of Histatin 5, thereby resulting in a mixture of procyanidin-Histatin 5 complexes. Moreover, gradual increases in the backbone-atom RMSDs of a Histatin 5 conformer bound to the compact and extended rotamers of procyanidin B1 indicate that procyanidin binding does not result in fixation of the Histatin 5 secondary structure (Figures 1.6 and 1.8), though tertiary structural changes in Histatin 5 were found not to occur upon binding EGCG.[31] In contrast, a mixture of tannin-peptide complexes resulting from tertiary structural changes has been observed upon binding of EGCG to the 70 residue proline-rich IB-5.[87] Future studies of conformational changes in Histatin 5 upon binding procyanidins with NMR using residual dipolar couplings (RDCs) and conformations of bound procyanidins using time-averaged NOEs could serve to further elucidate the mechanisms of procyanidin-Histatin 5 binding in aqueous solution.[93,106,107] 2D NMR studies showed that the primary sequence of Histatin 5 can affect tannin binding as well, perhaps due to some element of binding cooperativity, though the effect was not investigated in this study.[31,108]

It is estimated that 25% of the total protein in mammals consists of IUPs and efficient methods for predicting IUPs are currently being developed.[109–114] Highly accurate simulations of IUPs will most likely require modification of existing algorithms and force fields.[83,115–121] Intrinsic disorder can provide a receptor with additional functional properties compared with the folded state, including broader specificity to interact with a wider variety of ligands as well as the ability to interact with more ligands simultaneously.[34,80,122–125] The protein structure-function paradigm can thus be modified to encompass IUPs by including random coil, molten globule (containing secondary structure, but without compact tertiary structure), and folded states, along with their transitions.[126] It seems appropriate that intrinsic disorder imparts salivary peptides with the ability to bind a

greater variety of tannins than the folded state since, evolutionally, it would appear energetically costly to need to synthesize and process a large number of folded proteins capable of binding each species of potentially harmful tannin.[81] However, the energetic cost of broader specificity imparted to a peptide by intrinsic disorder may result in lower tannin binding affinities overall.[126,127] Tannins that do not bind strongly to salivary peptides would be expected to be more bioavailable, and could potentially be exploited for their antioxidant potential.[31] Mass spectrometry, with its rapid and sensitive screening ability, may be particularly well suited for determining the bioavailability of tannins.[44–47] More investigation of the potential of ESI-MS to screen the relative binding affinities of tannins for salivary peptides could be conducted using tannin-peptide complexes, concentrations, pH, and solvent conditions matching those used in studies employing other analytical techniques such as NMR and ITC as closely as possible.

References

[1] T. Swain and E. C. Bate-Smith. Flavonoid Compounds. In M. Florkin and H.S. Mason, editors, *Comparative Biochemistry*, page 764. Academic Press, New York and London, **1962**.

[2] D. W. Griffiths. Condensed Tannins. In J. P. Felix D'Mello, C. M. Duffus, and J. H. Duffus, editors, *Toxic Substances in Crop Plants*, pages 180–181. The Royal Society of Chemistry, Cambridge, **1991**.

[3] K. Khanbabaee and T. van Ree. Tannins: Classification and Definition. *Nat. Prod. Rep.*, *18*:641–649, **2001**.

[4] A. Bennick. Interaction of Plant Polyphenols with Salivary Proteins. *Critical Reviews in Oral Biology & Medicine*, *13*:184–196, **2002**.

[5] H. Mehansho, L. G. Butler, and D. M. Carlson. Dietary Tannins and Salivary Proline-Rich Proteins: Interactions, Induction, and Defense Mechanisms. *Ann. Rev. Nutr.*, *7*:423–440, **1987**.

[6] G. R. Beecher. Overview of Dietary Flavonoids: Nomenclature, Occurrence and Intake. *J. Nutr.*, *133*:3248S–3254S, **2003**.

[7] V. Koleckar, K. Kubikova, Z. Rehakova, K. Kuca, D. Jun, L. Jahodar, and L. Opletal. Condensed and Hydrolysable Tannins as Antioxidants Influencing the Health. *Mini Reviews in Medicinal Chemistry*, *8*:436–447, **2008**.

[8] K. T. Chung, T. Y. Wong, C. I. Wei, Y. W. Huang, and Y. Lin. Tannins and Human Health: a Review. *Critical Reviews in Food Science and Nutrition*, *38*:421–464, **1998**.

[9] T. N. Asquith and L. G. Butler. Interactions of Condensed Tannins with Selected Proteins. *Phytochemistry*, *25*:1591–1593, **1986**.

[10] S. Soares, N. Mateus, and V. de Freitas. Interaction of Different Classes of Salivary Proteins with Food Tannins. *FRIN*, *49*:807–813, **2012**.

[11] Y. Lu and A. Bennick. Interaction of Tannin with Human Salivary Proline-Rich Proteins. *Arch. Oral Biol.*, *43*:717–728, **1998**.

[12] N. Naurato, P. Wong, Y. Lu, K. Wroblewski, and A. Bennick. Interaction of Tannin with Human Salivary Histatins. *J. Agric. Food Chem.*, *47*:2229–2234, **1999**.

[13] F. Amado, M. João, C. Lobo, P. Domingues, J. A. Duarte, and R. Vitorino. Salivary Peptidomics. *Expert. Rev. Proteomics*, *7*:709–721, **2010**.

[14] M. S. Lamkin and F. G. Oppenheim. Structural Features of Salivary Function. *Crit. Rev. Oral Biol. Med.*, *4*:251–259, **1993**.

[15] P. de Sousa-Pereira, F. Amado, J. Abrantes, R. Ferreira, P. J. Esteves, and R. Vitorino. An Evolutionary Perspective of Mammal Salivary Peptide Families: Cystatins, Histatins, Statherin and PRPs. *Arch. Oral Biol.*, *58*:451–458, **2013**.

[16] M. P. Williamson. The Structure and Function of Proline-Rich Regions in Proteins. *Biochem. J.*, *297*:249–260, **1994**.

[17] P. A. Raj, M. Johnsson, M. J. Levine, and G. H. Nancollas. Salivary Statherin. Dependence on Sequence, Charge, Hydrogen Bonding Potency, and Helical Conformation for Adsorption to Hydroxyapatite and Inhibition of Mineralization. *J. Biol. Chem.*, *267*:5968–5976, **1992**.

[18] J. Muenzer, C. Bildstein, M. Gleason, and D. M. Carlson. Properties of Proline-Rich Proteins from Parotid Glands of Isoproterenol-Treated Rats. *J. Biol. Chem.*, *254*:5629–5634, **1979**.

[19] E. Jöbstl, J. O'Connell, J. Patrick A. Fairclough, and M. P. Williamson. Molecular Model for Astringency Produced by Polyphenol/Protein Interactions. *Biomacromolecules*, *5*:942–949, **2004**.

[20] I. Messana, T. Cabras, E. Pisano, M. T. Sanna, A. Olianas, B. Manconi, M. Pellegrini, G. Paludetti, E. Scarano, A. Fiorita, S. Agostino, A. M. Contucci, L. Calo, P. M. Picciotti, A. Manni, A. Bennick, A. Vitali, C. Fanali, R. Inzitari, and M. Castagnola. Trafficking and Postsecretory Events Responsible for the Formation of Secreted Human Salivary Peptides: A Proteomics Approach. *Molecular & Cellular Proteomics*, *7*:911–926, **2008**.

[21] M. Stubbs, J. Chan, A. Kwan, J. So, U. Barchynsky, M. Rassouli-Rahsti, R. Robinson, and A. Bennick. Encoding of Human Basic and Glycosylated Proline-Rich Proteins by the PRB Gene Complex and Proteolytic Processing of their Precursor Proteins. *Archives of Oral Biology*, *43*:753–770, **1998**.

[22] A. Bennick. Structural and Genetic Aspects of Proline-Rich Proteins. *J. Dent. Res.*, *66*:457–461, **1987**.

[23] D. M. Carlson. Salivary Proline-Rich Proteins: Biochemistry, Molecular Biology, and Regulation of Expression. *Critical Reviews in Oral Biology & Medicine*, *4*:495–502, **1993**.

[24] F. G. Oppenheim, T. Xu, F. M. McMillian, S. M. Levitz, R. D. Diamond, G. D. Offner, and R. F. Troxler. Histatins, a Novel Family of Histidine-Rich Proteins in Human Parotid Secretion. Isolation, Characterization, Primary Structure, and Fungistatic Effects on Candida Albicans. *J. Biol. Chem.*, *263*:7472–7477, **1988**.

[25] R. F. Troxler, G. D. Offner, T. Xu, J. C. Vanderspek, and F. G. Oppenheim. Structural Relationship Between Human Salivary Histatins. *Journal of Dental Research*, *69*:2–6, **1990**.

[26] L. M. Sabatini and E. A. Azen. Histatins, a Family of Salivary Histidine-Rich Proteins, are Encoded by at least Two Loci (HIS1 and HIS2). *Biochem. Biophys. Res. Commun.*, *160*:495–502, **1989**.

[27] M. Castagnola, R. Inzitari, D. V. Rossetti, C. Olmi, T. Cabras, V. Piras, P. Nicolussi, M. T. Sanna, M. Pellegrini, B. Giardina, and I. Messana. A Cascade of 24 Histatins (Histatin 3 Fragments) in Human Saliva. Suggestions for a Pre-Secretory Sequential Cleavage Pathway. *J. Biol. Chem*, *279*:41436–41443, **2004**.

[28] W. S. Jang, J. S. Bajwa, J. N. Sun, and M. Edgerton. Salivary Histatin 5 Internalization by Translocation, but Not Endocytosis, is Required for Fungicidal Activity in Candida albicans. *Molecular Microbiology*, *77*:354–370, **2010**.

[29] D. Brewer, H. Hunter, and G. Lajoie. NMR Studies of the Antimicrobial Salivary Peptides Histatin 3 and Histatin 5 in Aqueous and Nonaqueous Solutions. *Biochem. Cell. Biol.*, *76*:247–256, **1998**.

[30] P. A. Raj, E. Marcus, and D. K. Sukumaran. Structure of Human Salivary Histatin 5 in Aqueous and Nonaqueous Solutions. *Biopolymers*, *45*:51–67, **1998**.

[31] K. Wroblewski, R. Muhandiram, A. Chakrabartty, and A. Bennick. The Molecular Interaction of Human Salivary Histatins with Polyphenolic Compounds. *European Journal of Biochemistry*, *268*:4384–4397, **2001**.

[32] A. E. Hagerman and L. G. Butler. Protein Precipitation Method for the Quantitative Determination of Tannins. *J. Agric. Food Chem.*, *26*:809–812, **1978**.

[33] J. R. Bacon and M. J. C. Rhodes. Development of a Competition Assay for the Evaluation of the Binding of Human Parotid Salivary Proteins to Dietary Complex Phenols and Tannins Using a Peroxidase-Labeled Tannin. *J. Agric. Food Chem.*, *46*:5083–5088, **1998**.

[34] V. de Freitas and N. Mateus. Structural Features of Procyanidin Interactions with Salivary Proteins. *J. Agric. Food Chem.*, *49*:940–945, **2001**.

[35] R. A. Frazier, A. Papadopoulou, I. Mueller-Harvey, D. Kissoon, and R. J. Green. Probing Protein-Tannin Interactions by Isothermal Titration Microcalorimetry. *J. Agric. Food Chem.*, *51*:5189–5195, **2003**.

[36] C. Poncet-Legrand, C. Gautier, V. Cheynier, and A. Imberty. Interactions between Flavan-3-ols and Poly (L-Proline) Studied by Isothermal Titration Calorimetry: Effect of the Tannin Structure. *J. Agric. Food Chem.*, *55*:9235–9240, **2007**.

[37] J. M. Mcrae, R. J. Falconer, and J. A. Kennedy. Thermodynamics of Grape and Wine Tannin Interaction with Polyproline: Implications for Red Wine Astringency. *J. Agric. Food Chem.*, *58*:12510–12518, **2010**.

[38] E. R. Deaville, R. J. Green, I. Mueller-Harvey, I. Willoughby, and R. A. Frazier. Hydrolyzable Tannin Structures Influence Relative Globular and Random Coil Protein Binding Strengths. *J. Agric. Food Chem.*, *55*:4554–4561, **2007**.

[39] R. A. Frazier, E. R. Deaville, R. J. Green, E. Stringano, I. Willoughby, J. Plant, and I. Mueller-Harvey. Interactions of Tea Tannins and Condensed Tannins with Proteins. *J. Pharm. Biomed. Anal.*, *51*:490–495, **2010**.

[40] S. V. E. Prigent, A. G. J. Voragen, G. A. Van Koningsveld, A. Baron, C. M. G. C. Renard, and H. Gruppen. Interactions between Globular Proteins and Procyanidins of Different Degrees of Polymerization. *Journal of Dairy Science*, *92*:5843–5853, **2009**.

[41] C. Simon, K. Barathieu, M. Laguerre, J. M. Schmitter, E. Fouquet, I. Pianet, and E. J. Dufourc. Three-Dimensional Structure and Dynamics of Wine Tannin-Saliva Protein Complexes. A Multitechnique Approach. *Biochemistry*, *42*:10385–10395, **2003**.

[42] O. Cala, N. Pinaud, C. Simon, E. Fouquet, M. Laguerre, E. J. Dufourc, and I. Pianet. NMR and Molecular Modeling of Wine Tannins Binding to Saliva Proteins: Revisiting Astringency from Molecular and Colloidal Prospects. *The FASEB Journal*, *24*:4281–4290, **2010**.

[43] O. Cala, S. Fabre, E. Fouquet, E. J. Dufourc, and I. Pianet. NMR of Human Saliva Protein/Wine Tannin Complexes. Towards Deciphering Astringency with Physico-Chemical Tools. *Comptes Rendus Chimie*, *13*:449–452, **2010**.

[44] F. Canon, F. Paté, E. Meudec, T. Marlin, V. Cheynier, A. Giuliani, and P. Sarni-Manchado. Characterization, Stoichiometry, and Stability of Salivary Protein–Tannin Complexes by ESI-MS and ESI-MS/MS. *Anal. Bioanal. Chem.*, *395*:2535–2545, **2009**.

[45] F. Canon, A. Giuliani, F. Paté, and P. Sarni-Manchado. Ability of a Salivary Intrinsically Unstructured Protein to Bind Different Tannin Targets Revealed by Mass Spectrometry. *Anal. Bioanal. Chem.*, *398*:815–822, **2010**.

[46] P. Sarni-Manchado and V. Cheynier. Study of Non-Covalent Complexation between Catechin Derivatives and Peptides by Electrospray Ionization Mass Spectrometry. *J. Mass Spectrom.*, *37*:609–616, **2002**.

[47] S. Vergé, T. Richard, S. Moreau, S. Richelme-David, J. Vercauteren, J. C. Promé, and J. P. Monti. First Observation of Non-Covalent Complexes for a Tannin–Protein Interaction Model Investigated by Electrospray Ionisation Mass Spectroscopy. *Tetrahedron Letters*, *43*(13):2363–2366, **2002**.

[48] Q. Yan and A. Bennick. Identification of Histatins as Tannin-Binding Proteins in Human Saliva. *Biochem. J.*, *311*:341–347, **1995**.

[49] S. Soares, R. Vitorino, H. Osório, A. Fernandes, A. Venâncio, N. Mateus, F. Amado, and V. de Freitas. Reactivity of Human Salivary Proteins Families towards Food Polyphenols. *J. Agric. Food Chem.*, *59*:5535–5547, **2011**.

[50] P. G. Pietta. Flavonoids as Antioxidants. *Journal of natural products*, *63*:1035–1042, **2000**.

[51] A. E. Hagerman, K. M. Riedl, G. A. Jones, K. N. Sovik, N. T. Ritchard, P. W. Hartzfeld, and T. L. Riechel. High Molecular Weight Plant Polyphenolics (Tannins) as Biological Antioxidants. *J. Agric. Food Chem.*, *46*:1887–1892, **1998**.

[52] E. J. Helmerhorst. Characterization of Histatin 5 with Respect to Amphipathicity, Hydrophobicity, and Effects on Cell and Mitochondrial Membrane Integrity Excludes a Candidacidal Mechanism of Pore Formation. *Journal of Biological Chemistry*, *276*:5643–5649, **2001**.

[53] J. A. Loo. Studying Noncovalent Protein Complexes by Electrospray Ionization Mass Spectrometry. *Mass. Spectrom. Rev.*, *16*:1–23, **1997**.

[54] Y. Li, F. Heitz, C. Le Grimellec, and R. B. Cole. Hydrophobic Component in Noncovalent Binding of Fusion Peptides to Lipids as Observed by Electrospray Mass Spectrometry. *Rapid. Commun. Mass. Spectrom.*, *18*:135–137, **2004**.

[55] R. B. Cole. Some Tenets Pertaining to Electrospray Ionization Mass Spectrometry. *J. Mass. Spectrom.*, *35*:763–772, **2000**.

[56] I. Tarascou, K. Barathieu, C. Simon, M. A. Ducasse, Y. André, E. Fouquet, E. J. Dufourc, V. de Freitas, M. Laguerre, and I. Pianet. A 3D Structural and Conformational Study of Procyanidin Dimers in Water and Hydro-Alcoholic Media as Viewed by NMR and Molecular Modeling. *Magn. Reson. Chem.*, *44*:868–880, **2006**.

[57] Y. Li, F. Heitz, C. Le Grimellec, and R. B. Cole. Fusion Peptide-Phospholipid Noncovalent Interactions as Observed by Nanoelectrospray FTICR-MS. *Anal. Chem.*, *77*:1556–1565, **2005**.

[58] OpenEye Scientific Software Inc., Santa Fe, NM, USA. *FRED, version 2.2.5*, **2009**.

[59] M. McGann. FRED Pose Prediction and Virtual Screening Accuracy. *J. Chem. Inf. Model.*, *51*:578–596, **2011**.

[60] D. A. Case, T. A. Darden, T. E. Cheatham III, C. L. Simmerling, J. Wang, R. E. Duke, R. Luo, R. C. Walker, W. Zhang, K. M. Merz, B. P. Roberts, B. Wang, S. Hayik, A. Roitberg, G. Seabra, I. Kolossvai, K. F. Wong, F. Paesani, J. Vanicek, J. Liu, X. Wu, S. R. Brozell, T. Steinbrecher, H. Gohlke, Q. Cai, X. Ye, J. Wang, M. J. Hsieh, G. Cui, D. R. Roe, D. H. Mathews, M. G. Seetin, C. Sagui, V. Babin, T. Luchko, S. Gusarov, A. Kovalenko, and P. A. Kollman. *AMBER 11*. University of California, San Francisco, **2010**.

[61] CambridgeSoft Corporation, 100 Cambridge Park Drive, Cambridge, MA 02140. *ChemDraw Ultra 13.0*.

[62] Schrödinger, LLC. *The PyMOL Molecular Graphics System, Version 1.3*, *August* **2010**.

[63] W. Humphrey, A. Dalke, and K. Schulten. VMD: Visual Molecular Dynamics. *J. Mol. Graphics*, *14*:33–38, **1996**.

[64] D. S. Wishart, D. Arndt, M. Berjanskii, P. Tang, J. Zhou, and G. Lin. CS23D: A Web Server for Rapid Protein Structure Generation using NMR Chemical Shifts and Sequence Data. *Nucleic Acids Research*, *36*:W496–W502, **2008**.

[65] Y. Duan, C. Wu, S. Chowdhury, M. C. Lee, G. Xiong, W. Zhang, R. Yang, P. Cieplak, R. Luo, T. Lee, J. Caldwell, J. Wang, and P. Kollman. A Point-charge Force Field for Molecular Mechanics Simulations of Proteins Based on Condensed-Phase Quantum Mechanical Calculations. *J. Comput. Chem.*, *24*:1999–2012, **2003**.

[66] W. L. Jorgensen, J. Chandrasekbar, J. D. Madura, R. W. Impey, and M. L. Klein. Comparison of Simple Potential Functions for Simulating Liquid Water. *J. Chem. Phys.*, *79*:926–935, **1983**.

[67] M. Valiev, E. J. Bylaska, N. Govind, K. Kowalski, T. P. Straatsma, H. J. J. van Dam, D. Wang, J. Nieplocha, E. Apra, T. L. Windus, and W. A. de Jong. Nwchem: A Comprehensive and Scalable Open-Source Solution for Large Scale Molecular Simulations. *Comput. Phys. Commun.*, *181*:1477–1489, **2010**.

[68] J. Wang, R. M. Wolf, J. W. Caldwell, P. A. Kollman, and D. A. Case. Development and Testing of a General Amber Force Field. *J. Comput. Chem.*, *25*:1157–1174, **2004**.

[69] J. Wang, W. Wang, P. A. Kollman, and D. A. Case. Automatic Atom Type and Bond Type Perception in Molecular Mechanical Calculations. *J Mol. Graph. Modell.*, *25*:247–260, **2006**.

[70] M. Rueda, S. G. Kalko, F. J. Luque, and M. Orozco. The Structure and Dynamics of DNA in the Gas Phase. *J. Am. Chem. Soc.*, *125*:8007–8014, **2003**.

[71] J. Gidden, A. Ferzoco, E. S. Baker, and M. T. Bowers. Duplex Formation and the Onset of Helicity in Poly d(CG)n Oligonucleotides in a Solvent-Free Environment. *J. Am. Chem. Soc.*, *126*:15132–15140, **2004**.

[72] M. Rueda, F. J. Luque, and M. Orozco. Nature of Minor-Groove Binders-DNA Complexes in the Gas Phase. *J. Am. Chem. Soc.*, *127*:11690–11698, **2005**.

[73] M. Rueda, F. J. Luque, and M. Orozco. G-Quadruplexes can Maintain their Structure in the Gas Phase. *J. Am. Chem. Soc.*, *128*:3608–3619, **2006**.

[74] A. Arcella, G. Portella, M. L. Ruiz, R. Eritja, M. Vilaseca, V. Gabelica, and M. Orozco. Structure of Triplex DNA in the Gas Phase. *J. Am. Chem. Soc.*, *134*:6596–6606, **2012**.

[75] A. E. Hagerman and L. G. Butler. The Specificity of Proanthocyanidin-Protein Interactions. *Journal of Biological Chemistry*, *256*:4494–4497, **1981**.

[76] N. J. Baxter, T. H. Lilley, E. Haslam, and M. P. Williamson. Multiple Interactions between Polyphenols and a Salivary Proline-Rich Protein Repeat Result in Complexation and Precipitation. *Biochemistry*, *36*:5566–5577, **1997**.

[77] N. J. Baxter, T. H. Lilley, E. Haslam, and M. P. Williamson. Multiple Interactions between Polyphenols and a Salivary Proline-Rich Protein Repeat Result in Complexation and Precipitation. *Biochemistry*, *36*:5566–5577, **1997**.

[78] A. J. Charlton, N. J. Baxter, M. L. Khan, A. J. G. Moir, E. Haslam, A. P. Davies, and M. P. Williamson. Polyphenol/Peptide Binding and Precipitation. *J. Agric. Food Chem.*, *50*:1593–1601, **2002**.

[79] I. Pianet, Y. André, M. A. Ducasse, I. Tarascou, J. C. Lartigue, N. Pinaud, E. Fouquet, E. J. Dufourc, and M. Laguerre. Modeling Procyanidin Self-Association Processes and Understanding their Micellar Organization:A Study by Diffusion NMR and Molecular Mechanics. *Langmuir*, *24*:11027–11035, **2008**.

[80] A. J. Charlton, N. J. Baxter, T. H. Lilley, E. Haslam, C. J. McDonald, and M. P. Williamson. Tannin Interactions with a Full-Length Human Salivary Proline-Rich Protein Display a Stronger Affinity than with Single Proline-Rich Repeats. *FEBS Lett.*, *382*:289–292, **1996**.

[81] M. P. Williamson. The Structure and Function of Proline-Rich Regions in Proteins. *Biochem. J.*, *297*:249–260, **1994**.

[82] A. A. Adzhubei, M. J. E. Sternberg, and A. A. Makarov. Polyproline-II Helix in Proteins: Structure and Function. *Journal of Molecular Biology*, *425*:2100–2132, **2013**.

[83] J. Makowska, S. Rodziewicz-Motowidło, K. Bagińska, J. A. Vila, A. Liwo, L. Chmurzyński, and H. A. Scheraga. Polyproline II Conformation is One of Many Local Conformational States and is Not an Overall Conformation of Unfolded Peptides and Proteins. *PNAS*, *103*:1744–1749, **2006**.

[84] N. J. Murray and M. P. Williamson. Conformational Study of a Salivary Proline-Rich Protein Repeat Sequence. *Eur. J. Biochem.*, *219*:915–921, **1994**.

[85] N. J. Murray, M. P. Williamson, T. H. Lilley, and E. Haslam. Study of the Interaction Between Salivary Proline-Rich Proteins and a Polyphenol by ^{1}H NMR Spectroscopy. *Eur. J. Biochem.*, *219*:923–935, **1994**.

[86] C. Pascal, C. Poncet-Legrand, A. Imberty, C. Gautier, P. Sarni-Manchado, V. Cheynier, and A. Vernhet. Interactions between a Non Glycosylated Human Proline-Rich Protein and Flavan-3-ols are Affected by Protein Concentration and Polyphenol/Protein Ratio. *J. Agric. Food Chem.*, *55*:4895–4901, **2007**.

[87] F. Canon, R. Ballivian, F. Chirot, R. Antoine, P. Sarni-Manchado, J. Lemoine, and P. Dugourd. Folding of a Salivary Intrinsically Disordered Protein upon Binding to Tannins. *J. Am. Chem. Soc.*, *133*:7847–7852, **2011**.

[88] C. Pascal, F. Paté, V. Cheynier, and M. A. Delsuc. Study of the Interactions between a Proline-Rich Protein and a Flavan-3-ol by NMR: Residual Structures in the Natively Unfolded Protein Provides Anchorage Points for the Ligands. *Biopolymers*, *91*:745–756, **2009**.

[89] V. N. Uversky, J. R. Gillespie, and A. L. Fink. Why are "Natively Unfolded" Proteins Unstructured under Physiologic Conditions? *Proteins*, *41*:415–427, **2000**.

[90] S. Vucetic, C. J. Brown, A. K. Dunker, and Z. Obradovic. Flavors of Protein Disorder. *Proteins*, *52*:573–584, **2003**.

[91] W. Deng and C. L. M. J. Verlinde. Evaluation of Different Virtual Screening Programs for Docking in a Charged Binding Pocket. *J. Chem. Inf. Model.*, *48*:2010–2020, **2008**.

[92] E. Perola, W. P. Walters, and P. S. Charifson. A Detailed Comparison of Current Docking and Scoring Methods on Systems of Pharmaceutical Relevance. *Proteins*, *56*:235–249, **2004**.

[93] A. J. Charlton, E. Haslam, and M. P. Williamson. Multiple Conformations of the Proline-Rich Protein/Epigallocatechin Gallate Complex Determined by Time-Averaged Nuclear Overhauser Effects. *J. Am. Chem. Soc.*, *124*:9899–9905, **2002**.

[94] W. L. Jorgensen. Free Energy Calculations: A Breakthrough for Modeling Organic Chemistry in Solution. *Acc. Chem. Res.*, *22*:184–189, **1989**.

[95] Ajay and M. A. Murcko. Computational Methods to Predict Binding Free Energy in Ligand-Receptor Complexes. *J. Med. Chem.*, *38*:4953–4967, **1995**.

[96] T. Rodinger and R. Pomès. Enhancing the Accuracy, the Efficiency and the Scope of Free Energy Simulations. *Curr. Opin. Struct. Biol.*, *15*:164–170, **2005**.

[97] W. L. Jorgensen. The Many Roles of Computation in Drug Discovery. *Science*, *303*:1813–1818, **2004**.

[98] D. B. Kitchen, H. Decornez, J. R. Furr, and J. Bajorath. Docking and Scoring in Virtual Screening for Drug Discovery: Methods and Applications. *Nat. Rev. Drug Discov.*, *3*:935–949, **2004**.

[99] M. R. Shirts, D. L. Mobley, and J. D. Chodera. Alchemical Free Energy Calculations: Ready for Prime Time? In D.C. Spellmeyer and R. Wheeler, editors, *Annu. Rep. Comput. Chem.*, volume *3*, pages 41–59. Elsevier, Amsterdam, **2007**.

[100] D. L. Mobley, A. P. Graves, J. D. Chodera, A. C. McReynolds, B. K. Shoichet, and K. A. Dill. Predicting Absolute Ligand Binding Free Energies to a Simple Model Site. *Journal of Molecular Biology*, *371*:1118–1134, **2007**.

[101] S. E. Boyce, D. L. Mobley, G. J. Rocklin, A. P. Graves, K. A. Dill, and B. K. Shoichet. Predicting Ligand Binding Affinity with Alchemical Free Energy Methods in a Polar Model Binding Site. *Journal of Molecular Biology*, *394*:747–763, **2009**.

[102] D. L. Mobley and K. A. Dill. Binding of Small-Molecule Ligands to Proteins: "What You See" is Not Always "What You Get". *Structure*, *17*:489–498, **2009**.

[103] J. D. Chodera, D. L. Mobley, M. R. Shirts, R. W. Dixon, K. Branson, and V. S. Pande. Alchemical Free Energy Methods for Drug Discovery: Progress and Challenges. *Curr. Opin. Struct. Biol.*, *21*:150–160, **2011**.

[104] D. L. Mobley and P. V. Klimovich. Perspective: Alchemical Free Energy Calculations for Drug Discovery. *J. Chem. Phys.*, *137*:230901, **2012**.

[105] R. W. Hemingway. Exploring the Conformations of Polyflavanoids-An Approach to Understanding the Significance of Tannins. In J. Vercauteren, C. Cheze, and J. Triaud, editors, *Polyphenols Communications 96: 18th International Conference on Polyphenols*, volume *1*, pages 101–102, Paris, **1998**. INRA.

[106] G. Bouvignies, P. Markwick, R. Brüschweiler, and M. Blackledge. Simultaneous Determination of Protein Backbone Structure and Dynamics from Residual Dipolar Couplings. *J. Am. Chem. Soc.*, *128*(47):15100–15101, **2006**.

[107] M. Blackledge. Recent Progress in the Study of Biomolecular Structure and Dynamics in Solution from Residual Dipolar Couplings. *Prog. Nucl. Magn. Reson. Spectrosc.*, *46*:23–61, **2005**.

[108] S. Vergé, T. Richard, S. Moreau, A. Nurich, J. M. Merillon, J. Vercauteren, and J. P. Monti. First Observation of Solution Structures of Bradykinin-penta-o-galloyl-d-glucopyranose Complexes as Determined by NMR and Simulated Annealing. *Biochim. Biophys. Acta.*, *1571*:89–101, **2002**.

[109] A. K. Dunker, I. Silman, V. N. Uversky, and J. L. Sussman. Function and Structure of Inherently Disordered Proteins. *Curr. Opin. Struct. Biol.*, *18*:756–764, **2008**.

[110] P. Tompa. Intrinsically Unstructured Proteins. *Trends Biochem. Sci.*, *27*:527–533, **2002**.

[111] H. J. Dyson and P. E. Wright. Intrinsically Unstructured Proteins and their Functions. *Nat. Rev. Mol. Cell Biol.*, *6*:197–208, **2005**.

[112] P. E. Wright and H. J. Dyson. Intrinsically Unstructured Proteins: Re-Assessing the Protein Structure-Function Paradigm. *J. Mol. Biol.*, *293*:321–331, **1999**.

[113] M. R. Jensen, L. Salmon, G. Nodet, and M. Blackledge. Defining Conformational Ensembles of Intrinsically Disordered and Partially Folded Proteins Directly from Chemical Shifts. *J. Am. Chem. Soc.*, *132*:1270–1272, **2010**.

[114] A. De Simone, A. Cavalli, S. T. D. Hsu, W. Vranken, and M. Vendruscolo. Accurate Random Coil Chemical Shifts from an Analysis of Loop Regions in Native States of Proteins. *J. Am. Chem. Soc.*, *131*:16332–16333, **2009**.

[115] K. Lindorff-Larsen, N. Trbovic, P. Maragakis, S. Piana, and D. E. Shaw. Structure and Dynamics of an Unfolded Protein Examined by Molecular Dynamics Simulation. *J. Am. Chem. Soc.*, *134*:3787–3791, **2012**.

[116] J. Higo, Y. Nishimura, and H. Nakamura. A Free-Energy Landscape for Coupled Folding and Binding of an Intrinsically Disordered Protein in Explicit Solvent from Detailed All-Atom Computations. *J. Am. Chem. Soc.*, *133*:10448–10458, **2011**.

[117] D. A. Potoyan and G. A. Papoian. Energy Landscape Analyses of Disordered Histone Tails Reveal Special Organization of their Conformational Dynamics. *J. Am. Chem. Soc.*, *133*:7405–7415, **2011**.

[118] T. Terakawa and S. Takada. Multiscale Ensemble Modeling of Intrinsically Disordered Proteins: p53 N-Terminal Domain. *Biophys. J.*, *101*:1450–1458, **2011**.

[119] M. Knott and R. B. Best. A Preformed Binding Interface in the Unbound Ensemble of an Intrinsically Disordered Protein: Evidence from Molecular Simulations. *PLoS Comput. Biol.*, *8*:e1002605, **2012**.

[120] S. L. Kazmirski and V. Daggett. Simulations of the Structural and Dynamical Properties of Denatured Proteins: the "Molten Coil" State of Bovine Pancreatic Trypsin Inhibitor. *J. Mol. Biol.*, *277*:487–506, **1998**.

[121] K. B. Wong, J. Clarke, C. J. Bond, J. L. Neira, S. M. Freund, A. R. Fersht, and V. Daggett. Towards a Complete Description of the Structural and Dynamic Properties of the Denatured State of Barnase and the Role of Residual Structure in Folding. *J. Mol. Biol.*, *296*:1257–1282, **2000**.

[122] O. K. Abou-Zied, N. Al-Lawatia, M. Elstner, and T. B. Steinbrecher. Binding of Hydroxyquinoline Probes to Human Serum Albumin: Combining Molecular Modeling and Förster's Resonance Energy Transfer Spectroscopy to Understand Flexible Ligand Binding. *J. Phys. Chem. B*, *117*:1062–1074, **2013**.

[123] B. A. Shoemaker, J. J. Portman, and P. G. Wolynes. Speeding Molecular Recognition by Using the Folding Funnel: the Fly-Casting Mechanism. *PNAS*, *97*:8868–8873, **2000**.

[124] A. G. Turjanski, J. S. Gutkind, R. B. Best, and G. Hummer. Binding-Induced Folding of a Natively Unstructured Transcription Factor. *PLoS Comput. Biol.*, *4*:e1000060, **2008**.

[125] D. De Sancho and R. B. Best. Modulation of an IDP Binding Mechanism and Rates by Helix Propensity and Non-Native Interactions: Association of HIF1α with CBP. *Mol. BioSyst.*, *8*:256–267, **2012**.

[126] A. K. Dunker, J. D. Lawson, C. J. Brown, R. M. Williams, P. Romero, J. S. Oh, C. J. Oldfield, A. M. Campen, C. M. Ratliff, K. W. Hipps, J. Ausio, M. S. Nissen, R. Reeves, C. Kang, C. R. Kissinger, R. W. Bailey, M. D. Griswold, W. Chiu, E. C. Garner, and Z. Obradovic. Intrinsically Disordered Protein. *J. Mol. Graph. Model.*, *19*:26–59, **2001**.

[127] A. K. Dunker, E. Garner, S. Guilliot, P. Romero, K. Albrecht, J. Hart, Z. Obradovic, C. Kissinger, and J. E. Villafranca. Protein Disorder and the Evolution of Molecular Recognition: Theory, Predictions and Observations. *Pac. Symp. Biocomput.*, pages 473–484, **1998**.

Appendix

Supplemental Tables for Docked Procyanidin-Histatin 5 Complexes

Table S1. Average procyanidin docking scores for six Histatin 5 conformers +/- 2 standard deviations (PCB: Procyanidin B)

PCB	Docking score
PCB1	10 +/- 20
PCB2	10 +/- 20
PCB3	10 +/- 20
PCB4	20 +/- 10

Table S2. Average procyanidin rotamer docking scores for six Histatin 5 conformers +/- 2 standard deviations (PCBC: Procyanidin B compact rotamer; PCBE: Procyanidin B extended rotamer)

PCB rotamer	Docking score
PCB1C	20 +/- 10
PCB1E	10 +/- 20
PCB2C	10 +/- 10
PCB2E	10 +/- 20
PCB3C	20 +/- 10
PCB3E	0 +/- 20
PCB4C	20 +/- 10
PCB4E	10 +/- 10

Supplemental Tables for Procyanidin-Histatin 5 Binding Energies

Table S3. Average procyanidin-Histatin 5 binding energies for six Histatin 5 conformers +/- about 2 standard errors (kcal/mol) (PCB: Procyanidin B)

Liquid-phase procyanidin-Histatin 5 binding energies	
PCB1	-54.4 +/- 0.2
PCB2	-52.1 +/- 0.2
PCB3	-48.0 +/- 0.2
PCB4	-52.5 +/- 0.2
Gas-phase procyanidin-Histatin 5 binding energies	
PCB1	-82.8 +/- 0.2
PCB2	-86.4 +/- 0.2
PCB3	-83.1 +/- 0.2
PCB4	-86.1 +/- 0.2

Table S4. Average procyanidin rotamer-Histatin 5 binding energies for six Histatin 5 conformers +/- about 2 standard errors (kcal/mol) (PCBC: Procyanidin B compact rotamer; PCBE: Procyanidin B extended rotamer)

Liquid-phase procyanidin rotamer-Histatin 5 binding energies	
PCB1C	-49.3 +/- 0.3
PCB1E	-59.5 +/- 0.2
PCB2C	-52.2 +/- 0.3
PCB2E	-52.0 +/- 0.3
PCB3C	-40.0 +/- 0.2
PCB3E	-55.9 +/- 0.3
PCB4C	-54.5 +/- 0.4
PCB4E	-50.6 +/- 0.3
Gas-phase procyanidin rotamer-Histatin 5 binding energies	
PCB1C	-76.4 +/- 0.2
PCB1E	-89.1 +/- 0.2
PCB2C	-84.1 +/- 0.3
PCB2E	-88.8 +/- 0.2
PCB3C	-78.6 +/- 0.3
PCB3E	-87.6 +/- 0.3
PCB4C	-82.2 +/- 0.3
PCB4E	-89.9 +/- 0.3

Supplemental Tables for Procyanidin Ligand Strain

Table S5. Procyanidin strain energies +/- about 2 standard errors (kcal/mol) (PCB: Procyanidin B)

Liquid-phase procyanidin strain energies	
PCB1	5 +/- 5
PCB2	1 +/- 5
PCB3	2 +/- 4
PCB4	0 +/- 4
Gas-phase procyanidin strain energies	
PCB1	10 +/- 10
PCB2	3 +/- 6
PCB3	10 +/- 6
PCB4	8 +/- 6

Table S6. Procyanidin rotamer strain energies +/- about 2 standard errors (kcal/mol) (PCBC: Procyanidin B compact rotamer; PCBE: Procyanidin B extended rotamer)

Liquid-phase procyanidin rotamer strain energies	
PCB1C	-3 +/- 7
PCB1E	13 +/- 8
PCB2C	2 +/- 6
PCB2E	0 +/- 7
PCB3C	2 +/- 6
PCB3E	3 +/- 6
PCB4C	1 +/- 6
PCB4E	-1 +/- 6
Gas-phase procyanidin rotamer strain energies	
PCB1C	0 +/- 10
PCB1E	10 +/- 20
PCB2C	2 +/- 9
PCB2E	4 +/- 8
PCB3C	7 +/- 8
PCB3E	14 +/- 10
PCB4C	11 +/- 8
PCB4E	4 +/- 9

Supplemental Tables for Compact and Extended Procyanidin Rotamer Energies

Table S7. Compact - extended procyanidin rotamer self energies +/- about 2 standard errors (kcal/mol) (PCB: Procyanidin B)

Compact - extended rotamer self energies				
	liquid phase		gas phase	
PCB	Bound	Unbound	Bound	Unbound
PCB1	-50 +/- 10	-31 +/- 1	-30 +/- 20	-26 +/- 1
PCB2	-30 +/- 9	-32 +/- 1	-30 +/- 10	-29 +/- 1
PCB3	10 +/- 8	11 +/- 1	10 +/- 10	14 +/- 1
PCB4	-71 +/- 9	-73 +/- 1	-70 +/- 10	-81 +/- 1

Fair Use Evaluation Documentation

Compiled using the **Fair Use Evaluator** [cc] 2008 Michael Brewer & the Office for Information Technology Policy, http://librarycopyright.net/fairuse/

Name:	Joshua Shraberg
Job Title:	PhD student
Institution:	University of New Orleans
Title of Work Used:	NMR Studies of the Antimicrobial Salivary Peptides Histatin 3 and Histatin 5 in Aqueous and Nonaqueous Solution.
Copyright Holder:	D. Brewer, H. Hunter, and G. Lajoie/NRC Canada
Publication Status:	Published
Publisher:	Biochem. Cell Biol.
Place of Publication:	
Publication Year:	1998
Description of Work:	vol. 76: 247–256, Table 1
Date of Evaluation:	September 7, 2014
Date of Intended Use:	December 18, 2014

Describe the Purpose and Character of Your Intended Use:

dissertation

Fair — Unfair

Describe the Nature of Your Intended Use of the Copyrighted Work:

table of NMR chemical shifts

Fair — Unfair

Describe the Amount of Your Intended Use in Relation to the Copyrighted Work as a Whole:

table 1 on pg. 250 of pages 247–256

Fair — Unfair

Describe the Effect of Your Intended Use on the Potential Market or Value of the Copyrighted Work:

unknown

Fair — Unfair

The Average **"Fairness Level,"** Based on Your Rating of Each of the 4 **Factors, Is:**

[see tool disclaimer for important clarifying information]:

Fair — Unfair

Other Important Criteria:

website http://www.lib.umich.edu/copyright-office-mpublishing/copyrightability-charts-tables-and-graphs referred by Librarian Jeanne Pavy, Scholarly Communications Officer, Earl K. Long Library, University of New Orleans.

Based on the information and justification I have provided above, I, Joshua Shraberg, am asserting this use is **FAIR** under Section 107 of the U.S. Copyright Code.

Signature: Joshua Shraberg

Date of Signature: 9/8/2014

***Disclaimer:** This document is intended to help you* collect, organize & archive the information you might need to support your fair use evaluation. *It is not a source of legal advice or assistance. The results are only as good as the input you have provided by are intended to suggest next steps, and not to provide a final judgment. It is recommended that* you share this evaluation with a copyright specialist before proceeding with your intended use.

Fair Use Evaluation Documentation

Compiled using the **Fair Use Evaluator** [cc] 2008 Michael Brewer & the Office for Information Technology Policy, http://librarycopyright.net/fairuse/

Name:	Joshua Shraberg
Job Title:	PhD student
Institution:	University of New Orleans
Title of Work Used:	The molecular interaction of human salivary histatins with polyphenolic compounds.
Copyright Holder:	K. Wroblewski and R. Muhandiram and A. Chakrabartty and A. Bennick/FEBS
Publication Status:	Published
Publisher:	Eur. J. Biochem.
Place of Publication:	
Publication Year:	2001
Description of Work:	vol. 268: 4384–4397, Figure 4
Date of Evaluation:	September 7, 2014
Date of Intended Use:	December 18, 2014

Describe the Purpose and Character of Your Intended Use:

dissertation

Fair — Unfair

Describe the Nature of Your Intended Use of the Copyrighted Work:

bar graph of NMR chemical shifts

Fair — Unfair

Describe the Amount of Your Intended Use in Relation to the Copyrighted Work as a Whole:

Fig. 4 on pg. 4390 of pages 4384–4397

Fair — Unfair

Describe the Effect of Your Intended Use on the Potential Market or Value of the Copyrighted Work:

unknown

Fair — Unfair

The Average **"Fairness Level,"** Based on Your Rating of Each of the 4 Factors, Is:

[see tool disclaimer for important clarifying information]:

Fair — Unfair

Other Important Criteria:

website http://www.lib.umich.edu/copyright-office-mpublishing/copyrightability-charts-tables-and-graphs referred by Librarian Jeanne Pavy, Scholarly Communications Officer, Earl K. Long Library, University of New Orleans.

Based on the information and justification I have provided above, I, Joshua Shraberg, am asserting this use is **FAIR** under Section 107 of the U.S. Copyright Code.

Signature: Joshua Shraberg

Date of Signature: 9/8/2014

***Disclaimer:** This document is intended to help you* collect, organize & archive the information you might need to support your fair use evaluation. *It is not a source of legal advice or assistance. The results are only as good as the input you have provided by are intended to suggest next steps, and not to provide a final judgment. It is recommended that* you share this evaluation with a copyright specialist before proceeding with your intended use.

Thermodynamic Properties of Hofmeister-Anion Binding to a Hydrophobic Cavitand

Abstract

The effects of Hofmeister salts on complexation of an amphiphilic guest adamantane carboxylic acid to the hydrophobic surface of a deep-cavity cavitand have been investigated by Gibb et al. Adamantane-cavitand binding was found to be largely enthalpically driven, though adamantane binding in the presence of the salting-in anions perchlorate and thiocyanate was entropically driven. Gibb et al. also found that perchlorate-cavitand binding was enthalpically favorable, though entropically unfavorable. Potential-of-mean-force (PMF) calculations for perchlorate-cavitand and thiocyanate-cavitand complexation were performed using umbrella sampling with a modified version of the *sander* module from the Amber 9 software suite to further investigate the thermodynamic properties of Hofmeister-anion binding to the hydrophobic cavitand. The enthalpy for salting-in anion-cavitand complexation was calculated from the potential energy difference between the bound and unbound state (the potential energy of binding) along with the entropy. The binding entropy and enthalpy were also calculated using a finite difference approximation to the entropy. The enthalpy for perchlorate-cavitand complexation calculated from the binding energy and the finite difference approximation to the entropy was favorable with an unfavorable entropy. The binding enthalpy and entropy for thiocyanate-cavitand complexation calculated from the binding energy and finite difference approximation to the entropy were unfavorable and favorable, respectively, perhaps due to a classical hydrophobic effect. The orientation of the ligand, the number of water molecules displaced from the ligand and cavitand upon complexation, and the number of nearest-neighbor atom contacts between the ligand and the cavitand were also calculated. Additionally, the energetics of various interactions involved in salting-in anion-cavitand complexation including the anion-cavitand, anion-water, cavitand-water, and water-water interactions were assessed, though the data were inconclusive.

Introduction and Background

Salts arranged in a Hofmeister series were initially characterized by their effects on the solubility of protein cosolutes in water, though effects have since been observed for a variety of phenomena.[1–5] Hofmeister ions are typically ranked according to their ability to "salt out" or decrease the solubility of a cosolute.[2,6] For protein cosolutes, anions typically yield the Hofmeister series: $F^- \sim {SO_4}^{-2} > {HPO_4}^{-2} > AcO^- > Cl^- > {NO_3}^- > Br^- > {ClO_3}^- > I^- > {ClO_4}^- > SCN^-$.[4,7–9] Cations are more variable than anions, but for proteins generally yield the Hofmeister series: ${NH_4}^+ > K^+ \approx Na^+ > Li^+ > Mg^{2+} > {NMe_4}^+ \gg {CH_6N_3}^+$.[4,7–9] Conventionally, Hofmeister ions which increase the solubility of a cosolute ("salting-in" ions) have been termed chaotropes due to their ability to perturb the structure of the bulk solvent, whereas ions that enhance the structure of bulk solvent and therefore decrease cosolute solubility ("salting-out" ions) are termed kosmotropes.[2,6,10,11] However, the contribution of chaotropic and kosmotropic properties to the respective salting-in and salting-out effects of Hofmeister ions is still under investigation.[4,6,12,13] Some studies indicate Hofmeister effects result from ion-water interactions that substantially affect hydrogen bonding in the bulk solvent.[14] Other studies indicate Hofmeister salts do not affect hydrogen bonding in the bulk, but instead exert their effects through direct ion-cosolute interactions or interactions between ions and solvation-shell waters of the cosolute.[4,6,15–20] Moreover, in some instances salting-in anions were found to enhance solvent-water structure, whereas salting-out ions were found to distort the structure of solvent waters.[4,12,20] Salting-out effects have been suggested to be mainly the result of ion-water interactions.[2,4,6,18,19] Salting-in effects are greater for more weakly solvated anions than strongly solvated anions/cations and may be dictated by direct ion-cosolute interactions.[2,4,6,18–22] Additionally, several studies suggest increased solubilization of cosolutes by salting-in anions is significantly influenced by direct interactions between ions and hydrophobic surfaces of the cosolute.[4,6,20,22–28]

The effects of Hofmeister anions on binding of an amphiphilic guest adamantane carboxylic acid to the concave hydrophobic surface of an anionic (-6 charge) deep-cavity cavitand[4,29–33] (Fig-

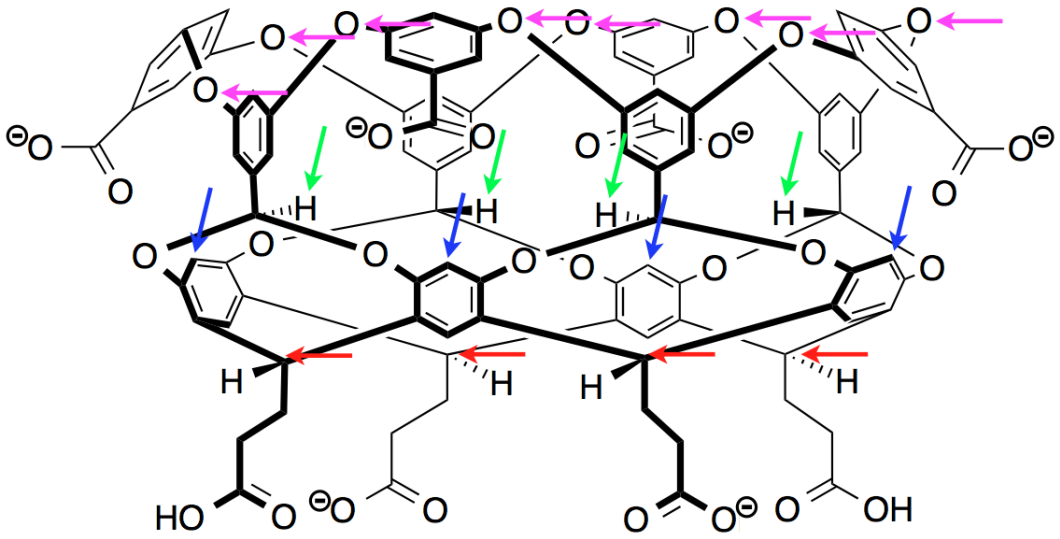

Figure 2.1. The host cavitand (-6 charge) (potential binding sites of Hofmeister anions are indicated with green and blue arrows. The bottom of the cavitand at z = 0 Å is indicated with red arrows, the limit of the inside of the cavitand from z = 0 to z = 7.3 Å with magenta arrows, and the limit of the lower region of the cavitand from z = 0 to about z = 4 Å also with green arrows)*

*adapted from a figure provided by Dr. Bruce Gibb, Department of Chemistry, Tulane University, New Orleans, LA 70118, USA.

ure 2.1) in water have been investigated by Gibb et al.[20] ITC experiments showed adamantane-cavitand complexation to be largely enthalpically driven with ΔH = -8.7 kcal mol^{-1}, though also entropically favorable (-TΔS = -0.4 kcal mol^{-1}).[20] Conversely, adamantane-cavitand complexation in the presence of the salting-in anions perchlorate ($NaClO_4$) and thiocyanate (NaSCN) was found to be entropically driven with -TΔS = -8.8 and -7.1 kcal mol^{-1}, respectively, and binding enthalpies of ΔH = 0.8 and -1.7 kcal mol^{-1}, respectively. Moreover, the presence of perchlorate and thiocyanate increased the binding free energy of the adamantane-cavitand complex by 1.1 and 0.3 kcal mol^{-1}, respectively, thus decreasing the association between adamantane and the hydrophobic cavitand, with perchlorate producing the greatest inhibition. NMR studies showed the binding free energies for perchlorate-cavitand and thiocyanate-cavitand complexation to be ΔG = -2.7 and -2.1 kcal mol^{-1}, respectively, with association constants of K_a = 95 and 33 M^{-1}, respectively.[20] In addition, complexation of the cavitand with perchlorate was found to be enthalpically favorable with ΔH = -10.62 kcal mol^{-1}, but entropically unfavorable with

$-T\Delta S = 7.94$ kcal mol^{-1}.[20]

To further investigate the thermodynamic properties of Hofmeister-anion binding to the concave surface of the hydrophobic cavitand studied by Gibb et al., perchlorate-cavitand and thiocyanate-cavitand binding free energies were determined from potential-of-mean-force (PMF) calculations using umbrella sampling with a modified version of the *sander* module from the Amber 9 software suite.[34–42] The binding enthalpy was approximated by the potential energy of binding (binding energy) and used to determine the binding entropy.[43] Additionally, the entropy and enthalpy of binding were calculated using a finite difference approximation to the entropy.[43–45] The perchlorate and thiocyanate binding modes, including the orientation of the ligand, the number of water molecules displaced from the ligand and cavitand upon complexation, and the number of nearest neighbor-atom contacts between the ligand and the cavitand, were also evaluated. In addition, the energetics of various interactions contributing to salting-in anion-cavitand complexation were assessed, including the anion-cavitand, anion-water, cavitand-water, and water-water interactions.

Methods

In-house scripts for processing MD trajectory data were written using Fortran 77 and Python 2.5.6. Three dimensional structures were rendered in VMD version 1.9.1[46] and data were plotted with gnuplot version 4.4.

Force field parameters and initial coordinates for the cavitand were the same as described in Ewell et al.[47] Perchlorate and thiocyanate parameters were obtained from studies by Baaden et al.[48] and Botti et al.[49], respectively. The systems were neutralized by addition of 7 sodium ions and solvated in boxes of 1176 TIP4P-Ew explicit waters.[50]

The perchlorate and thiocyanate ligands were harmonically restrained along the the central (z) axis of the cavitand 3 to 18 Å from the bottom of the host (Figure 2.1) in 0.5 Å increments with a 2 kcal/mol/Å^2 force constant for a total of 31 umbrella windows. The systems were equilibrated for 50 ps followed by 1 ns of MD simulation with a 1 fs time step and 12 Å nonbonded cutoff using a modified version of the *sander* module from Amber 9. Five 1 ns simulations were performed at each umbrella window for a total of 5 nanoseconds (5000000 time steps). Simulations were performed at constant temperature and pressure (NTP) under periodic boundary conditions using Langevin Dynamics temperature regulation with a collision frequency of 1 ps^{-1} at 298 K and a pressure of 1 bar. The SHAKE algorithm was used to constrain bond lengths involving hydrogens and long-range electrostatics were handled using the particle-mesh Ewald (PME) method. The sodium ions were restrained to be at least 10 Å from the host using half harmonic restraints with a force constant of 10 kcal/mol/Å^2. The PMF for each 1 ns trajectory was calculated using the Weighted Histogram Analysis Method (WHAM).[51,52]

Results and Data Analysis

Salting-In Anion-Cavitand Binding Free Energies

Perchlorate-cavitand and thiocyanate-cavitand binding free energies for each 1 ns trajectory were calculated as the difference between the free energy at z = 16 Å where the PMF became relatively constant (assumed to be the unbound state) and the global minimum free energy at z = 4.2 Å for perchlorate and z = 4.8 Å for thiocyanate (assumed to be the bound state), and averaged over the five 1 ns trajectories (Figure 2.2).

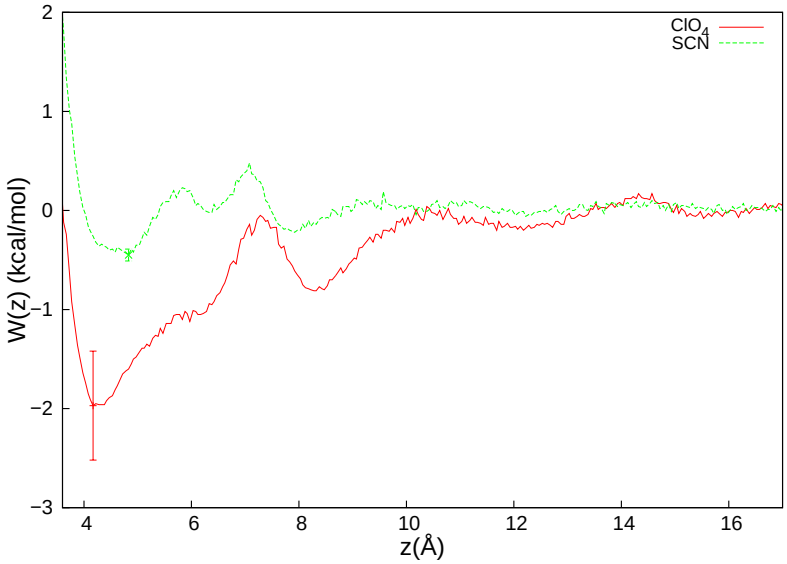

Figure 2.2. PMFs for perchlorate-cavitand and thiocyanate-cavitand binding as a function of the free energy coordinate (z) (the position of the minimum free energy is specified ± 2 standard errors)

The free energy for perchlorate-cavitand complexation (ΔG = -2.0 $\pm$ 0.6 kcal mol^{-1}) was found to be 1.6 kcal mol^{-1} more favorable than the free energy for thiocyanate-cavitand complexation (ΔG = -0.4 $\pm$ 0.1 kcal mol^{-1}) (Table 2.1).

Table 2.1. Binding free energies determined from the PMF of the perchlorate-cavitand and thiocyanate-cavitand complexes (kcal mol^{-1})

Guest	ΔG
ClO_4^-	-2.0 $\pm$ 0.6
SCN^-	-0.4 $\pm$ 0.1

Salting-In Anion-Cavitand Binding Enthalpies and Entropies

The salting-in anion-cavitand binding enthalpy was approximated by the difference between the potential energy (the binding energy) of the bound state (at around z = 4 and 5 Å for perchlorate and thiocyanate, respectively) and the unbound state (at around z = 16 Å) (Figure 2.3), which was calculated directly according to equation (1) along with the entropy (equation (2)).

$$\Delta H \approx E_{bound} - E_{unbound} \tag{1}$$

$$-T\Delta S = \Delta G - \Delta H \tag{2}$$

The enthalpy (potential energy) for perchlorate-cavitand complexation calculated using the bound and unbound states at around z = 4 and 16 Å, respectively, was favorable with ΔH = -8 $\pm$ 2 kcal mol^{-1}, though the entropy was unfavorable with -TΔS = 6 $\pm$ 2 kcal mol^{-1} (Table 2.2). However, fluctuations in the potential energy for thiocyanate-cavitand complexation along the free energy coordinate were too high to accurately calculate the binding enthalpy and entropy using the bound and unbound states at around z = 5 and 16 Å, respectively (Figure 2.3), such that the average potential energy from z = 12 to 18 Å (where the potential energy remained relatively constant) was used for the energy of the unbound state instead of the energy at z = 16 Å. The enthalpy (potential energy) for thiocyanate-cavitand complexation was found to be unfavorable (ΔH = 1 $\pm$ 1 kcal mol^{-1}) with a favorable entropy of -TΔS = -2 $\pm$ 1 kcal mol^{-1} (Table 2.2).

PMFs for perchlorate-cavitand and thiocyanate-cavitand binding were also calculated at temperatures of 328 K and 338 K using the protocol described above (see methods). The finite difference approximation to the entropy was used with binding free energies at 298 K and 328 K or 298 K and 338 K to calculate the entropy of salting-in anion-cavitand binding (equation (3)) and

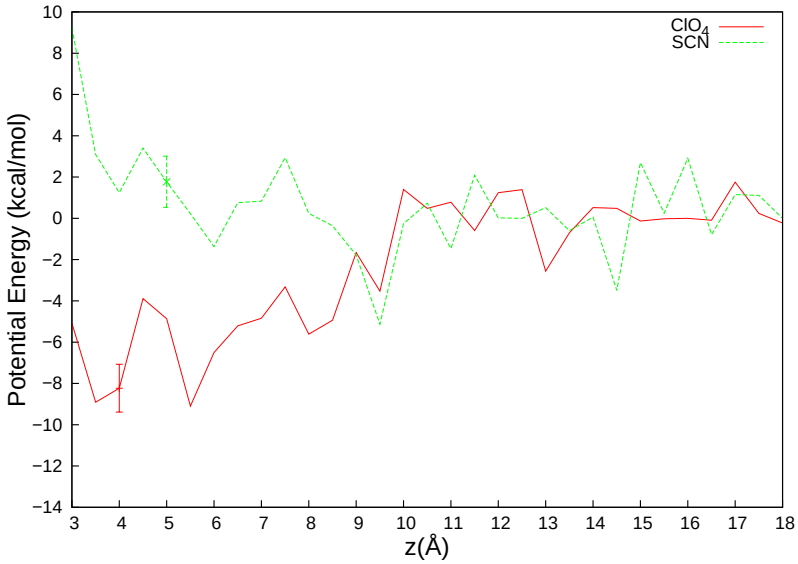

Figure 2.3. Potential energies for perchlorate-cavitand and thiocyanate-cavitand binding as a function of the free energy coordinate (z) (the position of the minimum free energy is specified ± 2 standard errors in the total potential energy and the average potential energy from z = 12 to 18 Å is plotted along the free energy coordinate for thiocyanate-cavitand binding)

the enthalpy (equation (4)) (Table 2.2).

$$\Delta S \approx -\left(\frac{\Delta G_2 - \Delta G_1}{T_2 - T_1}\right) \tag{3}$$

$$\Delta H = \Delta G + T\Delta S \tag{4}$$

The entropy for perchlorate-cavitand complexation calculated using the binding free energies at 298 K and 328 K was unfavorable with -TΔS = 4 ± 7 kcal mol^{-1}, while the enthalpy was favorable (ΔH = -6 ± 7 kcal mol^{-1}) (Table 2.2). The entropy for perchlorate-cavitand complexation using the binding free energies at 298 K and 338 K was also unfavorable with -TΔS = 1 ± 5 kcal mol^{-1}, though the enthalpy was favorable (ΔH = -3 ± 5 kcal mol^{-1}) (Table 2.2).

Table 2.2. Binding enthalpies and entropies of perchlorate-cavitand and thiocyanate-cavitand complexes at 298 K determined from the potential energy of binding at 298 K and the finite difference approximation to the entropy using binding free energies at 298 K and 328 K or 298 K and 338 K (kcal mol^{-1})

Method	Temperatures used	Guest	ΔH	-TΔS
Potential energy of binding	298 K	ClO_4^-	-8 ± 2	6 ± 2
		SCN^-	1 ± 1	-2 ± 1
Finite difference approximation	298 K and 328 K	ClO_4^-	-6 ± 7	4 ± 7
		SCN^-	0.5 ± 0.8	-1.0 ± 0.8
Finite difference approximation	298 K and 338 K	ClO_4^-	-3 ± 5	1 ± 5
		SCN^-	0.1 ± 0.9	-0.5 ± 0.9

Using the binding free energies at 298 K and 328 K, the entropy for thiocyanate-cavitand complexation was favorable with -TΔS = -1.0 ± 0.8 kcal mol^{-1}, while the binding enthalpy was unfavorable (ΔH = 0.5 ± 0.8 kcal mol^{-1}) (Table 2.2). Using the binding free energies at 298 K and 338 K, the entropy for thiocyanate-cavitand complexation was also favorable with -TΔS = -0.5 ± 0.9 kcal mol^{-1}, though the enthalpy was unfavorable (ΔH = 0.1 ± 0.9 kcal mol^{-1}) (Table 2.2).

Salting-In Anion-Cavitand Binding Modes

The number of perchlorate and thiocyanate solvation-shell waters was calculated using data for the perchlorate and thiocyanate radial distribution functions (RDFs) from studies by General et al.[53] and Botti et al.[49], respectively. The perchlorate ion lost an average of 12.6 ± 0.1 solvation-shell waters during transition from the unbound state at around z = 16 Å (16.4 ± 0.1 solvation-shell waters) to the bound state at around z = 4 Å (3.79 ± 0.09 solvation-shell waters) over the 5 ns of MD simulation (Figure 2.4 and Table 2.3). Thiocyanate lost an average of 5.62 ± 0.06 solvation-shell waters during transition from the unbound state at around z = 16 Å (9.61 ± 0.04 solvation-shell waters) to the bound state at around z = 5 Å (3.99 ± 0.04 solvation-shell waters) (Figure 2.4 and Table 2.3).

Table 2.3. Characteristics of perchlorate-cavitand and thiocyanate-cavitand binding modes averaged over 5 ns of MD simulation

Binding-mode characteristic	Guest	Bound state	Unbound state
number of guest solvation-shell waters	ClO_4^-	3.79 ± 0.09	16.4 ± 0.1
number of guest solvation-shell waters	SCN^-	3.99 ± 0.04	9.61 ± 0.04
number waters inside host	ClO_4^-	1.86 ± 0.04	4.5 ± 0.2
number waters inside host	SCN^-	1.72 ± 0.02	4.2 ± 0.1
% of time Cl occupied lower region of host	ClO_4^-	0.0 ± 0.0	0.0 ± 0.0
% of time O occupied lower region of host	ClO_4^-	95.9 ± 0.3	0.0 ± 0.0
% of time S occupied lower region of host	SCN^-	3.0 ± 0.9	0.0 ± 0.0
% of time N occupied lower region of host	SCN^-	0.0 ± 0.0	0.0 ± 0.0
angle of guest inside host (degrees)	SCN^-	103 ± 2	91 ± 3
number of Na^+ within 7 Å of guest	ClO_4^-	0.004 ± 0.007	0.5 ± 0.4
number of Na^+ within 7 Å of guest	SCN^-	0.06 ± 0.07	0.4 ± 0.4

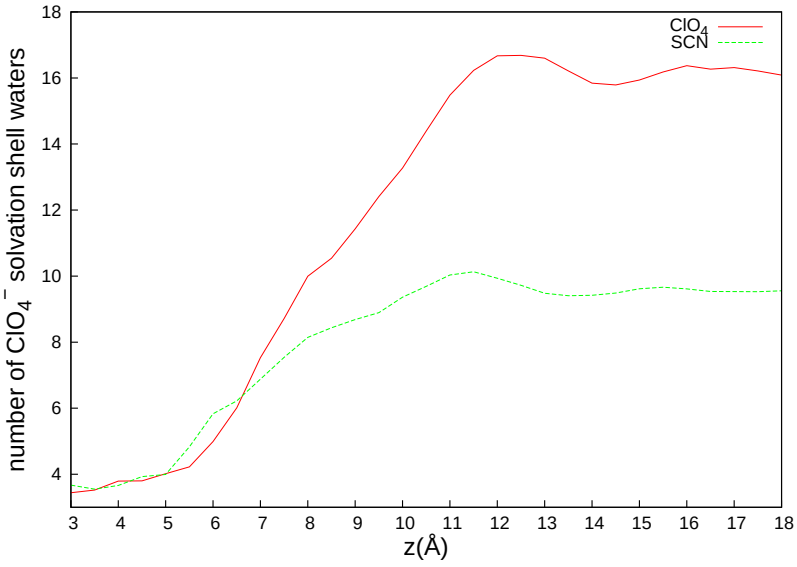

Figure 2.4. Average number of perchlorate-cavitand and thiocyanate-cavitand solvation-shell waters over 5 ns of MD simulation as a function of the free energy coordinate (z)

Perchlorate displaced an average of 2.6 $\pm$ 0.2 waters from the inside of the cavitand (below about z = 7.3 Å at the position of the eight oxygen atoms on the 32-membered ring constituting the rim of the host (Figure 2.1, magenta arrows)) during transition from the unbound state (4.5 $\pm$ 0.2 waters inside the host) to the bound state (1.86 $\pm$ 0.04 waters inside the host) over the 5 ns of MD (Figure 2.5 and Table 2.3).[47] Thiocyanate displaced an average of 2.5 $\pm$ 0.1 waters from inside the cavitand during transition from the unbound state (4.2 $\pm$ 0.1 waters inside the host) to the bound state (1.72 $\pm$ 0.02 waters inside the host) (Figure 2.5 and Table 2.3).

At least one oxygen atom from perchlorate occupied the lower region of the cavitand (below the position of the four benzyl hydrogen atoms at about z = 4 Å (Figure 2.1, green arrows)) an average of 95.9% $\pm$ 0.3% of the time in the bound state (Figure 2.6 and Table 2.3) over the 5 ns of MD simulation.[47] The sulfur atom of the thiocyanate ion occupied the lower region of the cavitand an average of 3.0% $\pm$ 0.9% of the time in the bound state (Figure 2.7 and Table 2.3), while the

nitrogen atom did not occupy the lower region of the cavitand for a significant amount of time (Figure 2.7 and Table 2.3).

The average angle of the sulfur atom of thiocyanate was 103° ± 2° (where thiocyanate is aligned with the central axis of the host and the sulfur atom is facing away from the bottom of the cavitand/toward the bulk solvent at 0°) in the bound state over the 5 ns of MD simulation (Figure 2.8 and Table 2.3). The average angle of thiocyanate was 91° ± 3° in the unbound state (Figure 2.8 and Table 2.3). The probability distribution for the angle of thiocyanate in the bound state, averaged over the 5 ns of MD, was bimodal with maxima at about 95° and 149° (Figure 2.9), while the probability distribution for the angle of thiocyanate in the unbound state was fairly constant (Figure 2.9), consistent with the data shown in Figure 2.8 and Table 2.3.

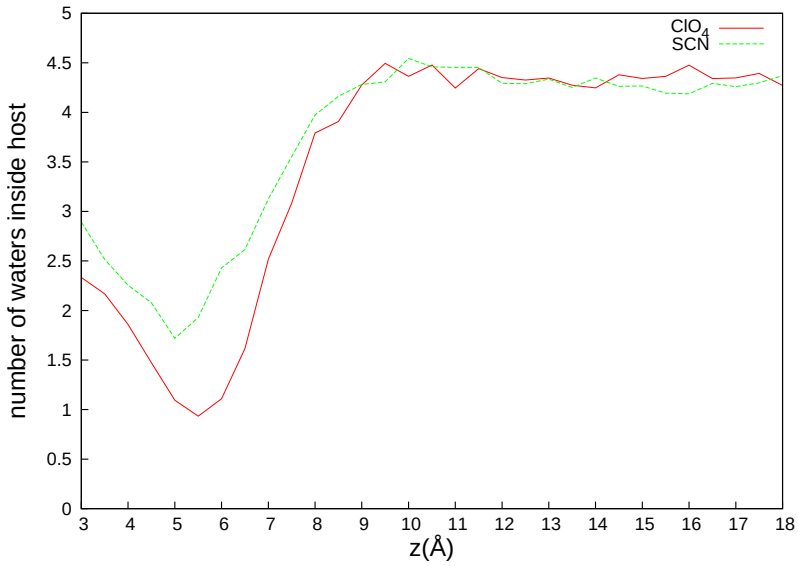

Figure 2.5. Average number of water molecules inside the cavitand (below about z = 7.3 Å) as a function of the free energy coordinate (z) over 5 ns of MD simulation

The percentage of nearest-neighbor atom contacts within a distance of 4 Å between anions and

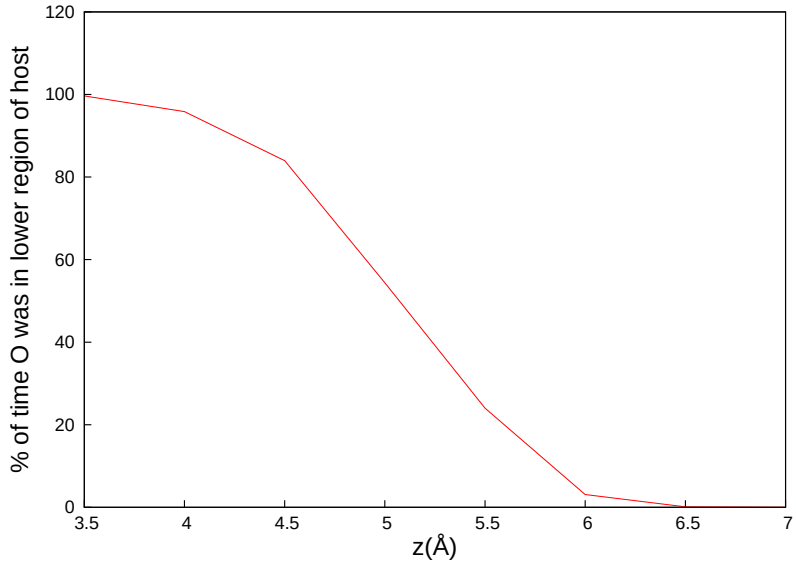

Figure 2.6. Average % of time a perchlorate oxygen was in the lower region (below about z = 4 Å) of the cavitand as a function of the free energy coordinate (z) over 5 ns of MD simulation

the cavitand in the bound state were calculated for the 5 ns of MD simulation with the HBonds Plugin in VMD using a donor-acceptor cutoff distance of 4 Å and a 180° cutoff angle. A greater number of cavitand atoms participated in nearest-neighbor contacts for the perchlorate-cavitand versus the thiocyanate-cavitand complex (data not shown) and the percentage of nearest-neighbor contacts during the 5 ns of MD was greater for the perchlorate-cavitand versus the thiocyanate-cavitand complex (Tables 2.4 and 2.5), perhaps due to the greater number of perchlorate atoms. The highest percentage of nearest-neighbor contacts for the perchlorate-cavitand complex involved the four benzyl hydrogen atoms at the limit of the lower region of the cavitand (Figure 2.1, green arrows) and the four aromatic hydrogen atoms (Figure 2.1, blue arrows) (greater than 35 % and 20 %, respectively) as well as the perchlorate oxygen atoms (Table 2.4), consistent with the data shown in Figure 2.6 and Table 2.3. The highest percentage of nearest-neighbor contacts for the thiocyanate-cavitand complex also involved the four benzyl hydrogen atoms in the lower region of the cavitand (Figure 2.1, green arrows) and four aromatic

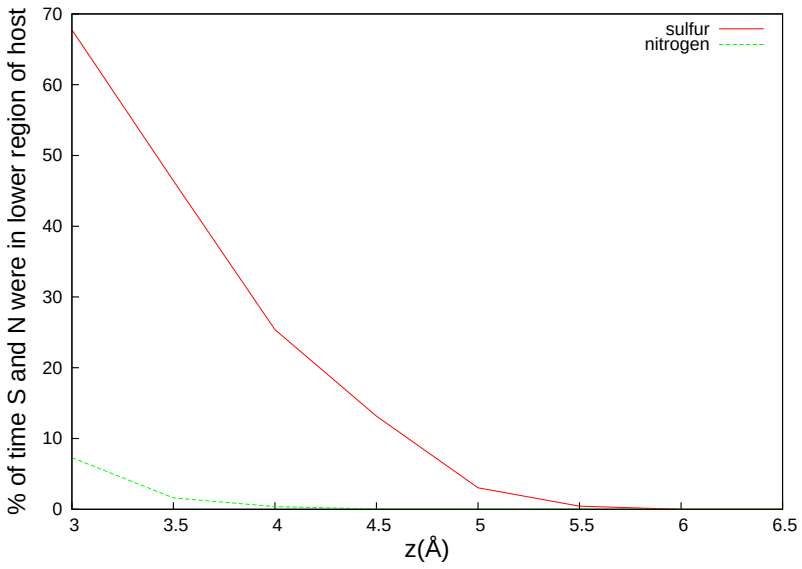

Figure 2.7. Average % of time the sulfur and nitrogen atoms of thiocyanate were in the lower region (below about z = 4 Å) of the cavitand as a function of the free energy coordinate (z) over 5 ns of MD simulation

hydrogen atoms (Figure 2.1, blue arrows) (greater than 35 % and 15 %, respectively) as well as the sulfur atom of thiocyanate (Table 2.5), consistent with the data shown in Figures 2.7-2.9 and Table 2.3.

On visual inspection, one oxygen atom from the perchlorate ion was observed to occupy the lower region of the cavitand for a significant amount of time during the 5 ns of MD simulation of the perchlorate-cavitand complex in the bound state (Figure 2.10(a)), consistent with the data shown in Figure 2.6 and Tables 2.3 and 2.4. Also, on visual inspection the sulfur atom of thiocyanate was found to be associated with the four benzyl hydrogen atoms at the position of the limit of the lower region of the cavitand (Figure 2.1, green arrows) and four aromatic hydrogen atoms (Figure 2.1, blue arrows) for a significant amount of time during simulation of the thiocyanate-cavitand complex in the bound state (Figure 2.10(b)), consistent with the data shown in Figure 2.7 and Tables 2.3 and 2.5.

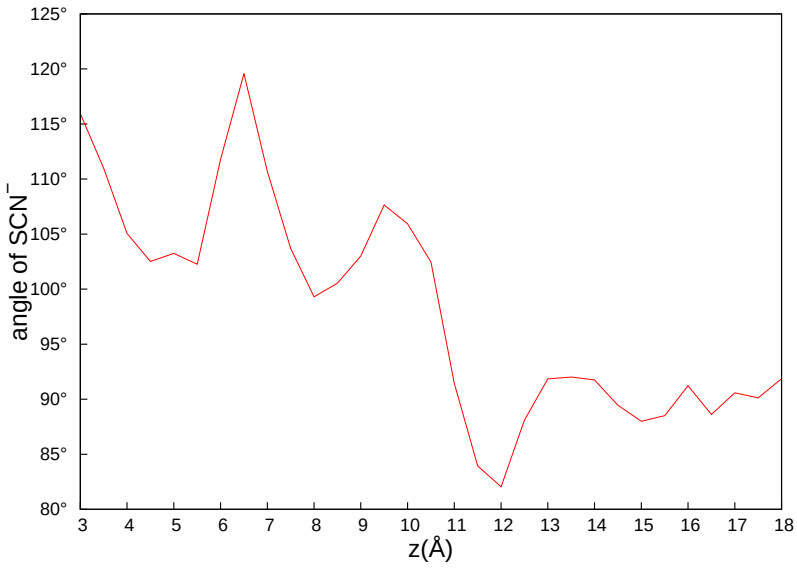

Figure 2.8. Average angle of thiocyanate as a function of the free energy coordinate (z) over 5 ns of MD simulation

An average of 0.004 ± 0.007 sodium ions were found within 7 Å of the perchlorate ion in the bound state at around z = 4 Å over the 5 ns of MD simulation, though 0.5 ± 0.4 sodium ions were found within 7 Å of perchlorate in the unbound state at around z = 16 Å (Figure 2.11 and Table 2.3). A maximum of 1.0 ± 0.2 sodium ions were found within 7 Å of perchlorate at z = 15.5 Å. An average of 0.06 ± 0.07 sodium ions were found within 7 Å of the thiocyanate ion at around z = 5 Å, while 0.4 ± 0.4 sodium ions were found within 7 Å of thiocyanate at around z = 16 Å (Figure 2.11 and Table 2.3). A maximum of 0.5 ± 0.2 sodium ions were found within 7 Å of thiocyanate at z = 17.5 Å.

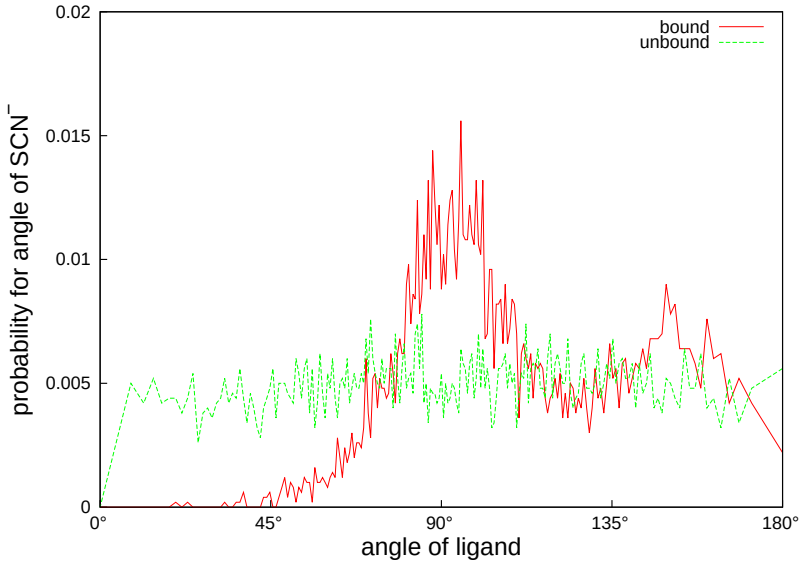

Figure 2.9. Probability distribution for the angle of thiocyanate in the bound (around z = 5 Å) and unbound (around z = 16 Å) state averaged over 5 ns of MD simulation

Table 2.4. Percentage of nearest-neighbor atom contacts less than 4 Å of perchlorate with benzyl and aromatic hydrogen atoms of the cavitand during 5 ns of MD simulation (benzyl H: benzyl hydrogen atom, aromatic H: aromatic hydrogen atom)

cavitand atom	perchlorate atom	nearest-neighbor contacts
cavitand-benzyl H1	perchlorate-O1	38.86%
cavitand-benzyl H1	perchlorate-Cl	18.34%
cavitand-benzyl H1	perchlorate-O2	36.66%
cavitand-benzyl H1	perchlorate-O3	37.06%
cavitand-aromatic H1	perchlorate-O2	22.02%
cavitand-aromatic H2	perchlorate-O1	21.76%
cavitand-benzyl H2	perchlorate-O1	38.9%
cavitand-aromatic H2	perchlorate-O3	22.56%
cavitand-benzyl H2	perchlorate-O3	40.14%
cavitand-benzyl H3	perchlorate-O2	36.48%
cavitand-benzyl H4	perchlorate-O4	39.62%
cavitand-aromatic H1	perchlorate-O1	23.7%
cavitand-benzyl H3	perchlorate-O1	39.64%
cavitand-benzyl H3	perchlorate-Cl	23.82%
cavitand-benzyl H3	perchlorate-O4	41.86%
cavitand-aromatic H3	perchlorate-O4	24.52%
cavitand-aromatic H4	perchlorate-O4	23.6%
cavitand-benzyl H2	perchlorate-O4	37.52%
cavitand-aromatic H3	perchlorate-O2	20.48%
cavitand-aromatic H3	perchlorate-O1	22.5%
cavitand-benzyl H4	perchlorate-O1	37.48%
cavitand-aromatic H1	perchlorate-Cl	3.54%
cavitand-aromatic H4	perchlorate-O1	24.6%
cavitand-benzyl H4	perchlorate-Cl	22.7%
cavitand-benzyl H4	perchlorate-O3	39.86%
cavitand-benzyl H2	perchlorate-Cl	23.86%
cavitand-aromatic H1	perchlorate-O4	23.26%
cavitand-aromatic H4	perchlorate-O3	26.96%
cavitand-aromatic H2	perchlorate-O4	19.32%
cavitand-aromatic H1	perchlorate-O3	23.94%
cavitand-benzyl H1	perchlorate-O4	35.66%
cavitand-benzyl H3	perchlorate-O3	39.72%
cavitand-benzyl H4	perchlorate-O2	39.28%
cavitand-aromatic H4	perchlorate-O2	26.42%
cavitand-benzyl H2	perchlorate-O2	41.78%
cavitand-aromatic H2	perchlorate-Cl	3.26%
cavitand-aromatic H4	perchlorate-Cl	4.7%
cavitand-aromatic H3	perchlorate-O3	24.96%
cavitand-aromatic H2	perchlorate-O2	21.16%
cavitand-aromatic H3	perchlorate-Cl	3.62%

Table 2.5. Percentage of nearest-neighbor atom contacts less than 4 Å of thiocyanate with benzyl and aromatic hydrogen atoms of the cavitand during 5 ns of MD simulation (benzyl H: benzyl hydrogen atom, aromatic H: aromatic hydrogen atom)

cavitand atom	thiocyanate atom	nearest-neighbor contacts
cavitand-benzyl H1	thiocyanate-C	10.8%
cavitand-benzyl H1	thiocyanate-N	25.76%
cavitand-aromatic H1	thiocyanate-N	11.08%
cavitand-benzyl H2	thiocyanate-N	25.72%
cavitand-aromatic H2	thiocyanate-S	18.08%
cavitand-benzyl H3	thiocyanate-S	35.66%
cavitand-benzyl H4	thiocyanate-S	36.18%
cavitand-benzyl H1	thiocyanate-S	37.1%
cavitand-benzyl H2	thiocyanate-C	12.7%
cavitand-aromatic H3	thiocyanate-N	8.9%
cavitand-benzyl H4	thiocyanate-N	25.12%
cavitand-aromatic H4	thiocyanate-S	16.68%
cavitand-benzyl H3	thiocyanate-C	12.24%
cavitand-aromatic H1	thiocyanate-S	19.4%
cavitand-benzyl H2	thiocyanate-S	37.22%
cavitand-aromatic H2	thiocyanate-N	11.62%
cavitand-benzyl H3	thiocyanate-N	28.08%
cavitand-benzyl H4	thiocyanate-C	9.84%
cavitand-aromatic H2	thiocyanate-C	1.96%
cavitand-aromatic H1	thiocyanate-C	1.98%
cavitand-aromatic H3	thiocyanate-S	16.22%
cavitand-aromatic H4	thiocyanate-N	9.74%
cavitand-aromatic H4	thiocyanate-C	1.44%
cavitand-aromatic H3	thiocyanate-C	1.34%

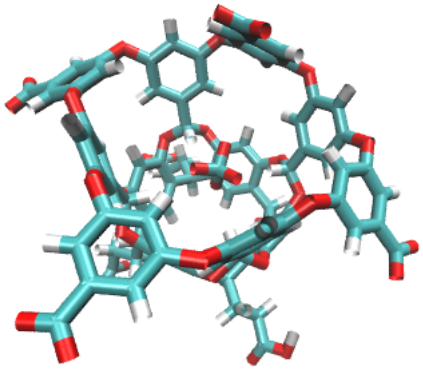

2.10(a) a potential perchlorate-cavitand binding mode at the minimum free energy around z = 4 Å

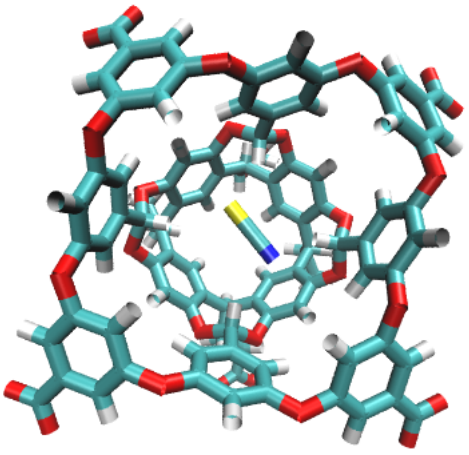

2.10(b) a potential thiocyanate-cavitand binding mode at the minimum free energy around z = 5 Å

Figure 2.10. Perchlorate-cavitand and thiocyanate-cavitand binding modes

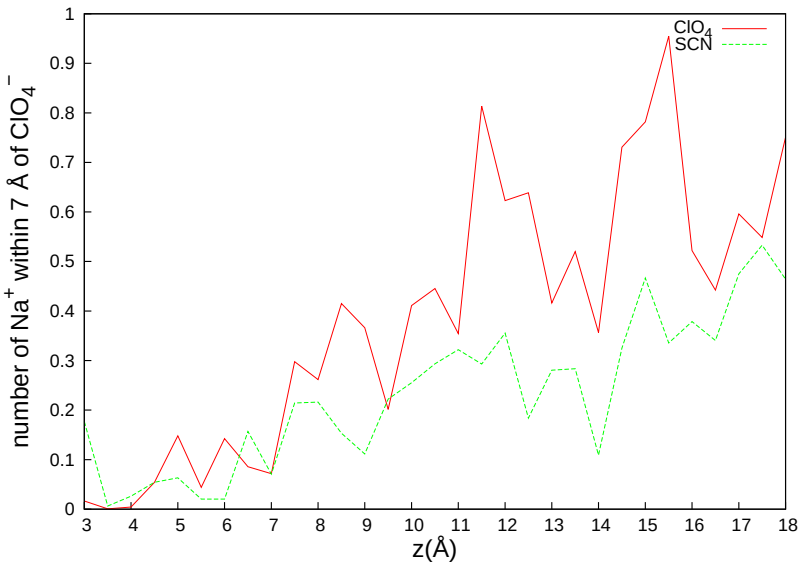

Figure 2.11. Average number of sodium ions within 7 Å of the perchlorate and thiocyanate ions over 5 ns of MD simulation

Discussion

The calculated relative binding free energies for perchlorate-cavitand and thiocyanate-cavitand complexation determined from their PMFs (ΔG = -2.0 and -0.4 kcal mol^{-1}, respectively (Table 2.1)) were in qualitative agreement with their experimentally determined binding free energies (ΔG = -2.7 and -2.1 kcal mol^{-1}, respectively).[20] However, the thiocyanate-cavitand binding free energy was rather low, perhaps due to insufficient sampling during the 5 ns of MD. Also, unbound configurations besides those at z = 16 Å were not included in the perchlorate-cavitand and thiocyanate-cavitand binding free energy calculations. Other methods for computing free energy changes such as free energy perturbation (FEP)[54–56] and thermodynamic integration (TI)[34] could possibly be used to increase sampling of unbound configurations of the anion and cavitand and improve the accuracy of salting-in anion-cavitand free energy calculations.[57–60]

The enthalpy for perchlorate-cavitand complexation calculated using the bound and unbound states at around z = 4 and 16 Å, respectively (ΔH = -8 kcal mol^{-1} (Table 2.2)), as well as the enthalpy for perchlorate-cavitand complexation calculated from the finite difference approximation to the entropy using binding free energies at 298 K and 328 K (ΔH = -6 kcal mol^{-1}) and 298 K and 338 K (ΔH = -3 kcal mol^{-1}) (Table 2.2) were favorable, in qualitative agreement with the experimentally determined perchlorate-cavitand binding enthalpy (ΔH = -10.62 kcal mol^{-1}).[20] The entropy for perchlorate-cavitand complexation calculated from the binding energy ($-T\Delta S$ = 6 kcal mol^{-1} (Table 2.2)) as well as the entropy calculated from the finite difference approximation to the entropy using binding free energies at 298 K and 328 K ($-T\Delta S$ = 4 kcal mol^{-1}) and 298 K and 338 K ($-T\Delta S$ = 1 kcal mol^{-1}) (Table 2.2) were unfavorable, in agreement with the experimentally determined perchlorate-cavitand binding entropy ($-T\Delta S$ = 7.94 kcal mol^{-1}).[20]

Fluctuations in the potential energy for thiocyanate-cavitand complexation along the free energy coordinate were too high to determine the enthalpy (binding energy) and entropy accurately

using the bound and unbound states at around z = 5 and 16 Å, respectively (Figure 2.3), so that the average potential energy from z = 12 to 18 Å was used for the energy of the unbound state. The enthalpy for thiocyanate-cavitand complexation calculated from the binding energy (ΔH = 1 kcal mol^{-1} (Table 2.2)) and the enthalpy calculated from the finite difference approximation to the entropy using binding free energies at 298 K and 328 K (ΔH = 0.5 kcal mol^{-1}) and 298 K and 338 K (ΔH = 0.1 kcal mol^{-1}) (Table 2.2) were unfavorable. The entropy for thiocyanate-cavitand complexation calculated from the binding energy (-TΔS = -2 kcal mol^{-1} (Table 2.2)) and the entropy calculated from the finite difference approximation to the entropy using binding free energies at 298 K and 328 K (-TΔS = -1.0 kcal mol^{-1}) and 298 K and 338 K (-TΔS = -0.5 kcal mol^{-1}) (Table 2.2) were favorable.

The perchlorate ion lost an average of about seven more solvation-shell waters than thiocyanate during transition from the unbound state to the bound state over the 5 ns of MD simulation (Figure 2.4 and Table 2.3), though perchlorate and thiocyanate displaced about the same number of waters from inside the cavitand upon binding (Figure 2.5 and Table 2.3). An average of about 4.5 and 4.2 water molecules occupied the inside of the cavitand in the unbound state in simulations of the perchlorate-cavitand and thiocyanate-cavitand complexes, respectively (Figure 2.5 and Table 2.3), consistent with previous studies which found the number of waters inside the cavitand averaged about 4.5, though the cavitand fluctuated between empty and full over the course of tens of nanoseconds.[47]

At least one oxygen from the perchlorate ion occupied the lower region of the cavitand an average of 95.9% of the time in the bound state over the 5 ns of MD simulation (Figure 2.6 and Table 2.3) and the highest percentage of nearest-neighbor contacts for the perchlorate-cavitand complex in the bound state during the 5 ns of MD involved the four benzyl hydrogen atoms in the lower region of the cavitand (Figure 2.1, green arrows), four aromatic hydrogen atoms (Figure 2.1, blue arrows), and the perchlorate oxygen atoms (Table 2.4). Moreover, on visual inspection one

oxygen was found to occupy the lower region of the cavitand for a significant amount of time during simulation of the perchlorate-cavitand complex in the bound state (Figure 2.10(a)). The chlorine atom of the perchlorate ion did not, on average, occupy the lower region of the cavitand for a significant amount of time in the bound state, as expected (data not shown). The sulfur atom of thiocyanate occupied the lower region of the cavitand an average of 3.0% of the time in the bound state during the 5 ns of MD (Figure 2.7 and Table 2.3), though nitrogen did not occupy the lower region of the cavitand for a significant amount of time (Figure 2.7 and Table 2.3). In addition, the highest percentage of nearest-neighbor contacts for the thiocyanate-cavitand complex in the bound state during the 5 ns of MD involved the four benzyl hydrogens in the lower region of the cavitand (Figure 2.1, green arrows), four aromatic hydrogens (Figure 2.1, blue arrows), and the sulfur atom of thiocyanate (Table 2.5). Also, on visual inspection, the sulfur atom of thiocyanate was found associated with the four benzyl hydrogen atoms in the lower region of the cavitand (Figure 2.1, green arrows) and four aromatic hydrogen atoms (Figure 2.1, blue arrows) for a significant amount of time in the bound state during simulation of the thiocyanate-cavitand complex (Figure 2.10(b)). Moreover, the sulfur atom of thiocyanate was, on average, facing toward the bottom of the cavitand at an angle of 103° (13° from perpendicular to the central axis of the host) (Figure 2.8 and Table 2.3) over the 5 ns of MD simulation and the probability distribution for the angle of thiocyanate, averaged over the 5 ns of MD, was bimodal with maxima at about 95° and 149° (Figure 2.9) in the bound state, implying the thiocyanate-cavitand complex possesses two binding modes. However, the average angle of thiocyanate was 91° (nearly perpendicular to the central axis of the host) (Figure 2.8 and Table 2.3) and the probability distribution for the angle of thiocyanate was relatively constant in the unbound state (Figure 2.9), indicating no long-range correlation between the angle of the unbound ligand and the cavitand.

Few sodium ions (0.004 sodium ions, on average, over the 5 ns of MD simulation) were found within 7 Å of the perchlorate ion in the bound state at around z = 4 Å, indicating little ion pairing occurs in the perchlorate-cavitand complex (Figure 2.11 and Table 2.3), though a larger number

of sodium ions (0.5 sodium ions, on average, over the 5 ns of MD) were found within 7 Å of perchlorate in the unbound state at around z = 16 Å and one sodium ion was found within 7 Å of perchlorate at z = 15.5 Å. Also, few sodium ions (0.06 sodium ions on average) were found within 7 Å of thiocyanate in the bound state at around z = 5 Å, though 0.4 sodium ions were found within 7 Å of thiocyanate in the unbound state at around z = 16 Å (Figure 2.11 and Table 2.3) and a maximum of 0.5 sodium ions were found within 7 Å of thiocyanate at z = 17.5 Å. Data for the energetic analysis of various interactions contributing to salting-in anion-cavitand complexation, including the anion-cavitand, anion-water, cavitand-water, and water-water interactions was inconclusive possibly due to insufficient sampling during the 5 ns of MD.

ITC and NMR studies[20] indicate complexation of perchlorate with the hydrophobic cavitand is enthalpically driven (ΔH = -10.62 kcal mol^{-1} and -$T\Delta S$ = 7.94 kcal mol^{-1}), possibly occurring via a nonclassical (enthalpically driven) hydrophobic effect.[61–70] Also, the enthalpy for perchlorate-cavitand complexation calculated from the binding energy and the finite difference approximation to the entropy were favorable with an unfavorable entropy, suggesting salting-in anion-cavitand binding is enthalpically driven. In addition, analysis of nearest-neighbor contacts between salting-in anions and the cavitand showed a greater number of cavitand atoms involved in nearest-neighbor contacts for the perchlorate-cavitand versus the thiocyanate-cavitand complex (data not shown) and the percentage of nearest-neighbor contacts was greater for the perchlorate-cavitand complex (Tables 2.4 and 2.5) which, together with the calculated binding free energies of ΔG = -2.0 and -0.4 kcal mol^{-1} (Table 2.1), respectively (as well as the experimentally determined binding free energies of ΔG = -2.7 and -2.1 kcal mol^{-1},[20] respectively), suggests salting-in anion-cavitand complexation is enthalpically driven, possibly occurring via electrostatic interactions between the anion and cavitand. However, the entropy for thiocyanate-cavitand complexation calculated from the binding energy and finite difference approximation to the entropy was favorable with an unfavorable enthalpy and studies by Ewell et al. show the free energy for displacing all waters from the cavitand to be around

ΔG = 5 kcal mol^{-1} with an enthalpy of ΔH = 20 kcal mol^{-1} and an entropy of $-T\Delta S$ = -15 kcal mol^{-1} at 298 K,[47] suggesting salting-in anion-cavitand complexation may occur via a classical hydrophobic effect.[39–41,43,71–78] Additionally, though the highest percentage of nearest-neighbor contacts for the perchlorate-cavitand and thiocyanate-cavitand complexes involved the four benzyl hydrogens in the lower region of the cavitand (Figure 2.1, green arrows), four aromatic hydrogens (Figure 2.1, blue arrows), the sulfur atom of thiocyanate, and the oxygen atoms of perchlorate (Tables 2.4 and 2.5), interactions of the perchlorate oxygens and thiocyanate nitrogen with other cavitand atoms or water may also contribute to salting-in anion-cavitand complexation. Energetic analysis of the Lennard-Jones and electrostatic components of pairwise interactions between anion and cavitand atoms could be used to further elucidate the mechanism(s) of Hofmeister anion-cavitand binding. Assessment of Hofmeister anion-cavitand complexation in solvents of varying polarity could also be used to further investigate the anion-cavitand binding mechanism(s).[63,69] Salting-in anion-cavitand binding affinity should be affected by solvent polarity and polarizability such that solvents of higher polarity/lower polarizability would increase anion-cavitand binding driven by a solvent-mediated hydrophobic effect and decrease anion-cavitand binding driven by electrostatic interactions between the anion and cavitand.[63,69] Additionally, solvents of increasing polarity/lower polarizability should result in more favorable binding enthalpies versus entropies for anion-cavitand binding mediated by an enthalpically driven nonclassical hydrophobic effect.

References

[1] F. Hofmeister. Zur Lehre von der Wirkung der Salze. *Arch. Exp. Pathol. Pharmakol.*, *24*:247–260, **1888**.

[2] K. D. Collins and M. W. Washabaugh. The Hofmeister Effect and the Behaviour of Water at Interfaces. *Q. Rev. Biophys.*, *18*:323–422, **1985**.

[3] W. Kunz, J. Henle, and B. W. Ninham. 'Zur Lehre von der Wirkung der Salze'(about the science of the effect of salts): Franz Hofmeister's Historical Papers. *Curr. Opin. Colloid. Interface Sci.*, *9*:19–37, **2004**.

[4] B. C. Gibb. Supramolecular Assembly and Binding in Aqueous Solution: Useful Tips Regarding the Hofmeister and Hydrophobic Effects. *Isr. J. Chem.*, *51*:798–806, **2011**.

[5] M. D. Baer and C. J. Mundy. An *ab initio* Approach to Understanding the Specific Ion Effect. *Faraday Discuss.*, *160*:89–101, **2013**.

[6] Y. Zhang and P. S. Cremer. Interactions between Macromolecules and Ions: The Hofmeister Series. *Curr. Opin. Chem. Biol.*, *10*:658–663, **2006**.

[7] P. H. von Hippel and K. Y. Wong. The Effect of Ions on the Kinetics of Formation and the Stability of the Collagen-Fold. *Biochemistry*, *1*:664–674, **1962**.

[8] P. H. von Hippel and K. Y. Wong. The Collagen $\leftrightarrow$ Gelatin Phase Transition. I. Further Studies of the Effects of Solvent Environment and Polypeptide Chain Composition. *Biochemistry*, *2*:1387–1398, **1963**.

[9] P. H. von Hippel and K. Y. Wong. Neutral Salts: The Generality of their Effects on the Stability of Macromolecular Conformations. *Science*, *145*:577–580, **1964**.

[10] M. D. Baer, V. T. Pham, J. L. Fulton, G. K. Schenter, M. Balasubramanian, and C. J. Mundy. Is Iodate a Strongly Hydrated Cation? *J. Phys. Chem. Lett.*, *2*:2650–2654, **2011**.

[11] K. D. Collins. Charge Density-Dependent Strength of Hydration and Biological Structure. *Biophys. J.*, *72*:65–76, **1997**.

[12] R. Zangi. Can Salting-In/Salting-Out Ions be Classified as Chaotropes/Kosmotropes? *J. Phys. Chem. B*, *114*:643–650, **2010**.

[13] Y. Marcus. Effect of Ions on the Structure of Water: Structure Making and Breaking. *Chem. Rev.*, *109*:1346–1370, **2009**.

[14] R. Mancinelli, A. Botti, F. Bruni, M. A. Ricci, and A. K. Soper. Perturbation of Water Structure due to Monovalent Ions in Solution. *Phys. Chem. Chem. Phys.*, *9*:2959–2967, **2007**.

[15] A. W. Omta, M. F. Kropman, S. Woutersen, and H. J. Bakker. Influence of Ions on the Hydrogen-Bond Structure in Liquid Water. *J. Chem. Phys.*, *119*:12457–12461, **2003**.

[16] A. W. Omta. Negligible Effect of Ions on the Hydrogen-Bond Structure in Liquid Water. *Science*, *301*:347–349, **2003**.

[17] A. P. Lyubartsev, K. Laasonen, and A. Laaksonen. Hydration of L^+ Ion. An *ab initio* Molecular Dynamics Simulation. *J. Chem. Phys.*, *114*:3120–3126, **2001**.

[18] Y. Zhang and P. S. Cremer. Chemistry of Hofmeister Anions and Osmolytes. *Annu. Rev. Phys. Chem.*, *61*:63–83, **2010**.

[19] Y. Zhang, S. Furyk, D. E. Bergbreiter, and P. S. Cremer. Specific Ion Effects on the Water Solubility of Macromolecules: PNIPAM and the Hofmeister Series. *J. Am. Chem. Soc.*, *127*:14505–14510, **2005**.

[20] C. L. D. Gibb and B. C. Gibb. Anion Binding to Hydrophobic Concavity is Central to the Salting-In Effects of Hofmeister Chaotropes. *J. Am. Chem. Soc.*, *133*:7344–7347, **2011**.

[21] T. Arakawa and S. N. Timasheff. Preferential Interactions of Proteins with Salts in Concentrated Solutions. *Biochemistry*, *21*:6545–6552, **1982**.

[22] S. C. Flores, J. Kherb, and P. S. Cremer. Direct and Reverse Hofmeister Effects on Interfacial Water Structure. *J. Phys. Chem. C*, *116*:14408–14413, **2012**.

[23] A. Hamabata and P. H. von Hippel. Model Studies on the Effects of Neutral Salts on the Conformational Stability of Biological Macromolecules. II. Effects of Vicinal Hydrophobic Groups on the Specificity of Binding of Ions to Amide Groups. *Biochemistry*, *12*:1264–1271, **1973**.

[24] A. Hamabata, S. Chang, and P. H. von Hippel. Model Studies on the Effects of Neutral Salts on the Conformational Stability of Biological Macromolecules. III. Solubility of Fatty Acid Amides in Ionic Solutions. *Biochemistry*, *12*:1271–1278, **1973**.

[25] R. L. Baldwin. How Hofmeister Ion Interactions Affect Protein Stability. *Biophys. J.*, *71*:2056–2063, **1996**.

[26] R. Zangi, M. Hagen, and B. J. Berne. Effect of Ions on the Hydrophobic Interaction between Two Plates. *J. Am. Chem. Soc.*, *129*:4678–4686, **2007**.

[27] M. Lund, L. Vrbka, and P. Jungwirth. Specific Ion Binding to Nonpolar Surface Patches of Proteins. *J. Am. Chem. Soc.*, *130*:11582–11583, **2008**.

[28] L. M. Pegram, T. Wendorff, R. Erdmann, I. Shkel, D. Bellissimo, D. J. Felitsky, and M. T. Record. Why Hofmeister Effects of Many Salts Favor Protein Folding but not DNA Helix Formation. *Proc. Natl. Acad. Sci.*, *107*:7716–7721, **2010**.

[29] C. L. D. Gibb and B. C. Gibb. Well-Defined, Organic Nanoenvironments in Water: The Hydrophobic Effect Drives a Capsular Assembly. *J. Am. Chem. Soc.*, *126*:11408–11409, **2004**.

[30] S. Liu and B. C. Gibb. High-Definition Self-Assemblies Driven by the Hydrophobic Effect: Synthesis and Properties of a Supramolecular Nanocapsule. *Chem. Commun.*, *2008*:3709–3716, **2008**.

[31] S. Liu, S. E. W. Loup, C. L. D. Gibb, and B. C. Gibb. An Improved Synthesis of 'Octa-Acid' Deep-Cavity Cavitand. *Supramolecular Chemistry*, *23*:480–485, **2011**.

[32] H. Gan and B. C. Gibb. Guest-Mediated Switching of the Assembly State of a Water-Soluble Deep-Cavity Cavitand. *Chem. Commun.*, *49*:1395–1397, **2013**.

[33] D. J. Cram. Cavitands: Organic Hosts with Enforced Cavities. *Science*, *219*:1177–1183, **1983**.

[34] J. G. Kirkwood. Statistical Mechanics of Fluid Mixtures. *Journal of Chemical Physics*, *3*:300–313, **1935**.

[35] G. M. Torrie and J. P. Valleau. Nonphysical Sampling Distributions in Monte Carlo Free-Energy Estimation: Umbrella Sampling. *Journal of Computational Physics*, *23*:187–199, **1977**.

[36] C. Pangali, M. Rao, and B. J. Berne. On a Novel Monte Carlo Scheme for Simulating Water and Aqueous Solutions. *Chemical Physics Letters*, *55*:413–417, **1978**.

[37] D. W. Rebertus, B. J. Berne, and D. Chandler. A Molecular Dynamics and Monte Carlo Study of Solvent Effects on the Conformational Equilibrium of n-butane in CCl_4. *Journal of Chemical Physics*, *70*:3395–3400, **1979**.

[38] C. Pangali, M. Rao, and B. J. Berne. A Monte Carlo Simulation of the Hydrophobic Interaction. *Journal of Chemical Physics*, *71*:2975–2981, **1979**.

[39] S. W. Rick and B. J. Berne. Free Energy of the Hydrophobic Interaction from Molecular Dynamics Simulations: The Effects of Solute and Solvent Polarizability. *J. Phys. Chem. B*, *101*:10488–10493, **1997**.

[40] S. W. Rick. Free Energy, Entropy and Heat Capacity of the Hydrophobic Interaction as a Function of Pressure. *J. Phys. Chem. B*, *104*:6884–6888, **2000**.

[41] S. W. Rick. Heat Capacity Change of the Hydrophobic Interaction. *J. Phys. Chem. B*, *107*:9853–9857, **2003**.

[42] D.A. Case, T.A. Darden, T.E. Cheatham III, C.L. Simmerling, J. Wang, R.E. Duke, R. Luo, R.C. Walker, W. Zhang, K.M. Merz, B.P. Roberts, B. Wang, S. Hayik, A. Roitberg, G. Seabra, I. Kolossvai, K.F. Wong, F. Paesani, J. Vanicek, J. Liu, X. Wu, S.R. Brozell, T. Steinbrecher, H. Gohlke, Q. Cai, X. Ye, J. Wang, M.J. Hsieh, G. Cui, D.R. Roe, D.H. Mathews, M.G. Seetin, C. Sagui, V. Babin, T. Luchko, S. Gusarov, A. Kovalenko, and P.A. Kollman. *AMBER 11*. University of California, San Francisco, **2010**.

[43] D. E. Smith and A. D. J. Haymet. Free Energy, Entropy, and Internal Energy of Hydrophobic Interactions: Computer Simulations. *J. Chem. Phys.*, *98*:6445–6454, **1993**.

[44] L. R. Olano and S. W. Rick. Hydration Free Energies and Entropies for Water in Protein Interiors. *J. Am. Chem. Soc.*, *126*:7991–8000, **2004**.

[45] H. Yu and S. W. Rick. Free Energies and Entropies of Water Molecules at the Inhibitor-Protein Interface of DNA Gyrase. *J. Am. Chem. Soc.*, *131*:6608–6613, **2009**.

[46] W. Humphrey, A. Dalke, and K. Schulten. VMD: Visual Molecular Dynamics. *J. Mol. Graphics*, *14*:33–38, **1996**.

[47] J. Ewell, B. C. Gibb, and S. W. Rick. Water Inside a Hydrophobic Cavitand Molecule. *J. Phys. Chem. B*, *112*:10272–10279, **2008**.

[48] M. Baaden, F. Berny, C. Madic, and G. Wipff. M^{3+} Lanthanide Cation Solvation by Acetonitrile: The Role of Cation Size, Counterions, and Polarization Effects Investigated by Molecular Dynamics and Quantum Mechanical Simulations. *J. Phys. Chem. A*, *104*:7659–7671, **2000**.

[49] A. Botti, S. E. Pagnotta, F. Bruni, and M. A. Ricci. Solvation of KSCN in Water. *J. Phys. Chem. B*, *113*:10014–10021, **2009**.

[50] H. W. Horn, W. C. Swope, J. W. Pitera, J. D. Madura, T. J. Dick, G. L. Hura, and T. H. Gordon. Development of an Improved Four-Site Water Model for Biomolecular Simulations: TIP4P-Ew. *The Journal of Chemical Physics*, *120*:9665–9678, **2004**.

[51] A. Ferrenberg and R. Swendsen. Optimized Monte Carlo Data Analysis. *Phys. Rev. Lett.*, *63*:1195–1198, **1989**.

[52] S. Kumar, D. Bouzida, R. H. Swendsen, P. A. Kollman, and J. M. Rosenberg. The Weighted Histogram Analysis Method for Free-Energy Calculations on Biomolecules. I. The Method. *Journal of Computational Chemistry*, *13*:1011–1021, **1992**.

[53] I. J. General, E. K. Asciutto, and J. D. Madura. Structure of Aqueous Sodium Perchlorate Solutions. *J. Phys. Chem. B*, *112*:15417–15425, **2008**.

[54] R. W. Zwanzig. High-Temperature Equation of State by a Perturbation Method. I. Nonpolar Gases. *J. Chem. Phys.*, *22*:1420–1426, **1954**.

[55] M. R. Shirts, D. L. Mobley, and J. D. Chodera. Alchemical Free Energy Calculations: Ready for Prime Time? In D.C. Spellmeyer and R. Wheeler, editors, *Annu. Rep. Comput. Chem.*, volume *3*, pages 41–59. Elsevier, Amsterdam, **2007**.

[56] W. L. Jorgensen and L. L. Thomas. Perspective on Free-Energy Perturbation Calculations for Chemical Equilibria. *J. Chem. Theory Comput.*, *4*:869–876, **2008**.

[57] W. L. Jorgensen. Free Energy Calculations: A Breakthrough for Modeling Organic Chemistry in Solution. *Acc. Chem. Res.*, *22*:184–189, **1989**.

[58] D. A. Pearlman. A Comparison of Alternative Approaches to Free Energy Calculations. *J. Phys. Chem.*, *98*:1487–1493, **1994**.

[59] Ajay and M. A. Murcko. Computational Methods to Predict Binding Free Energy in Ligand-Receptor Complexes. *J. Med. Chem.*, *38*:4953–4967, **1995**.

[60] T. Rodinger and R. Pomès. Enhancing the Accuracy, the Efficiency and the Scope of Free Energy Simulations. *Curr. Opin. Struct. Biol.*, *15*:164–170, **2005**.

[61] J. M. Sturtevant and G. Velicelebi. Calorimetric Study of the Interaction of Lysozyme with Aqueous 1-Propanol. *Biochemistry*, *20*:3091–3096, **1981**.

[62] M. R. Eftink and J. C. Harrison. Calorimetric Studies of *p*-Nitrophenol Binding to α- and β-Cyclodextrin. *Bioorganic Chemistry*, *10*:388–398, **1981**.

[63] F. Diederich, D. B. Smithrud, E. M. Sanford, T. B. Wyman, D. R. Ferguson, D. R. Carcanague, I. Chao, and K. N. Houk. Solvent Effects in Molecular Recognition. *Acta Chemica Scandinavica*, *46*:205–215, **1992**.

[64] S. B. Ferguson, E. M. Seward, F. Diederich, E. M. Sanford, A. Chou, P. I. Szweda, and C. B. Knobler. Strong Enthalpically Driven Complexation of Neutral Benzene Guests in Aqueous Solution. *J. Org. Chem.*, *53*:5593–5595, **1988**.

[65] K. Harata, K. Tsuda, K. Uekama, M. Otagiri, and F. Hirayama. Complex Formation of Hexakis(2,3,6-tri-*O*-methyl)-α-Cyclodextrin with Substituted Benzenes in Aqueous Solution. *Journal of Inclusion Phenomena*, *6*:135–142, **1988**.

[66] S. B. Ferguson, E. M. Sanford, E. M. Seward, and F. Diederich. Cyclophane-Arene Inclusion Complexation in Protic Solvents: Solvent Effects versus Electron Donor-Acceptor Interactions. *J. Am. Chem. Soc.*, *113*:5410–5419, **1991**.

[67] D. B. Smithrud, T. B. Wyman, and F. Diederich. Enthalpically Driven Cyclophane-Arene Inclusion Complexation: Solvent-Dependent Calorimetric Studies. *J. Am. Chem. Soc.*, *113*:5420–5426, **1991**.

[68] R. U. Lemieux. How Water Provides the Impetus for Molecular Recognition in Aqueous Solution. *Acc. Chem. Res.*, *29*:373–380, **1996**.

[69] E. A. Meyer, R. K. Castellano, and F. Diederich. Interactions with Aromatic Rings in Chemical and Biological Recognition. *Angew. Chem. Int. Ed.*, *42*:1210–1250, **2003**.

[70] R. J. Bingham, J. B. C. Findlay, S. Y. Hsieh, A. P. Kalverda, A. Kjellberg, C. Perazzolo, S. E. V. Phillips, K. Seshadri, C. H. Trinh, W. B. Turnbull, G. Bodenhausen, and S. W. Homans. Thermodynamics of Binding of 2-Methoxy-3-isopropylpyrazine and 2-Methoxy-3-isobutylpyrazine to the Major Urinary Protein. *J. Am. Chem. Soc.*, *126*:1675–1681, **2004**.

[71] D. Harries, D. C. Rau, and V. A. Parsegian. Solutes Probe Hydration in Specific Association of Cyclodextrin and Adamantane. *J. Am. Chem. Soc.*, *127*:2184–2190, **2005**.

[72] H. S. Frank and M. W. Evans. Free Volume and Entropy in Condensed Systems III. Entropy in Binary Liquid Mixtures; Partial Molal Entropy in Dilute Solutions; Structure and Thermodynamics in Aqueous Electrolytes. *Journal of Chemical Physics*, *13*:507–532, **1945**.

[73] F. H. Stillinger. Structure in Aqueous Solutions of Nonpolar Solutes from the Standpoint of Scaled-Particle Theory. *J. Solution Chem.*, *2*:141–158, **1973**.

[74] N. T. Southall, K. A. Dill, and A. D. J. Haymet. A View of the Hydrophobic Effect. *J. Phys. Chem. B*, *106*:521–533, **2002**.

[75] S. Granick and S. C. Bae. Chemistry. A Curious Antipathy for Water. *Science*, *322*:1477–1478, **2008**.

[76] D. Chandler. Interfaces and the Driving Force of Hydrophobic Assembly. *Nature*, *437*:640–647, **2005**.

[77] L. R. Pratt and A. Pohorille. Hydrophobic Effects and Modeling of Biophysical Aqueous Solution Interfaces. *Chem. Rev.*, *102*:2671–2692, **2002**.

[78] L. R. Pratt and D. Chandler. Theory of the Hydrophobic Effect. *Journal of Chemical Physics*, *67*:3683–3704, **1977**.

Vita

Joshua Shraberg received his B.S. and M.S. in Cell and Molecular Biology from Tulane University in 2001 and 2002, respectively. He specialized in Biochemistry at the University of New Orleans in the Computational Chemistry lab of Dr. Steven Rick.